NASA TN D-136

TECHNICAL NOTE
D-136

THE EFFECTS OF THRUST REVERSAL AT MACH NUMBERS UP TO 0.86 ON THE LONGITUDINAL AND BUFFETING CHARACTERISTICS OF A TYPICAL JET-TRANSPORT AIRPLANE CONFIGURATION

By Fred B. Sutton and Jack J. Brownson

Ames Research Center
Moffett Field, Calif.

NATIONAL AERONAUTICS AND SPACE ADMINISTRATION

WASHINGTON

March 1960

NATIONAL AERONAUTICS AND SPACE ADMINISTRATION

TECHNICAL NOTE D-136

THE EFFECTS OF THRUST REVERSAL AT MACH NUMBERS UP TO 0.86 ON THE LONGITUDINAL AND BUFFETING CHARACTERISTICS OF A TYPICAL JET-TRANSPORT AIRPLANE CONFIGURATION

By Fred B. Sutton and Jack J. Brownson

SUMMARY

An investigation has been made to determine the effects of thrust reversal at relatively high speeds on the longitudinal and buffeting characteristics of a typical jet-transport airplane configuration. Wind-tunnel tests were conducted through ranges of angles of attack and jet-nozzle pressure ratios for forward and reverse thrust at Mach numbers from 0.40 to 0.86.

The results of the investigation show that thrust reversal can be used as a very effective method of speed control for jet-transport airplanes making steep, relatively rapid descents from operational altitudes. Use of thrust reversers can more than double the cruise drag of such aircraft, and the test results show that at a constant Mach number of about 0.80 the initial rate of descent from cruising altitudes can be increased from about 5000 feet per minute to over 12,000 feet per minute. Thrust reversal had only small effects on the longitudinal stability and trim characteristics of the model at the relatively low lift coefficients required for rapid descents by jet-transport aircraft. Operation of the reversers at a Mach number of 0.80 and an assumed initial altitude of 30,000 feet with complete tail-pipe blockage and the simulated power normally required for level flight resulted in a small stabilizing movement of the aerodynamic center corresponding to about 2 percent of the mean aerodynamic chord and about a $+1^{\circ}$ change in the horizontal-tail angle required for trim.

Reverse thrust resulted in reductions in lift-curve slope and reduced the lift coefficients at which static-longitudinal instability occurred. However, these lift coefficients were usually higher than the lift coefficients of interest for reverser operation at high speeds.

The effects of thrust reversal on the buffeting characteristics of both the wing and tail of the model were small. At the relatively low lift coefficients associated with steep high-speed descents, these effects were negligible.

INTRODUCTION

The relatively high operational altitudes of current jet-transport aircraft have caused much concern over flight techniques for rapid descents to lower altitudes. The tendency of these aircraft to accelerate quickly in nose-down attitudes and the dynamic-pressure limitations of such speed-arresting devices as spoilers and dive brakes combine to make descents from cruising altitudes relatively slow, if speed placards and structural limitations are not to be exceeded. The successful development of thrust reversers for reducing the landing roll of jet aircraft has suggested that these devices could be used to provide speed braking. Such usage would permit relatively steep and rapid descents from cruising altitudes at controlled velocities near cruising speeds, provided the efflux from the reversers did not induce adverse effects on the stability and buffeting characteristics of the airplane.

The present investigation was conducted in the Ames 12-foot pressure wind tunnel to determine the effects of thrust reversal at relatively high speeds upon the longitudinal and buffeting characteristics of a model having a configuration typical of current jet-transport airplanes with pod-mounted engines suspended from sweptback wings. The model employed cascade-type reversers similar to those described in reference 1 as configuration 4. Tests were conducted over a Mach number range of 0.40 to 0.86 at a Reynolds number of 2,000,000. Thrust was obtained by supplying cold compressed air to the nacelle exhaust nozzles for a range of ratios of jet total pressure to stream static pressures which varied from 1.0 (jet off) to 3.5. At Mach numbers near 0.80 and with an assumed altitude of 30,000 feet, full-scale thrust outputs of as much as 6500 pounds per engine were simulated.

NOTATION

a	mean-line designation, fraction of chord over which design load is uniform
a.c.	aerodynamic center
$\frac{b}{2}$	wing semispan perpendicular to the plane of symmetry, ft
BM	bending moment, ft-lb
$\bar{c}$	wing mean aerodynamic chord, ft
C_L	lift coefficient, $\frac{\text{lift}}{q_\infty S}$

C_m pitching-moment coefficient about the quarter point of the wing mean aerodynamic chord, $\frac{\text{pitching moment}}{q_\infty S \bar{c}}$

C_X longitudinal force coefficient, $\frac{X}{q_\infty S}$

h altitude, ft

i_t incidence of the horizontal tail with respect to the wing-root chord, deg

l_t tail length, distance between the quarter points of the mean aerodynamic chords of the wing and the horizontal tail, measured parallel to the plane of symmetry, ft

M free-stream Mach number

$\frac{P_n}{P_\infty}$ jet-pressure ratio (ratio of total pressure in the nacelle plenum to the free-stream pressure)

q_∞ free-stream dynamic pressure, $\frac{\rho_\infty V_\infty^2}{2}$, lb/sq ft

S area of semispan wing, sq ft

T thrust, lb

V_∞ velocity, ft/sec

W weight flow of air, lb/min

X longitudinal force parallel to stream and positive in a dragwise direction, lb

α angle of attack of the center line of the fuselage, deg

$\frac{\partial C_m}{\partial i_t}$ tail effectiveness parameter, measured at a constant angle of attack

MODEL DESCRIPTION

The design of the model was based on the geometry of several current jet-transport airplanes. All of the aircraft employed four podded engines suspended beneath low-mounted sweptback wings of comparatively high aspect ratio. The geometric parameters selected for the model generally represent an average of those for the airplanes considered. The semispan test technique was employed for the investigation because it permitted a larger

model with consequently higher Reynolds numbers and because it greatly simplified the supply of compressed air to the jet-exhaust nozzles. The model represented to about 0.066 scale, the right-hand side of the hypothetical four-engine jet transport. The geometry and details of the model are shown in figure 1. A photograph of the model mounted in the wind tunnel is shown in figure 2.

The wing had 35° of sweepback, an aspect ratio of 7.0, a taper ratio of 0.30, and employed NACA 65 series thickness distributions. These distributions of thickness were combined with an a = 1.0 mean line having an ideal lift coefficient of 0.40 to form sections parallel to the air stream. The thickness-chord ratio was tapered in two sections from 0.14 at the root to 0.11 at 0.30 b/2 and from 0.11 at 0.30 b/2 to 0.09 at the tip. The wing was untwisted and had 5° of dihedral. Construction was of steel and the surfaces were polished smooth. An air duct was machined within the wing and extended from the root to the spanwise position of the outboard nacelle (0.70 b/2).

Thrust conditions scaled to represent the output of full-sized turbojet engines were simulated by ejecting compressed air from scaled nacelle exhaust nozzles. The air was ducted through the wing, down the hollow struts supporting dummy engine nacelles, into the nacelle plenum chambers and exhausted, either through the exhaust nozzles or thrust reversers. The nacelles and struts were constructed of steel and were attached to the lower surface of the wing at 0.4 and 0.7 of the wing semispan. The usual air inlets in the nose of the nacelle were faired over and the nacelles were constructed as simple bodies of revolution having an NACA form 111 for the forebodies and portions of an NACA form 221 for the after sections. Coordinates of the nacelles are listed in table I. The thrust simulation requirements of the investigation demanded more air than could be ducted at the allowable line pressure through wing-nacelle struts having the same thickness-chord and strut-chord to wing-chord ratios as the full-scale airplanes used as a basis for the model design. Consequently, the thickness-chord ratio of the struts was increased from about 0.08 to 0.115 and the ratio of strut chord to wing mean aerodynamic chord was increased from about 0.50 to about 0.65. The struts had NACA 65A011.5 thickness distributions parallel to the air stream. Figure 1(b) presents strut and nacelle details.

A cascade-type thrust reverser similar to the unit presented in reference 1 as configuration 4 was mounted at the aft end of each nacelle. This arrangement consisted primarily of cascade elements mounted circumferentially in each side of the jet tail pipe. Reverse thrust was obtained by simulating internal doors in the jet tail pipes with wedge-shaped plugs (see fig. 1(c)). These plugs blocked or partially blocked the normal jet exits and forced the efflux through the cascades which turned it approximately 160°. For forward thrust and power-off conditions, the solid plugs were replaced with tubular inserts which closed off the

interior cascade openings and served as jet tail pipes. Also, for forward thrust and power-off conditions the exterior reverser openings were faired over with thin sleeves (see fig. 1(c)).

The fuselage employed for these tests consisted of a cylindrical midsection with simple fairings fore and aft. Fuselage coordinates are listed in table I. The fuselage had a fineness ratio of 11.5 and was located with respect to the wing so that the upper surface of the wing was nearly tangent to the fuselage center line at the plane of symmetry. The angle of incidence of the wing root with respect to the fuselage center line was 2°. The fuselage was relieved at the wing-fuselage juncture and the resultant gap sealed with sponge rubber to maintain an air seal, yet minimize mechanical restraint of the wing by the fuselage. The fuselage was constructed of Fiberglas and aluminum shells bolted to a heavy steel structural member.

The all-movable horizontal tail had an aspect ratio of 4.0, a taper ratio of 0.5, a sweepback angle of 35°, and NACA 65A009 thickness distributions parallel to the air stream. It had no dihedral and its incidence axis was at 50.5 percent of the tail root chord. Tail volume was 0.625. The tail was constructed of solid aluminum and the surfaces were polished smooth.

Fundamental bending frequencies were determined for some of the model components. The wing with nacelles and struts mounted had a frequency of about 25 cycles per second. The horizontal-tail frequency was about 60 cycles per second.

APPARATUS

The investigation was conducted in the Ames 12-foot pressure wind tunnel. Static-aerodynamic forces and moments were measured with the lever-type balance system. Steady-state and fluctuating bending moments of the wing and horizontal tail were measured with strain gages installed near the wing and tail roots (see fig. 1(a)). The strain-gage outputs were fed into electronic instrumentation which analyzed data samples corresponding to several thousand cycles of bending moment. This apparatus, which is described in detail in reference 2, provided the largest peak values of successive 10-second samples of data and the steady-state bending moments.

Compressed air used for jet thrust simulation was piped from a remote reservoir to the model. An arrangement of flexible bellows was employed at the juncture of the air line with the floating frame of the wind-tunnel scale system to eliminate any restraining effects of the air line. A controller was installed on the line to regulate and maintain air pressure at any desired level between -10 and +30 psig. Stagnation

pressures and temperatures at the inlets to the jet nozzles were measured with pressure and temperature probes. Air flow through the system was measured by means of a standard ASME sharp-edged orifice.

TESTS

The longitudinal and buffeting characteristics of the model were investigated at Mach numbers varying from 0.40 to 0.86 at a Reynolds number of 2,000,000. Tests were made through an angle-of-attack range of -4° to $+14^\circ$ at Mach numbers up to 0.70, from -4° to $+12^\circ$ at Mach numbers up to 0.83, and from -4° to $+10^\circ$ at a Mach number of 0.86. At each angle of attack, forward and reverse thrust conditions were generally varied from power off ($P_n/p_\infty = 1.0$) to simulated thrust outputs exceeding those normally required by a full-scale airplane for level flight. Reverse thrust was usually obtained with the tail pipe completely blocked (see fig. 1(c)); however, some testing was done at Mach numbers of 0.40, 0.70, and 0.80 to determine the effect of partial tail-pipe blockage (fig. 1(c)).

The model was tested with a tail incidence angle of -2° at all test Mach numbers. In addition, tests were made at Mach numbers of 0.40, 0.70, and 0.80 with tail incidence angles of 0° and -4° and with the horizontal tail removed.

REDUCTION OF DATA

Thrust Data

The basic thrust parameter used for this investigation was the exhaust jet-pressure ratio P_n/p_∞ and, as used herein, the term represents the average of total-pressure measurements in the inboard and outboard nacelle plenums divided by free-stream static pressure. The variations with this average pressure ratio of the total model forward thrust, the total reverse thrust, the average reverse-thrust ratio, and the total weight flows for forward and full-reverse thrust conditions are presented in figure 3 for zero stream velocity at atmospheric pressure. Operation of the thrust reversers at constant jet-pressure ratio reduced the weight flow by approximately 7 percent. The effect of this loss on the test data is believed to be relatively unimportant since most full-scale reverser installations will probably induce similar effects on the weight flows of full-scale engines.

Force and Moment Data

The basic data obtained for the various thrust conditions at constant angle of attack and Mach number were reduced to conventional form. Lift coefficient is shown as a function of angle of attack, and longitudinal-force coefficient and pitching-moment coefficient are shown as functions of lift coefficient. The data for these presentations were obtained by cross-plotting the constant angle-of-attack data at several constant jet-pressure ratios. Tabulations of the basic data are available at the Ames Research Center.

Buffet Data

Fluctuations of the bending moments at the roots of the wing and horizontal tail were measured for various test conditions as an indication of relative buffeting. These measurements were made simultaneously with measurements of the longitudinal characteristics and are presented herein as functions of model lift coefficient for several constant jet-pressure ratios. Steady-state bending moments were also measured at the wing and tail roots for each test condition and are also shown as functions of lift coefficient and jet-pressure ratio.

Corrections

The data have been corrected for constriction effects due to the tunnel walls by the method of reference 3, for tunnel-wall interference originating from lift on the model by the method of reference 4, and for drag tares caused by aerodynamic forces on the turntable upon which the model was mounted. The corrections to dynamic pressure, Mach number, angle of attack, drag coefficient, and pitching-moment coefficient are listed in table II. No corrections have been made for wind-tunnel-wall constraint on the efflux of the jets; however, computations indicated that at the Mach numbers and longitudinal-force coefficients of the subject investigation such effects would be negligible.

RESULTS AND DISCUSSION

The basic longitudinal characteristics of the model for several forward and reverse thrust conditions are presented for several horizontal-tail incidence angles, and with the horizontal tail removed in figures 4 through 21. All reverse-thrust results were obtained with full tail-pipe blockage except for those presented in figures 16 through 18 which

present measurements made with partial tail-pipe blockage. Unless otherwise stated, use of the expression reverse thrust denotes complete tail-pipe blockage. Figures 22 through 34 show, for selected conditions, the effects of thrust reverser operation on the various longitudinal parameters of the model, on the effectiveness of the horizontal tail, and on wing and tail buffeting. Figures 35 and 36 summarize the effects of thrust reverser operation on the performance of a hypothetical airplane similar to the model.

Effects of Forward and Reverse Thrust on the Longitudinal Characteristics

A
3
2
1

Figures 4 through 9 show the effects of forward and reverse thrust on the basic longitudinal characteristics of the model at Mach numbers ranging from 0.40 to 0.86. In general, the effects of forward thrust on lift were negligible compared to the effects of reverse thrust. Operation of the thrust reversers with complete tail-pipe blockage resulted in lift-curve slope reductions which increased with increasing jet-pressure ratio. This effect is summarized for several Mach numbers in figure 22. With reverse thrust, large reductions in lift-curve slope occurred at jet-pressure ratios near those required for steady level flight.

The effects of thrust reversal on the longitudinal-force coefficient characteristics of the model were large. For example, the drag of the model (positive longitudinal force) was more than doubled by operation of the thrust reversers at test conditions approximating full-scale cruise. (See fig. 7(b) for $M = 0.80$, $P_n/p_\infty = 3.0$, and $C_L = 0.30$.) These effects are summarized for several Mach numbers in figure 23 which shows net longitudinal-force coefficient (longitudinal-force coefficient for forward or reverse thrust less the longitudinal-force coefficient for power off) as a function of jet-pressure ratio. It is of interest to note that for the conditions shown, the net reverse thrust exceeded the net forward thrust and that this effect increased with increasing Mach number. This result is believed to be at least partly due to a combination of flow separation associated with the reverser efflux and separation stemming from compressibility effects.

As was the case for the lift characteristics, the effects of forward thrust on the pitching-moment characteristics were negligible compared to the effects of reverse thrust (figs. 4 through 9). The most pronounced effect of reverse thrust was to induce, at constant lift coefficient, a nose-up increment of pitching moment which became progressively larger with increasing jet-pressure ratio and Mach number. This result was opposite to the anticipated effects of the direct thrust forces. Use of the thrust reversers resulted in considerable reductions in the lift coefficients at which abrupt changes in the slopes of the pitching-moment

curves occurred. However, it should be noted that, at most Mach numbers, these lift coefficients were considerably larger than those required for normal cruising flight. The effect of reverse thrust on the slopes of the pitching-moment curves was small up to moderate lift coefficients. Figure 24 is representative of this effect and indicates that the largest slope changes occurred at the higher Mach numbers and jet-pressure ratios. The data for the tail-off presented in figures 19 through 21 show similar effects of thrust reversal on pitching moment. Therefore, it would appear that the nose-up increment of pitching moment associated with thrust reversal is at least partly due to changes in wing lift distribution caused by the reverser efflux.

A 3 2 1

The pitching-moment increment due to the horizontal tail and the tail-effectiveness parameter, $\partial C_m/\partial i_t$, are shown as functions of angle of attack for several thrust conditions in figures 25 and 26, respectively. Generally, the effect of thrust reversal on tail effectiveness was small; this was also the case at low lift coefficients for the pitching-moment increment due to the horizontal tail. However, at higher angles of attack, reverse thrust caused moderate increases of the pitching-moment contribution of the tail. This effect probably accounts for some of the nose-up increment of pitching moment previously noted for conditions of reverse thrust.

The effects of diverting only about 50 percent of the jet tail-pipe efflux through the reversers are shown in figures 16 through 18. This test condition approached zero thrust and resulted in a comparatively small reverse-thrust increment which was almost independent of jet-pressure ratio. The effects of such reverser operation on the lift and pitching-moment characteristics of the model were similar to the effects of reverser operation with complete tail-pipe blockage but were of considerably smaller magnitude.

Effects of Mach Number

The variation of longitudinal-force coefficient with Mach number at a lift coefficient of 0.30 is shown in figure 27 for several thrust conditions. It was anticipated that the Mach number for longitudinal-force divergence would be decreased as a result of the separated flow over portions of the model immersed in the flow field from the reverser. However, this effect was not apparent, and the Mach number for drag divergence was not affected by operation of the thrust reverser. The effects of Mach number on the slopes of the lift and pitching-moment curves are presented in figure 28 also for a constant lift coefficient of 0.30 and several thrust conditions. Reverse thrust, as noted previously, caused significant reductions in the lift-curve slopes and increased the variation of lift-curve slope with Mach number. Also, reverse thrust had

only a small effect on the variation of the slopes of the pitching-moment curves with Mach number except at the highest test Mach number where moderately stabilizing slope changes occurred.

Effects of Thrust Reversal on the Buffet Characteristics of the Model

Relative buffeting as indicated by the fluctuating wing and tail bending moments, ΔBM, is shown for several Mach numbers in figures 29 through 34 for various conditions of forward and reverse thrust. Also shown in these figures are the average (steady-state) bending moments measured simultaneously with the fluctuating values. In general, over the relatively low-lift-coefficient range of interest for high-speed operation of the thrust reversers, the effect of thrust reversal on wing buffeting was small (figs. 29 through 31). Thrust reversal usually resulted in small increases in the fluctuating bending moments at the higher pressure ratios and Mach numbers. Also, for these conditions, the abrupt increase in fluctuating bending moment associated with buffet boundaries usually occurred at lower lift coefficients than was the case with forward thrust. This effect of thrust reversal is probably associated with the reductions in lift-curve slope described previously. It is of interest to note that the fluctuating bending moment of the wing root usually did not exceed 10 percent of the steady-state bending moment, and that this value is probably higher than would be the case for a full-scale airplane having the same configuration because of differences in the resonance characteristics of the model and full-scale wings (see ref. 2).

Figures 32 through 34 show the effects of thrust reversal on the relative buffeting of the horizontal tail. The largest of these effects was the reduction in the model lift coefficient at which abrupt increases in fluctuating bending moment occurred. As was the case for the wing, these lift coefficients were considerably higher than those of interest for thrust reverser operation at high speeds.

Summation of the Effects of Thrust Reversal on the Characteristics of a Hypothetical Airplane

The effects of thrust reversal on the maximum rate of descent at several constant Mach numbers and on some of the longitudinal characteristics of a hypothetical jet-transport airplane were estimated from the test results and are shown in figures 35 and 36, respectively. It was assumed that the airplane weighed 200,000 pounds, had a wing area of 2750 square feet, and was initially operating at 30,000 feet with the jet-pressure ratios required for level flight at that altitude.

Approximate rates of descent were calculated from the following relation:

$$\frac{dh}{dt} = \frac{V_\infty(\text{thrust-drag})}{\text{gross weight}}$$

The maximum rates of descent possible at several constant Mach numbers for the power-off condition are compared in figure 35 with the rates of descent available with thrust reversal. Use of the reverser with complete tail-pipe blockage permitted the initial rate of descent from an altitude of 30,000 feet and at a constant Mach number of 0.80 to be increased from about 5200 feet per minute to about 12,800 feet per minute. In an emergency situation, this could represent the difference between a safe controlled descent at high speed and incapacitation of the occupants of the airplane from anoxia (see ref. 5).

Figure 36 shows some of the effects of thrust reversal on the longitudinal characteristics of the hypothetical jet-transport airplane making a high-speed descent. Operation of the reverser at a Mach number of 0.80 and at an initial altitude of 30,000 feet with complete tail-pipe blockage and the pressure ratios normally required for level flight resulted in a small stabilizing movement of the aerodynamic center (from about 56-percent $\bar{c}$ to about 58-percent $\bar{c}$) and about a 1° increase in the horizontal-tail incidence required for trim.

CONCLUSIONS

A wind-tunnel investigation has been made to evaluate the effects of thrust reversal upon the longitudinal and buffeting characteristics of a hypothetical jet-transport airplane configuration at relatively high speeds. The Mach number range was from 0.40 to 0.86. The following conclusions were indicated:

1. Thrust reversal can be used as a very effective method of speed control for jet-transport airplanes making steep, relatively rapid descents from operational altitudes. Use of thrust reversers can more than double the cruise drag of such aircraft and, at a constant Mach number of about 0.80, will permit the initial rate of descent from cruising altitudes to be increased from about 5000 feet per minute to over 12,000 feet per minute.

2. Thrust reversal had only small effect on the longitudinal stability and trim characteristics of the model, at least, at the lift coefficients required for rapid descents by jet-transport aircraft. Operation of the reversers at a Mach number of 0.80 and an assumed initial altitude of 30,000 feet with complete tail-pipe blockage and at jet-pressure ratios

normally required for level flight resulted in a small stabilizing movement of the aerodynamic center corresponding to about 2 percent of the mean aerodynamic chord and about a 1^{o} increase in the horizontal-tail incidence required for trim.

3. Reverse thrust resulted in reductions in lift-curve slope and reduced the lift coefficients at which static-longitudinal instability occurred. However, these lift coefficients were usually considerably higher than the lift coefficients of interest for reverser operation at high speeds.

4. The effects of thrust reversal on the buffeting characteristics of both the wing and tail of the model were small. At the relatively low lift coefficients associated with the steep, high-speed descents these effects could be neglected.

A
3
2
1

Ames Research Center
National Aeronautics and Space Administration
Moffett Field, Calif., Nov. 16, 1959

REFERENCES

1. Henzel, James G., Jr., and McArdle, Jack G.: Preliminary Performance Data of Several Tail-Pipe-Cascade-Type Model Thrust Reversers. NACA RM E55F09, 1955.

2. Sutton, Fred B., and Lautenberger, J. Walter, Jr.: A Buffet Investigation at High Subsonic Speeds of Several Wing-Fuselage-Tail Combinations Having Sweptback Wings with NACA 64A Thickness Distributions, Fences, a Leading-Edge Extension, and Body Contouring. NACA RM A57F06a, 1957.

3. Herriot, John G.: Blockage Corrections for Three-Dimensional-Flow Closed-Throat Wind Tunnels, With Consideration of the Effect of Compressibility. NACA Rep. 995, 1950. (Supersedes NACA RM A7B28)

4. Sivells, James C., and Salmi, Rachel M.: Jet-Boundary Corrections for Complete and Semispan Swept Wings in Closed Circular Wind Tunnels. NACA TN 2454, 1951.

5. Butchart, Stanley P., Fischel, Jack, Tremant, Robert A., and Robinson, Glenn H.: Flight Studies of Problems Pertinent to High-Speed Operation of Jet Transports. NASA MEMO 3-2-59H, 1959.

TABLE I.- MODEL COORDINATES

(a) Coordinates of fuselage			
Distance from nose, in.	Radius, in.	Distance from nose, in.	Radius, in.
0	0	40.00	5.000
.50	.934	50.00	5.000
1.00	1.314	59.00	5.000
2.00	1.842	65.00	4.960
4.00	2.557	71.00	4.834
8.00	3.477	77.00	4.609
12.00	4.080	83.00	4.266
16.00	4.497	89.00	3.767
20.00	4.775	95.00	3.028
24.00	4.939	105.00	1.514
28.44	5.000	115.00	0
(b) Coordinates of nacelles			
0	0	7.421	1.618
.257	.336	9.032	1.606
.482	.507	10.832	1.543
.932	.760	12.632	1.430
1.832	1.088	14.432	1.365
3.632	1.436	15.064	1.365
5.432	1.585	17.893	1.365
7.021	1.618	18.697	1.365

TABLE II.- CORRECTIONS TO DATA

(a) Corrections for constriction effects

Corrected Mach number	Uncorrected Mach number	$\frac{q_{corrected}}{q_{uncorrected}}$
0.40	0.399	1.005
.60	.597	1.006
.70	.696	1.008
.80	.792	1.012
.83	.820	1.014
.86	.847	1.017

(b) Corrections for tunnel-wall interference

$\Delta\alpha = 0.460C_L$

$\Delta C_D = 0.0069C_L^2$

$\Delta C_{m_{tail\ off}} = K_1 C_{L_{tail\ off}}$

$\Delta C_{m_{tail\ on}} = K_1 C_{L_{tail\ off}} - \left[(K_2 C_{L_{tail\ off}} - \Delta\alpha)\frac{\partial C_m}{\partial i_t}\right]$

M	K_1	K_2
0.40	0.0024	0.73
.60	.0028	.76
.70	.0035	.79
.80	.0044	.83
.83	.0048	.84
.86	.0052	.85

All dimensions in inches unless otherwise specified.
Fuselage coordinates given in table I.
Wing dihedral angle, 5°.
See figure 1(b) for vertical location of nacelles.

$S = 6.00\ \text{Ft.}^2$

$\lambda = 0.30$

$A = 7.00$

$\bar{c} = 17.231$

$\bar{c} = 10.181$

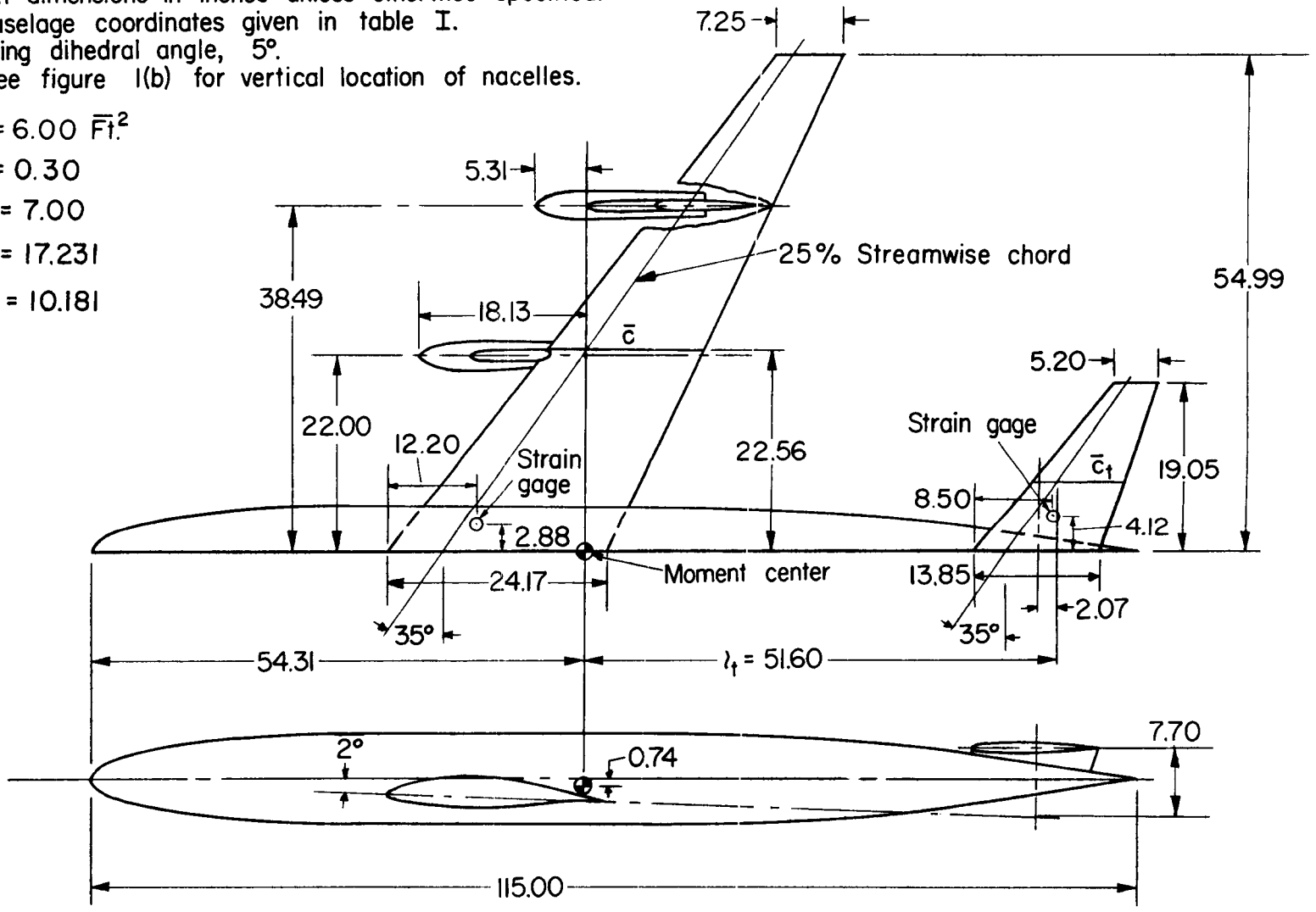

(a) General arrangement.

Figure 1.- Geometry of model.

All dimensions in inches unless otherwise specified.

Nacelle coordinates given in table I.

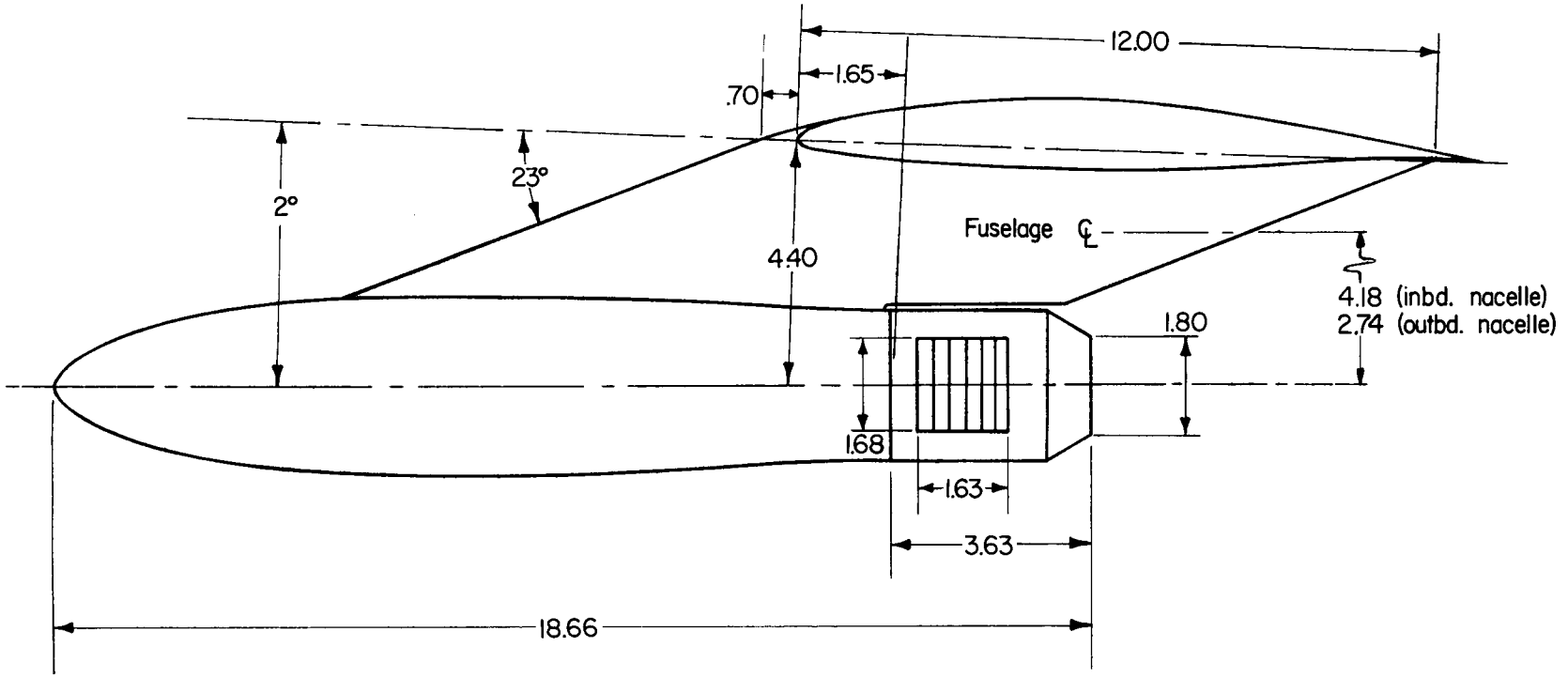

(b) Nacelle and strut details.

Figure 1.- Continued.

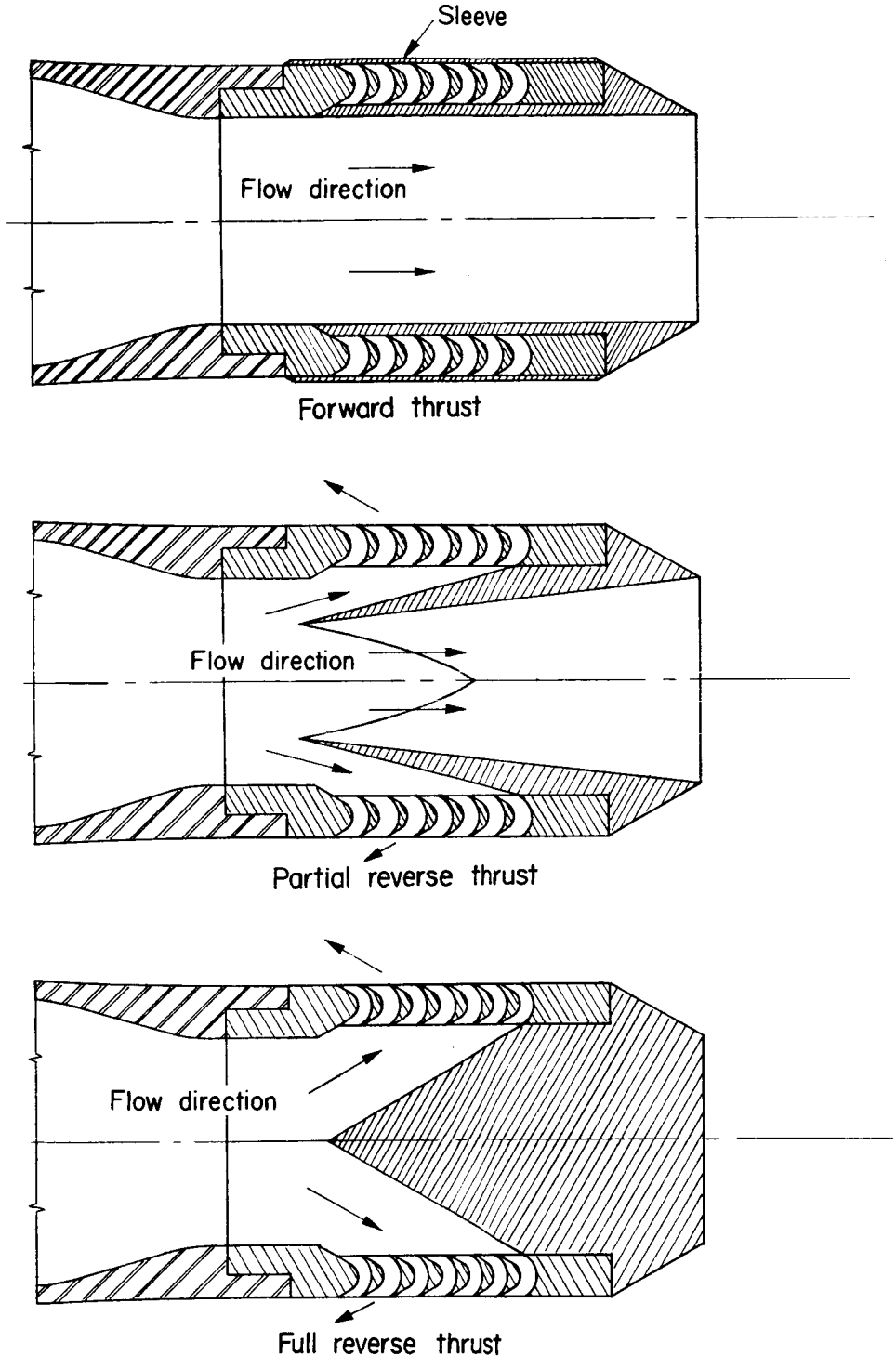

(c) Reverser details.

Figure 1.- Concluded.

A-24456

Figure 2.- Model in the wind tunnel.

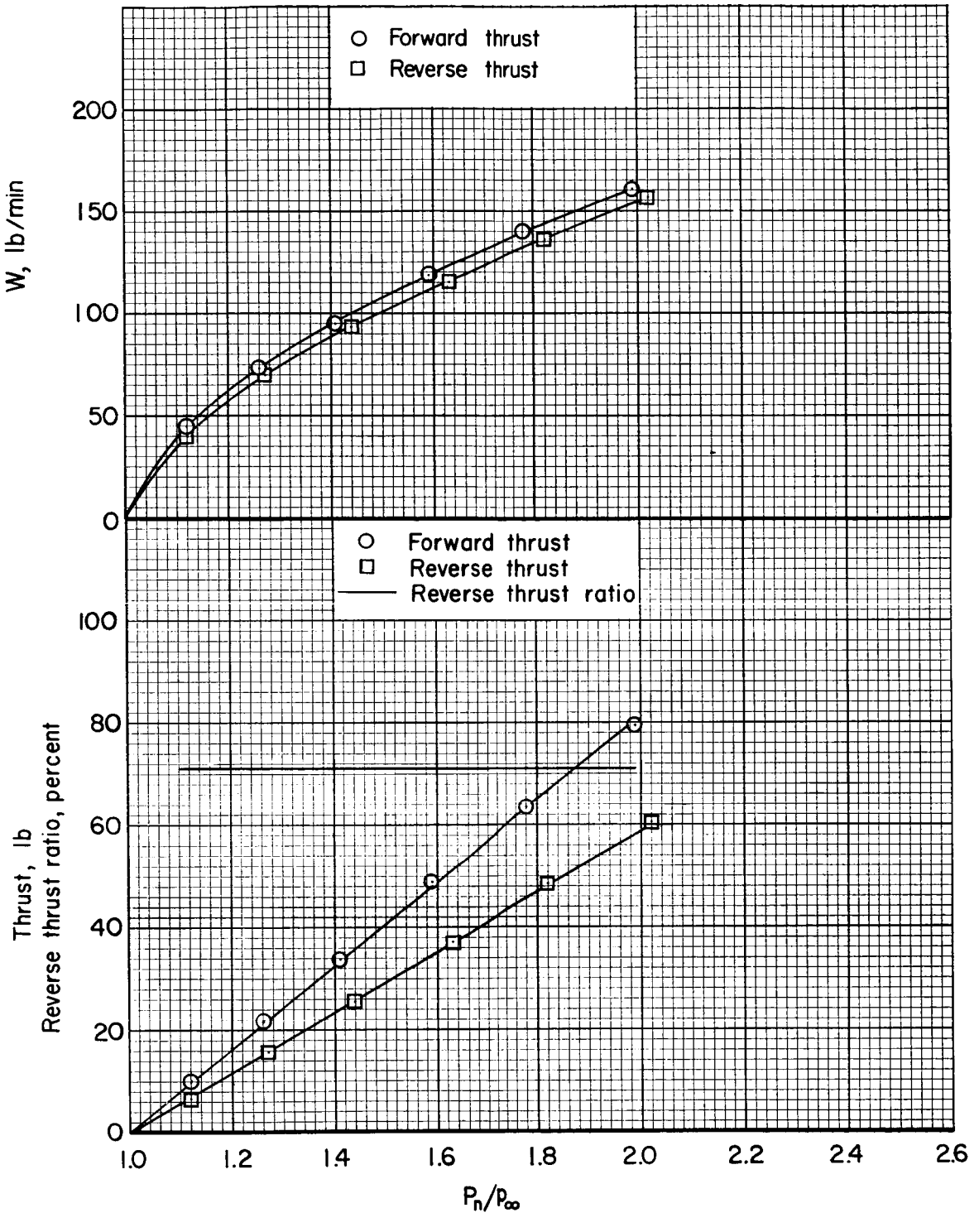

Figure 3.- Forward and full-reverse thrust characteristics of the model; M = 0.

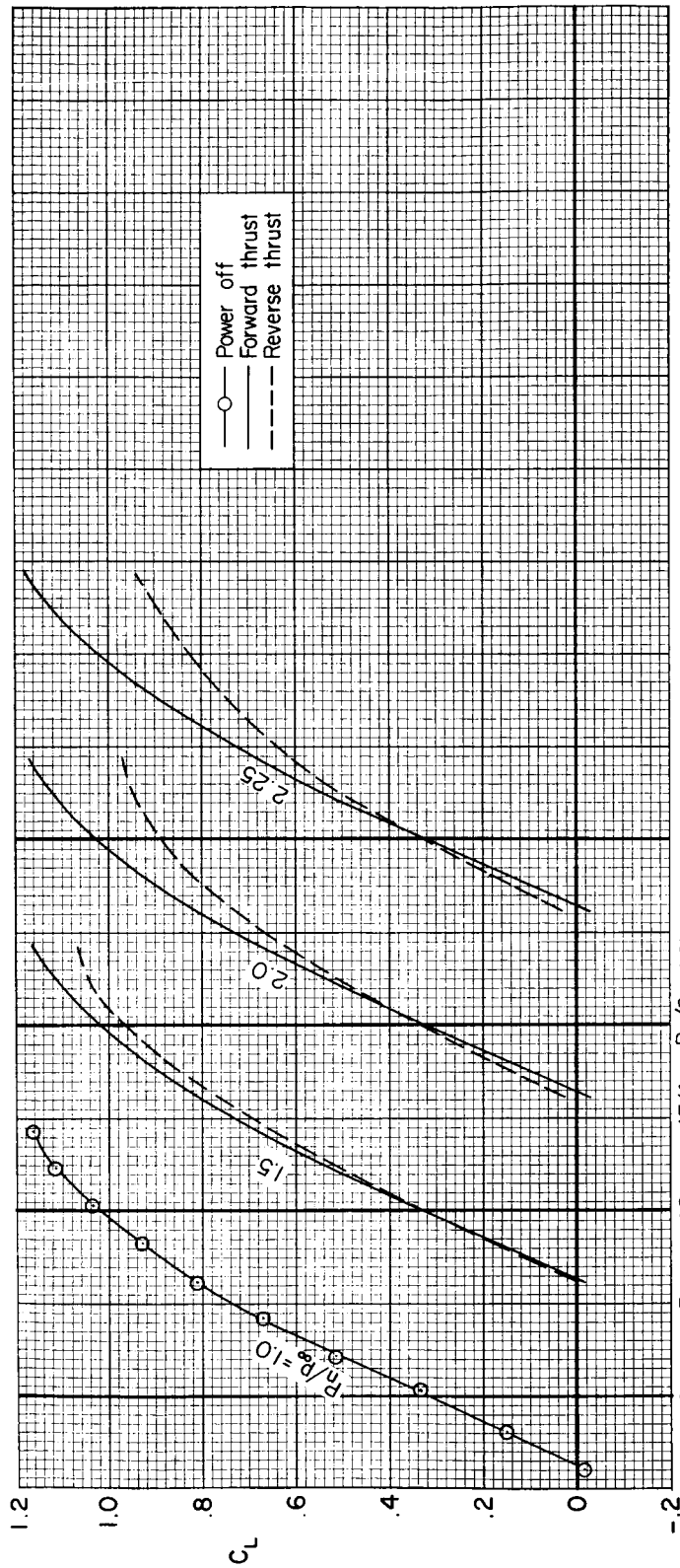

(a) C_L vs. α

Figure 4.- The effect of forward and reverse thrust on the longitudinal characteristics of the model; $i_t = -2^o$, M = 0.40.

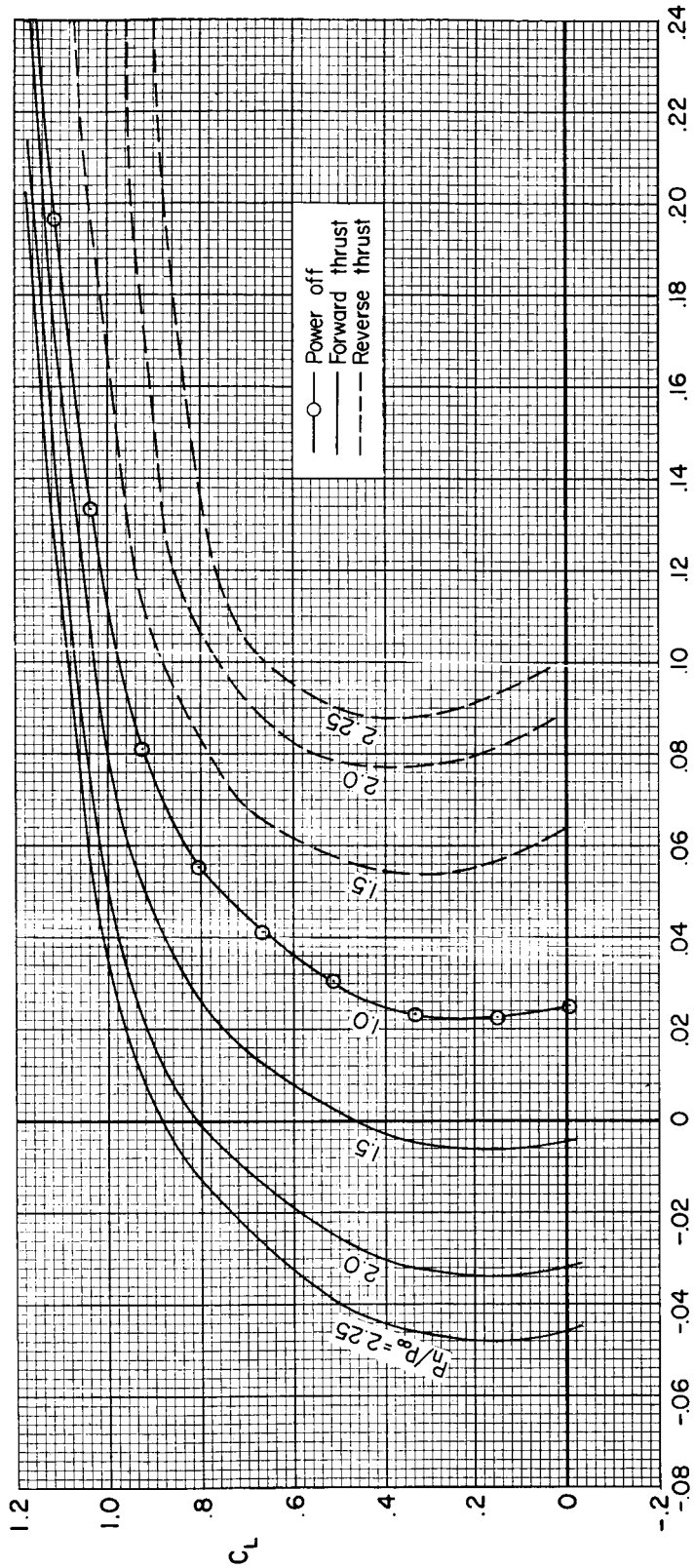

(b) C_X vs. C_L

Figure 4.- Continued.

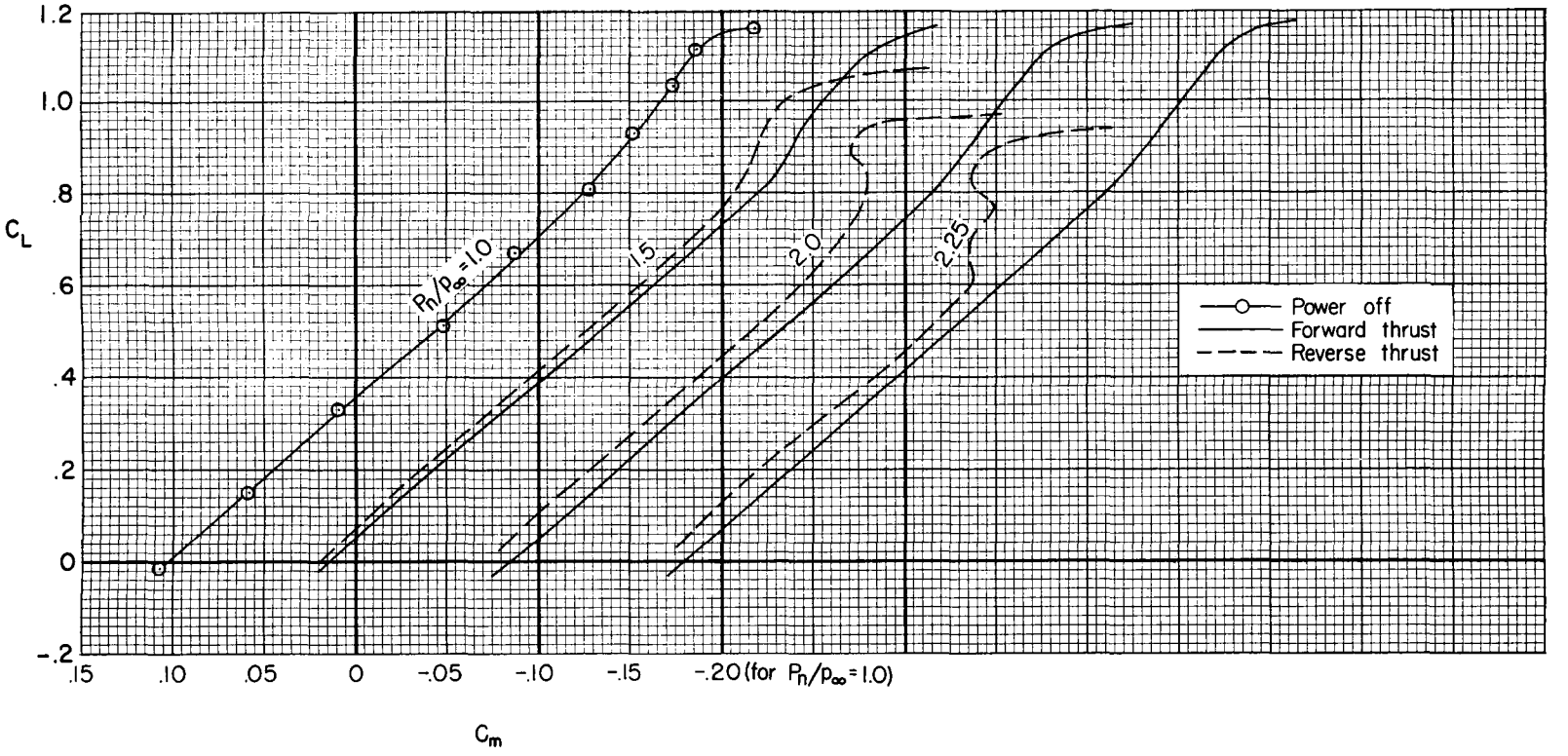

(c) C_m vs. C_L

Figure 4.- Concluded.

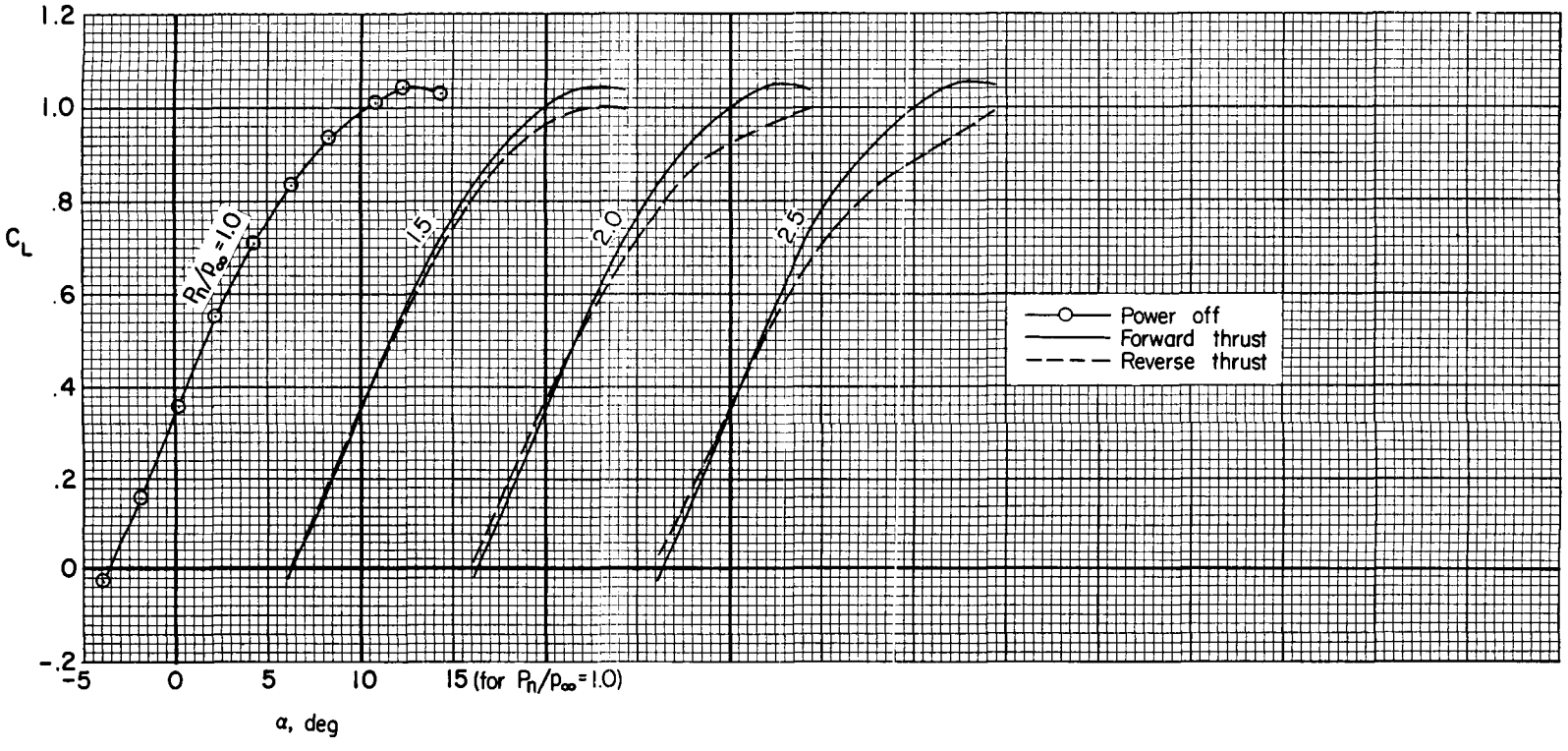

(a) C_L vs. α

Figure 5.- The effect of forward and reverse thrust on the longitudinal characteristics of the model; $i_t = -2^\circ$, M = 0.60.

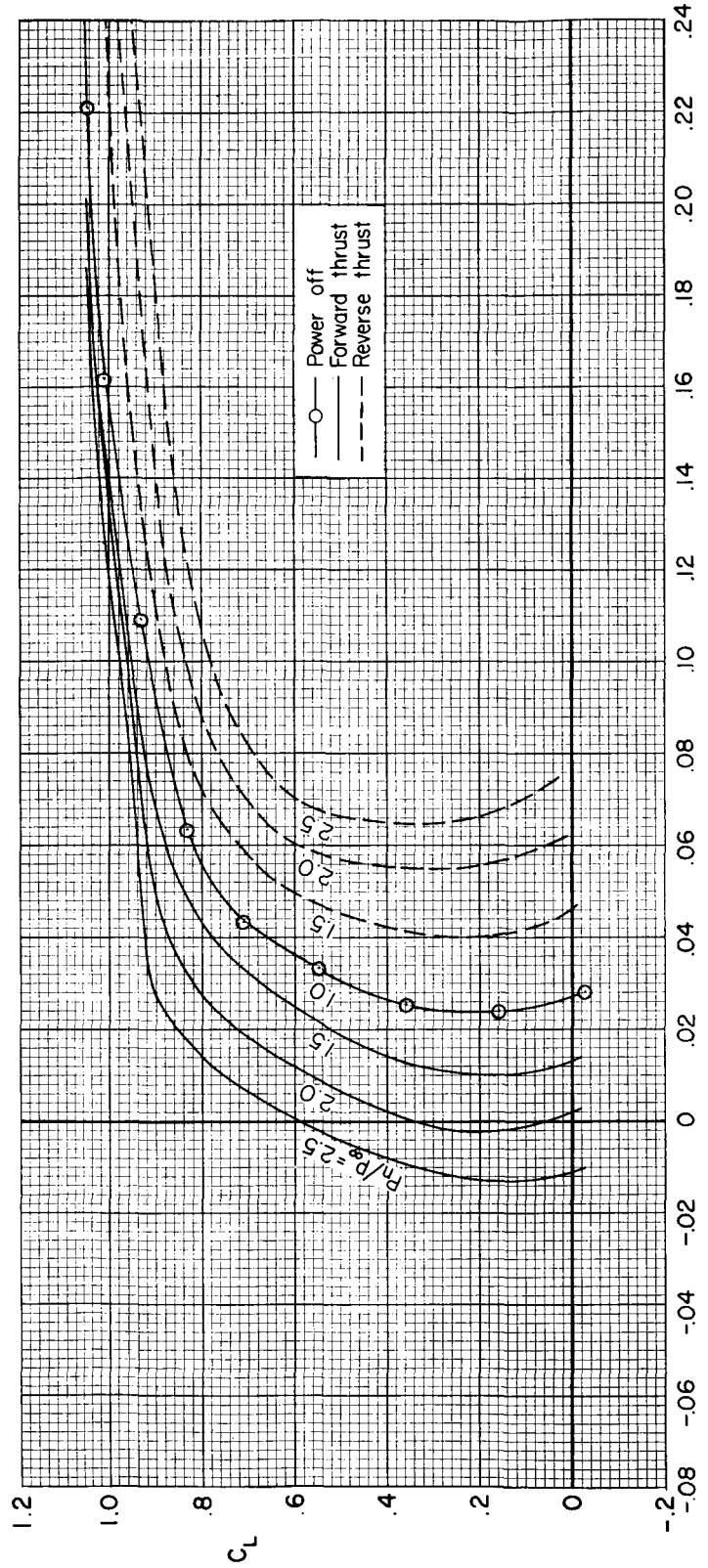

(b) C_X vs. C_L

Figure 5.- Continued.

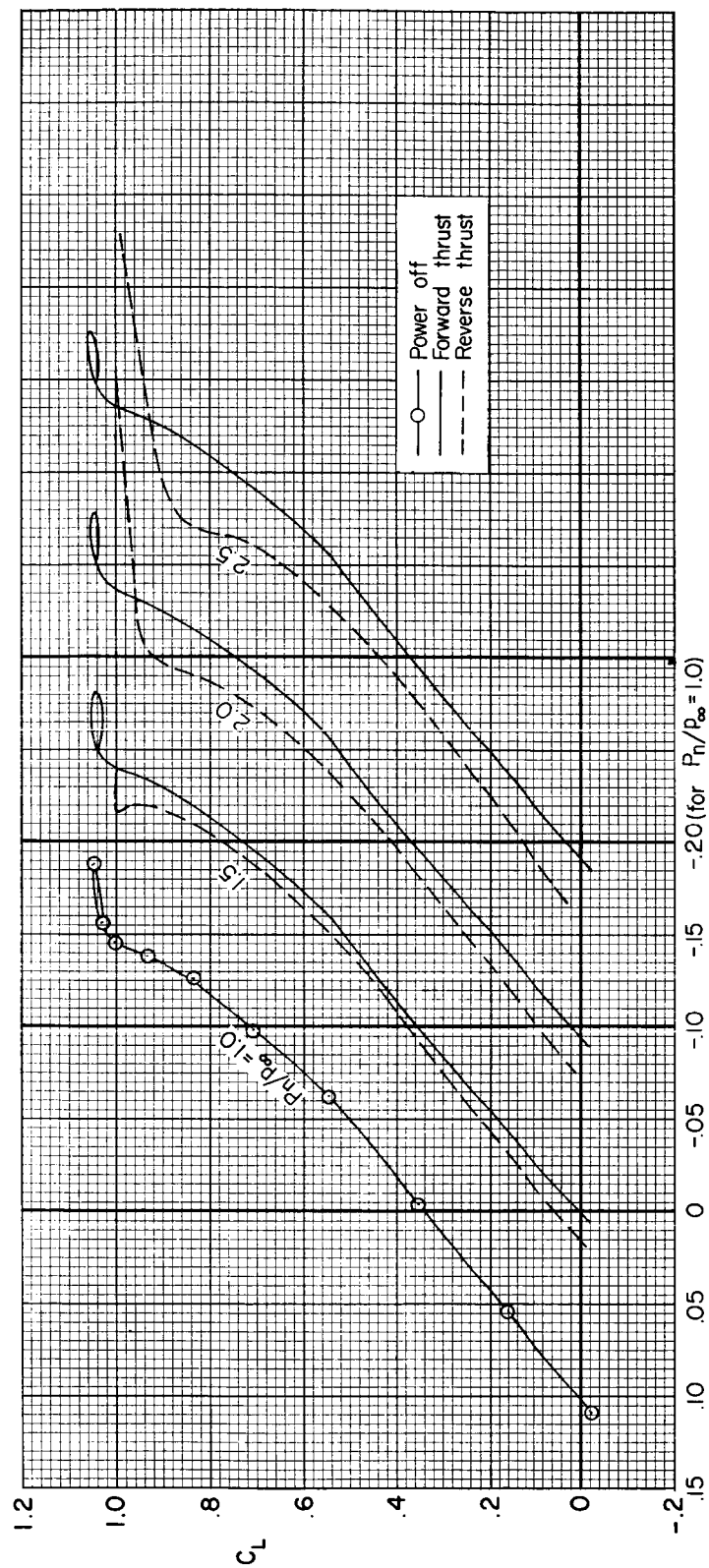

(c) C_m vs. C_L

Figure 5.- Concluded.

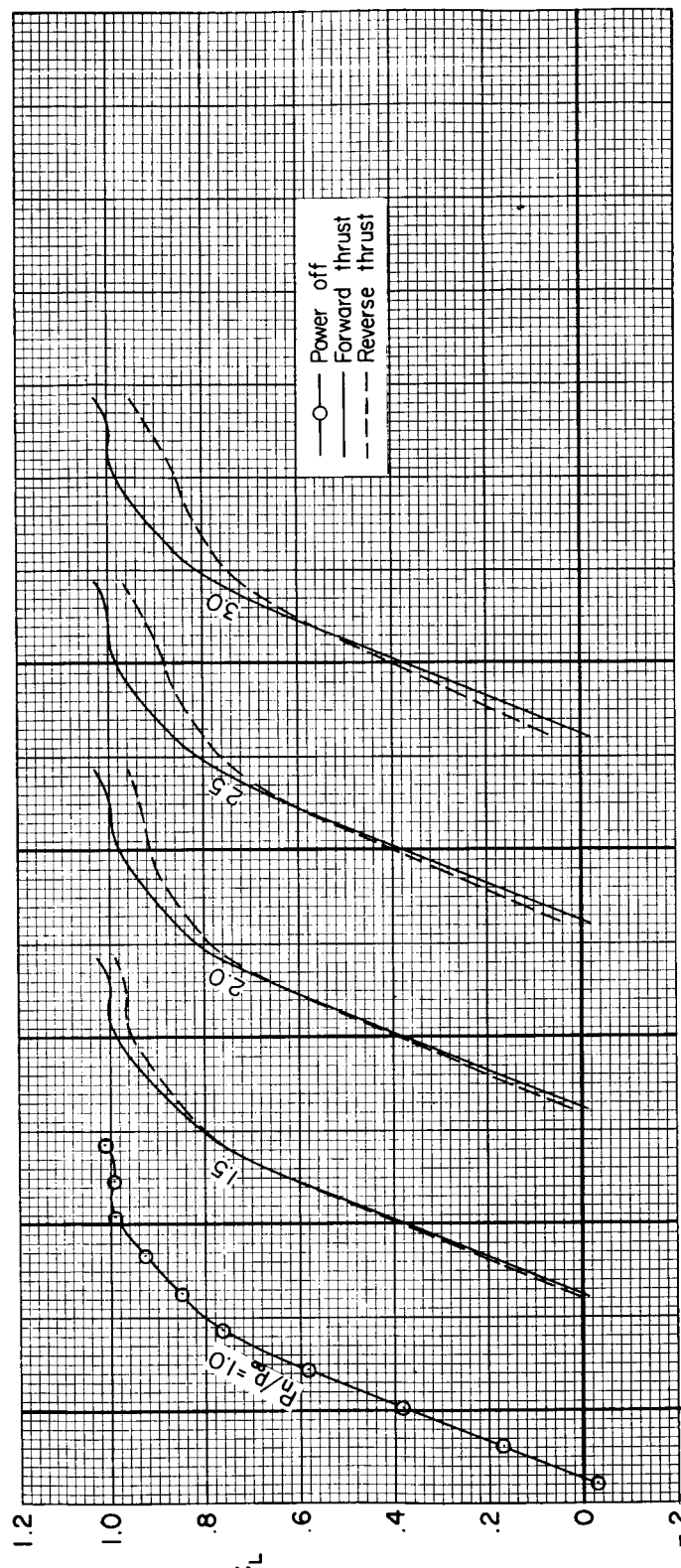

(a) C_L vs. α

Figure 6.- The effect of forward and reverse thrust on the longitudinal characteristics of the model; $i_t = -2^o$, M = 0.70.

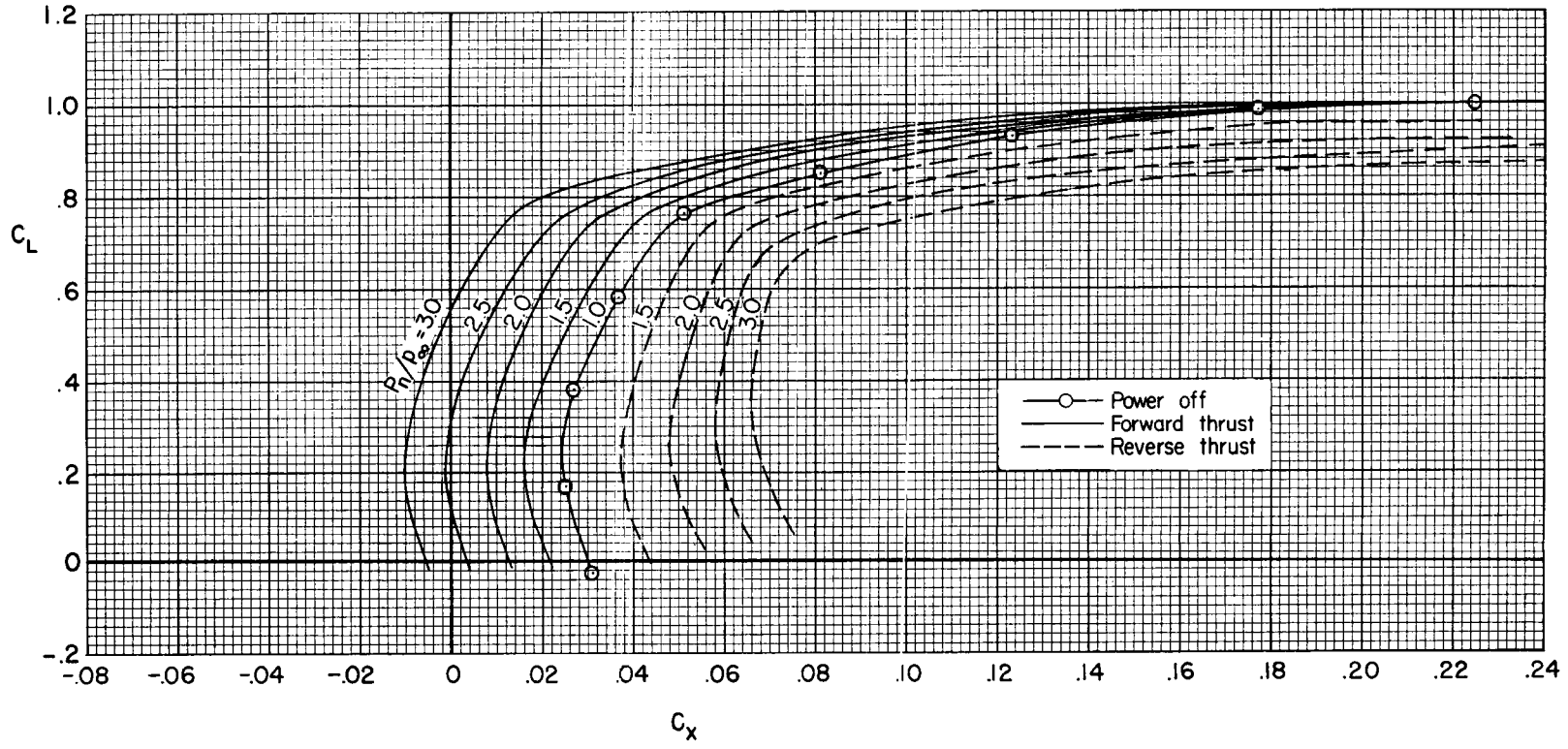

(b) C_X vs. C_L

Figure 6.- Continued.

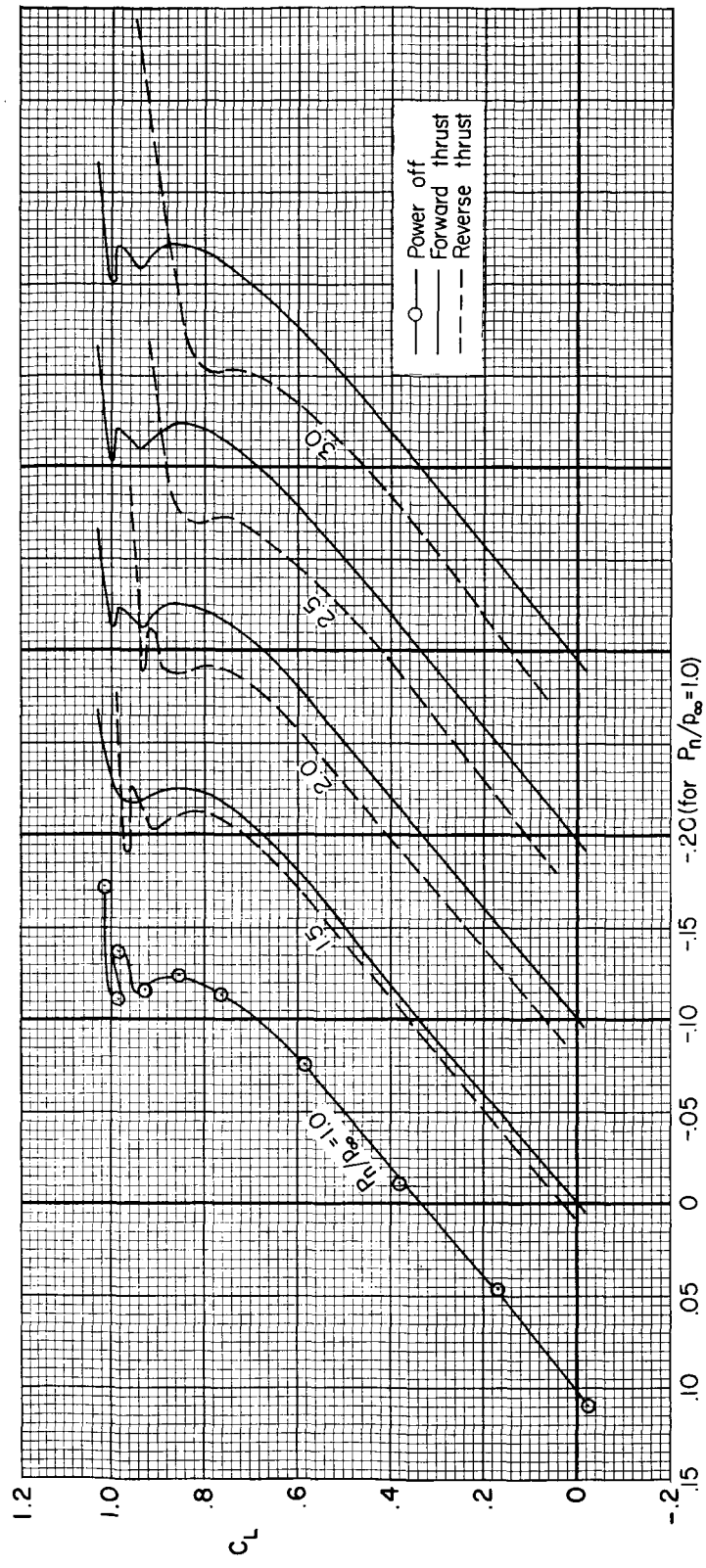

(c) C_m vs. C_L

Figure 6.- Concluded.

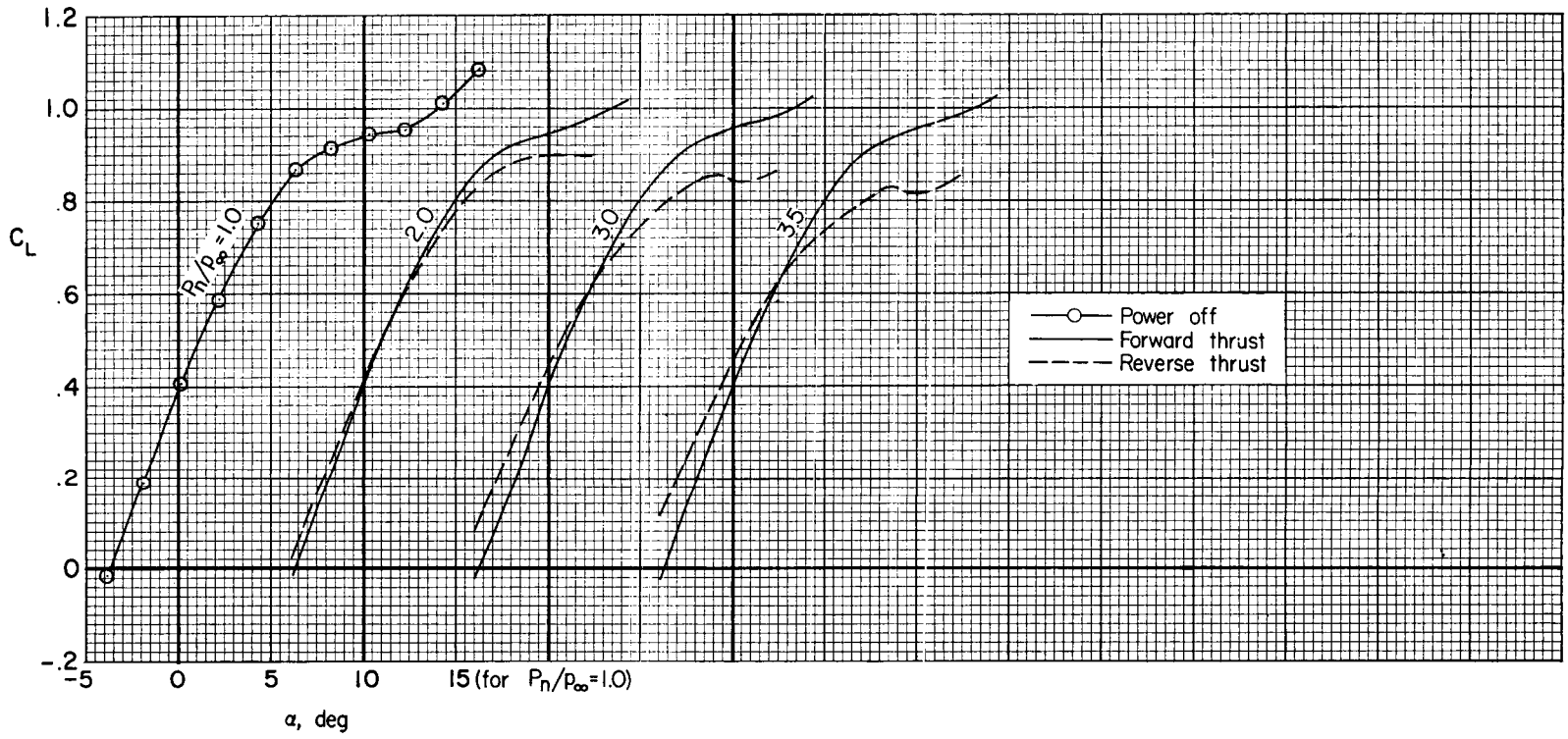

(a) C_L vs. α

Figure 7.- The effect of forward and reverse thrust on the longitudinal characteristics of the model; $i_t = -2^\circ$, M = 0.80.

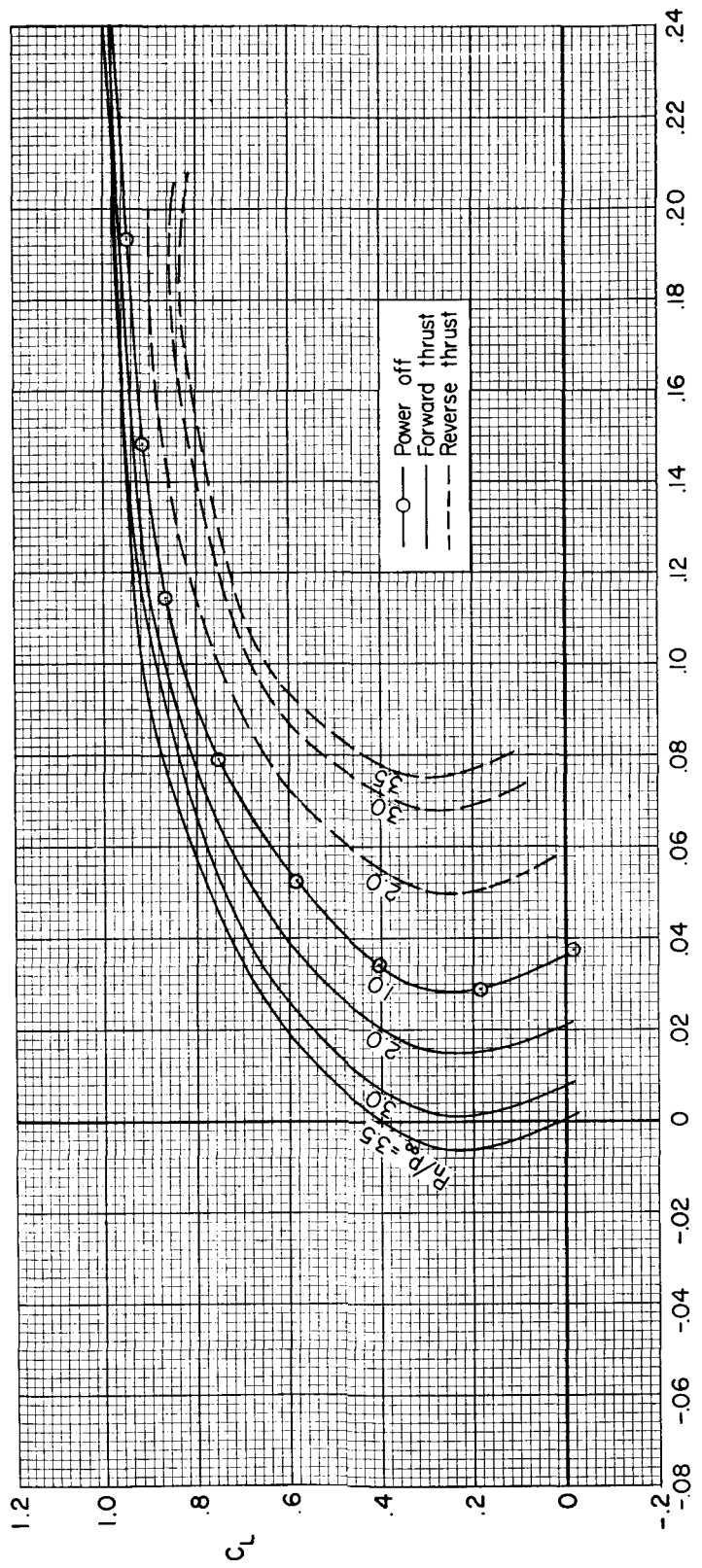

(b) C_X vs. C_L

Figure 7.- Continued.

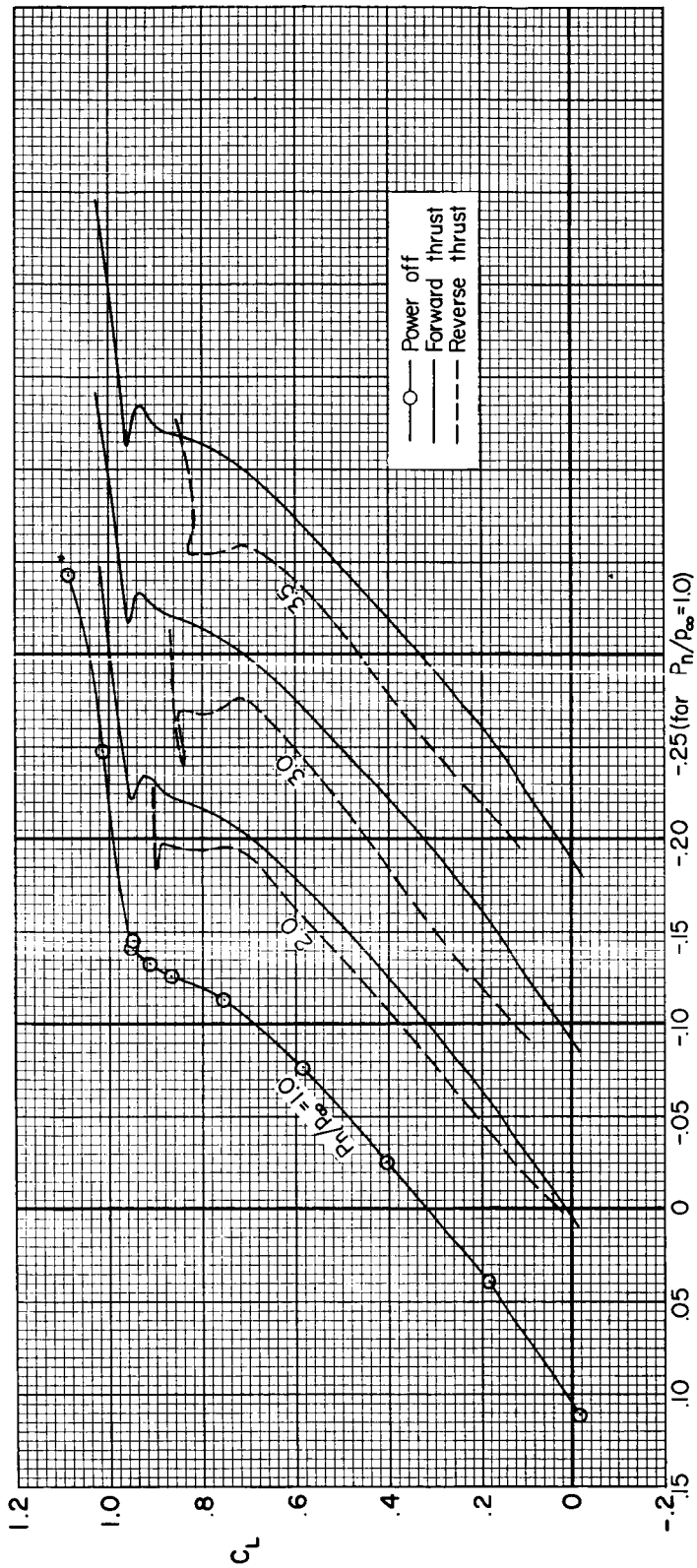

(c) C_m vs. C_L

Figure 7.- Concluded.

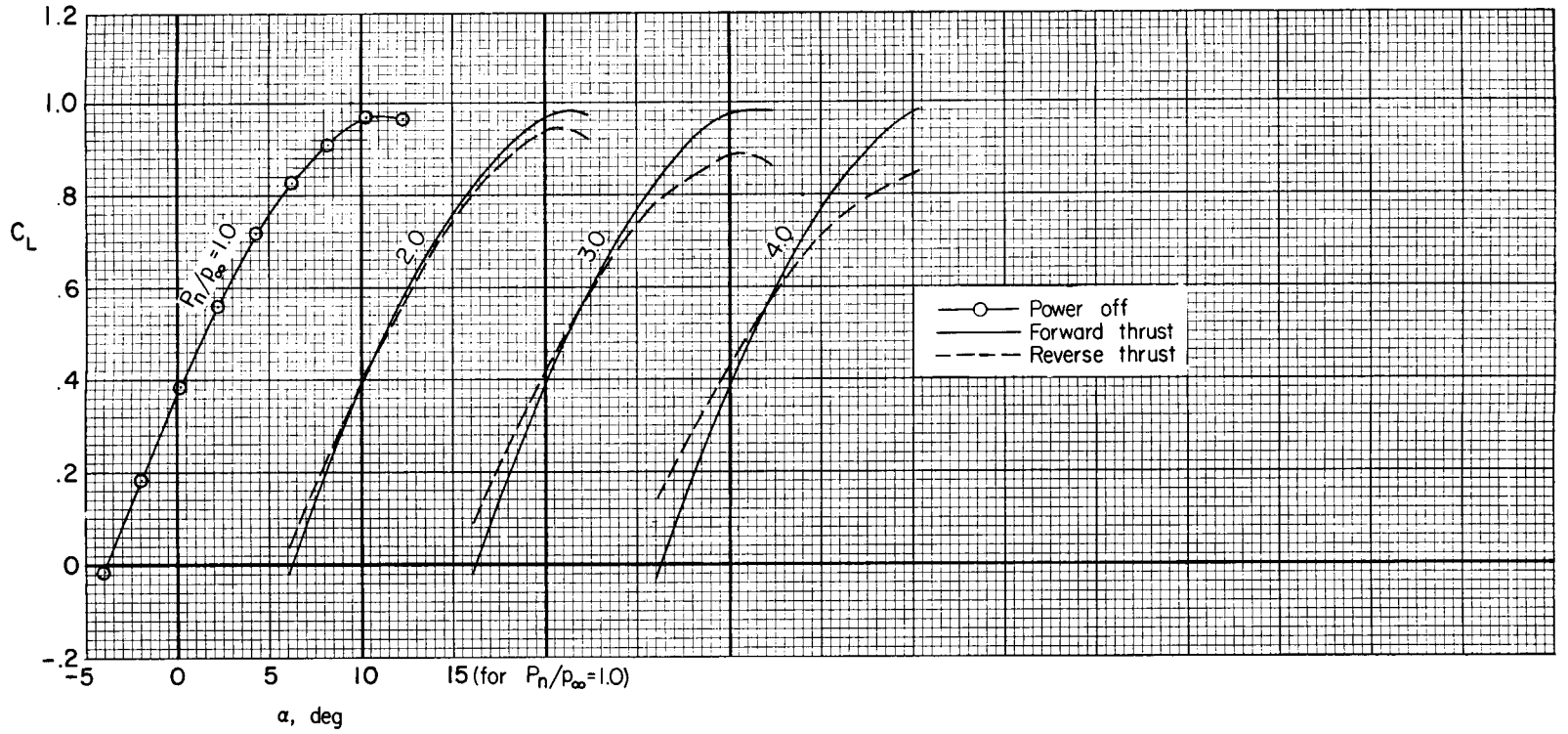

(a) C_L vs. α

Figure 8.- The effect of forward and reverse thrust on the longitudinal characteristics of the model; $i_t = -2^\circ$, M = 0.83.

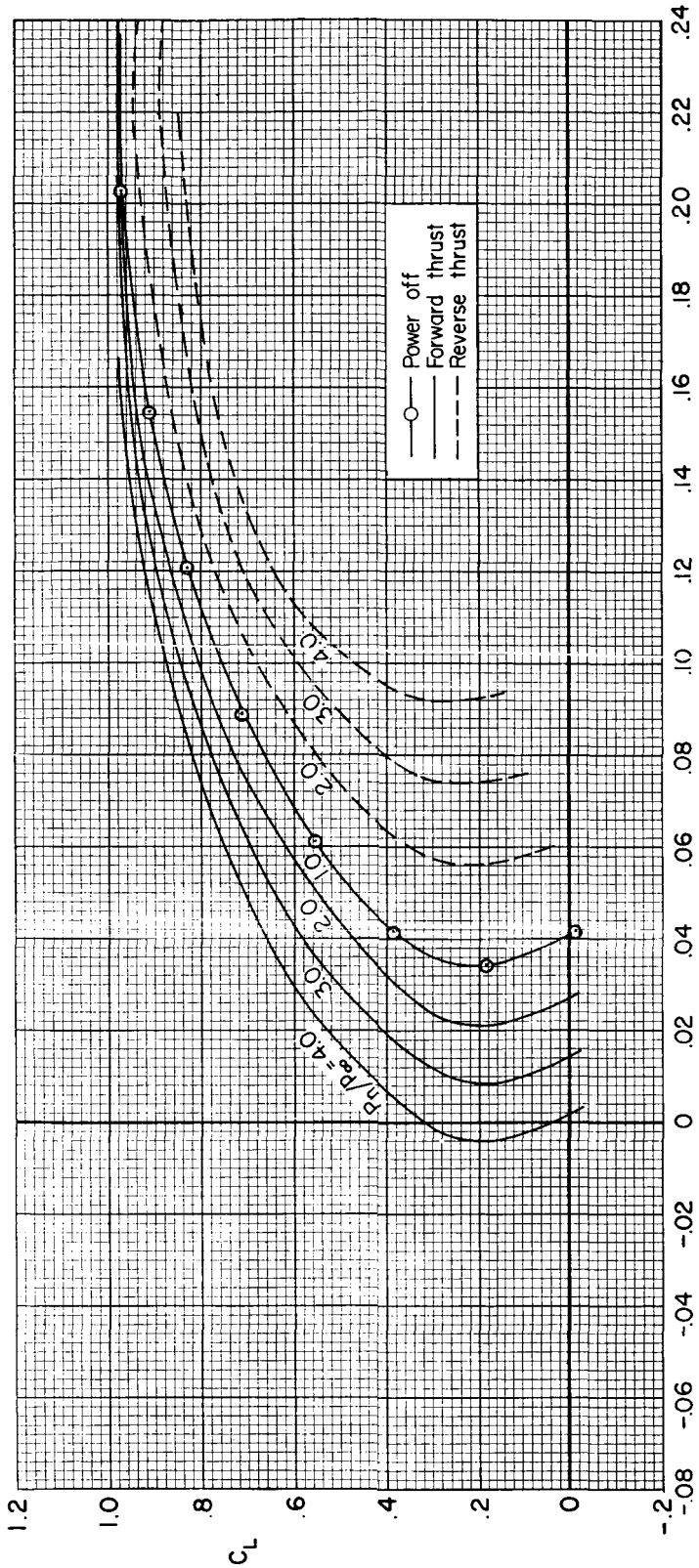

(b) C_X vs. C_L

Figure 8.- Continued.

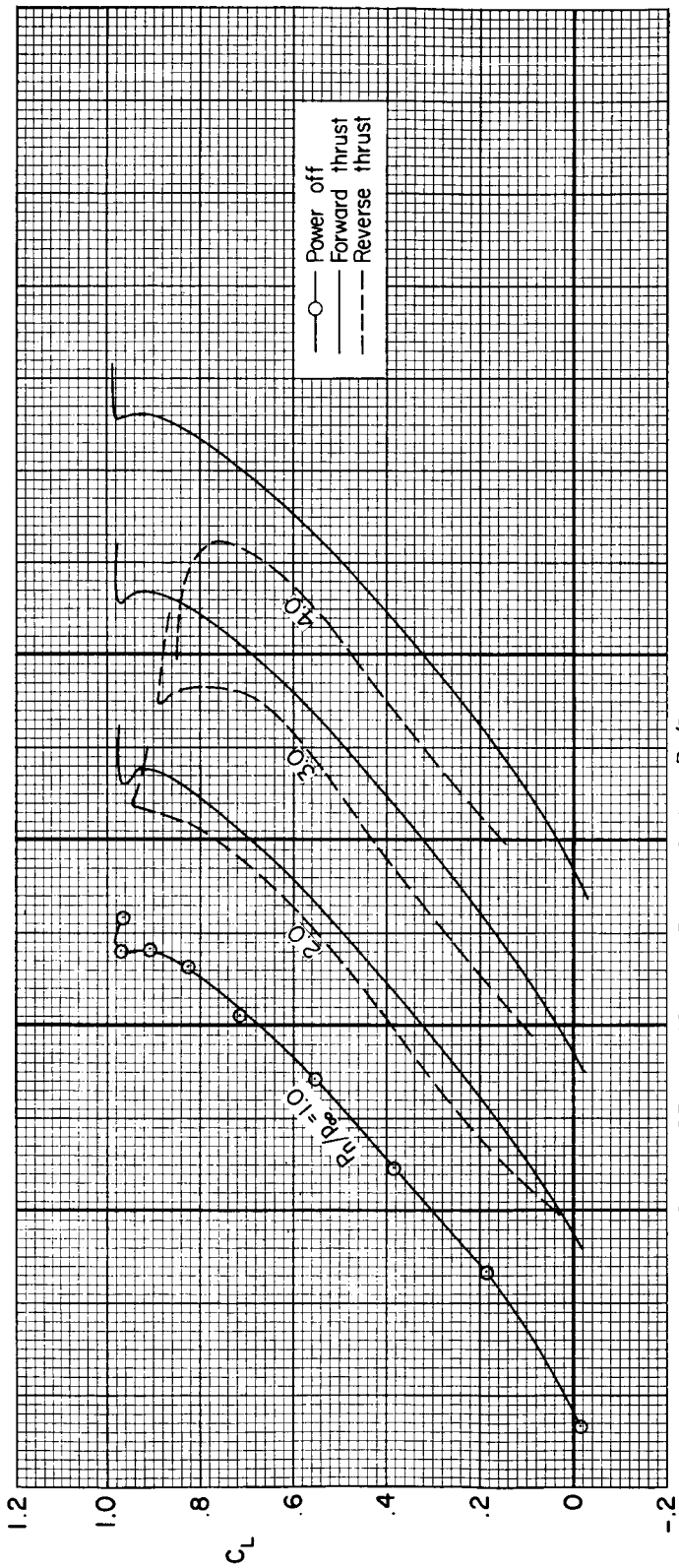

(c) C_m vs. C_L

Figure 8.- Concluded.

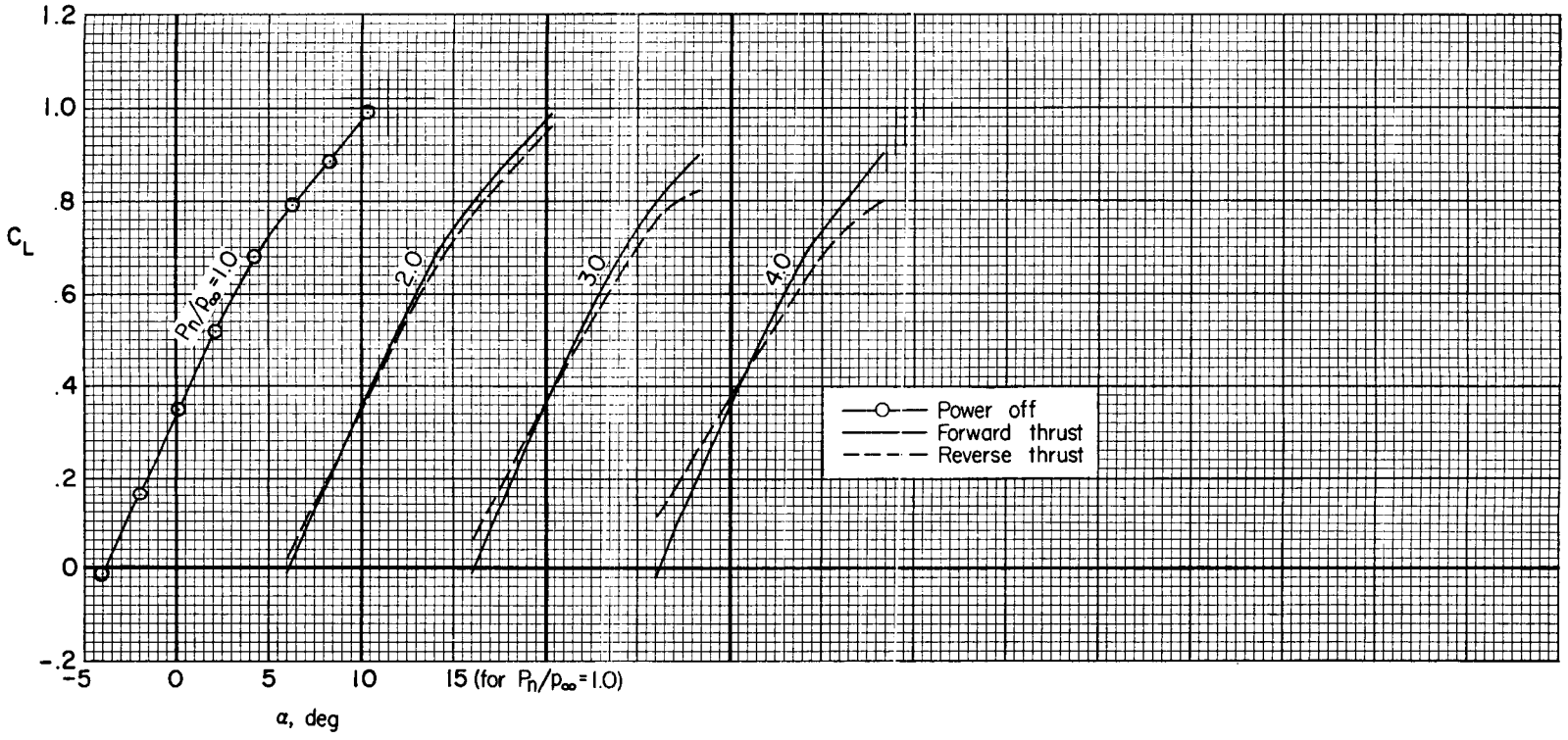

(a) C_L vs. α

Figure 9.- The effect of forward and reverse thrust on the longitudinal characteristics of the model; $i_t = -2^\circ$, M = 0.86.

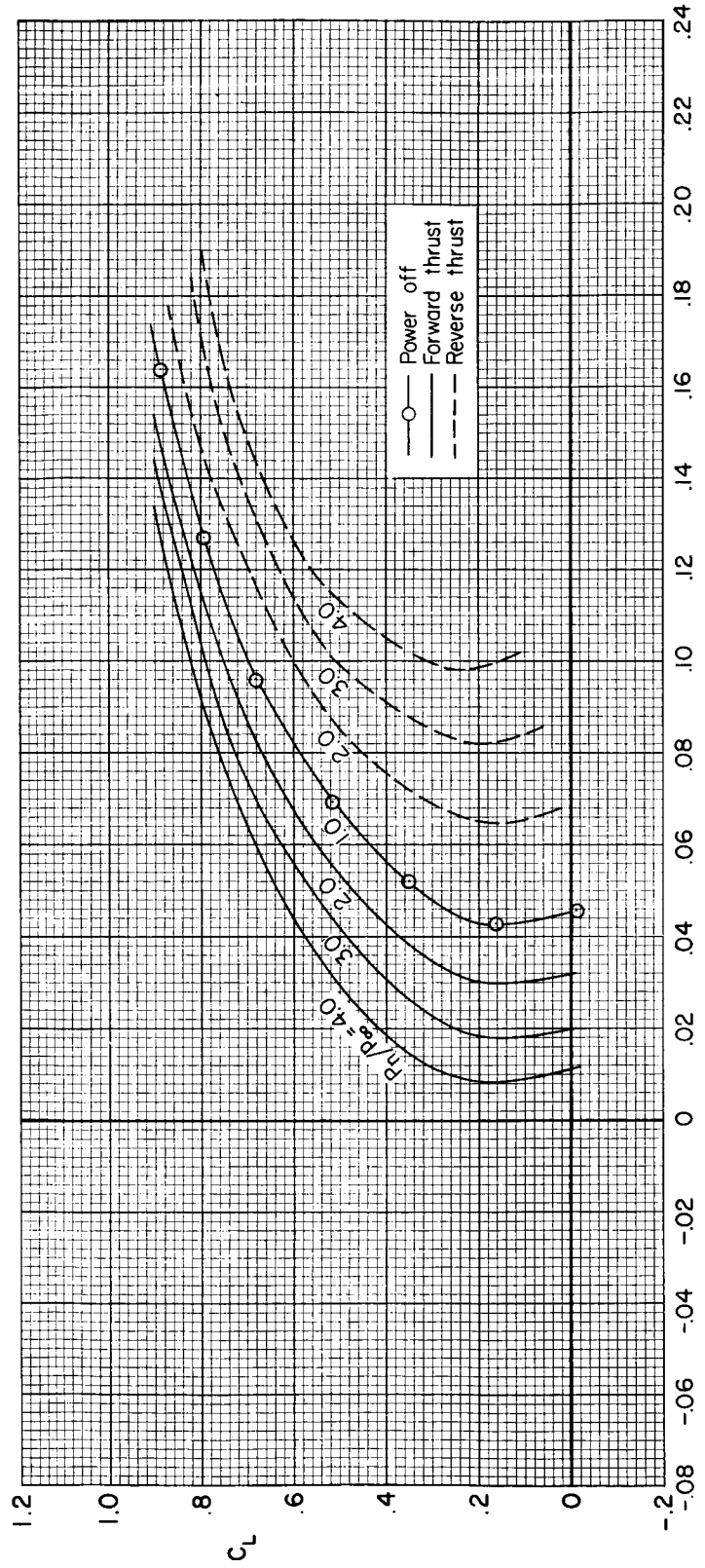

(b) C_X vs. C_L

Figure 9.- Continued.

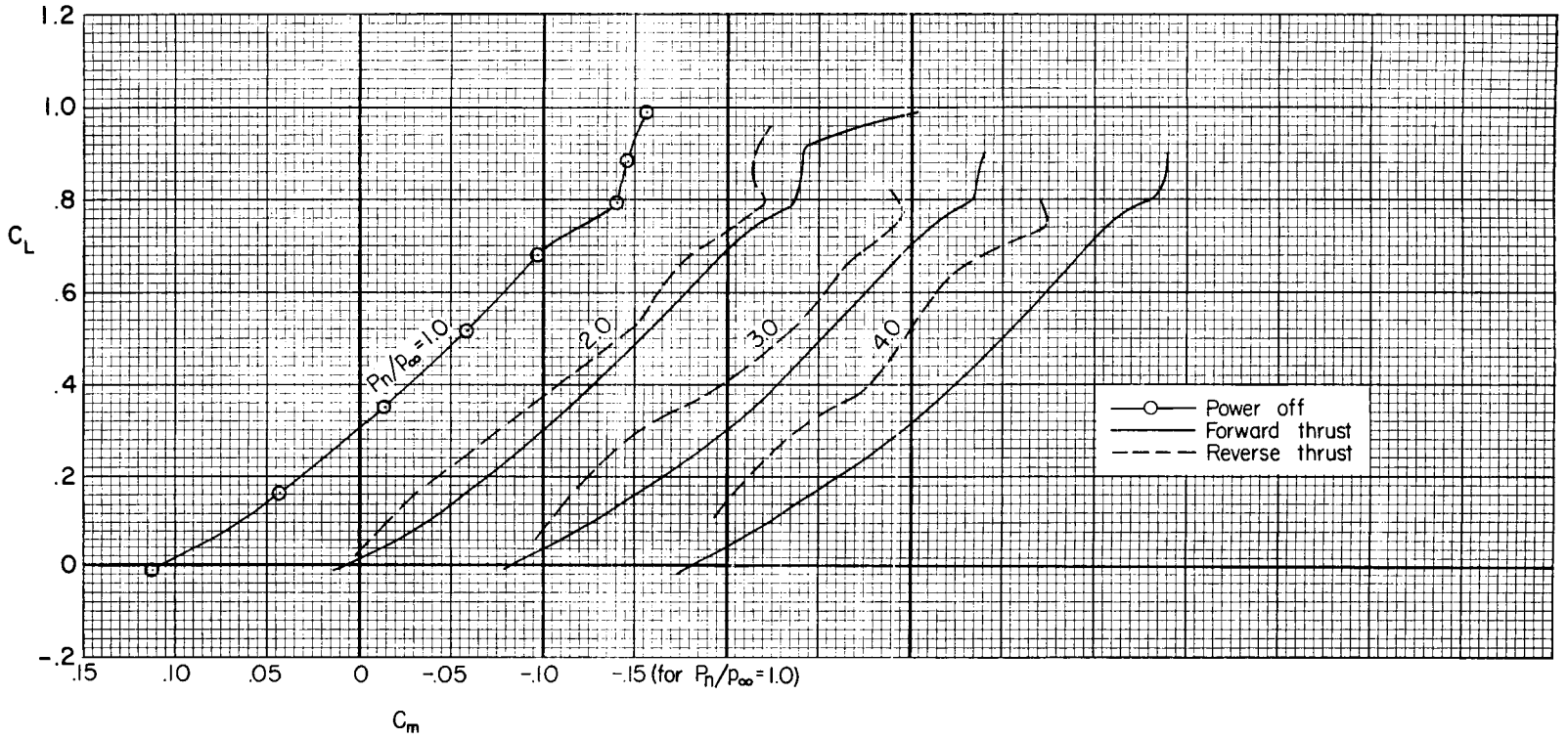

(c) C_m vs. C_L

Figure 9.- Concluded.

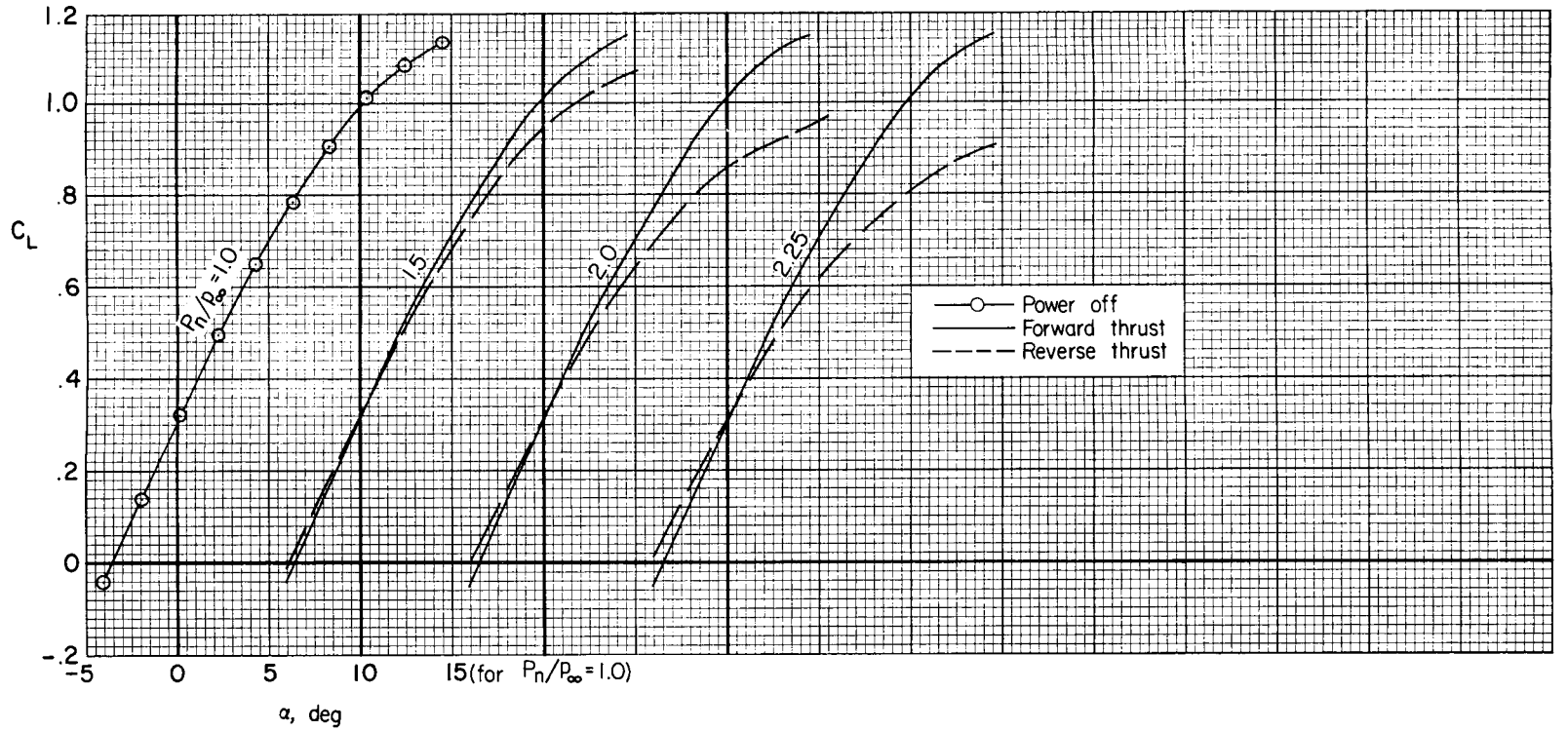

(a) C_L vs. α

Figure 10.- The effect of forward and reverse thrust on the longitudinal characteristics of the model; $i_t = -4^o$, M = 0.40.

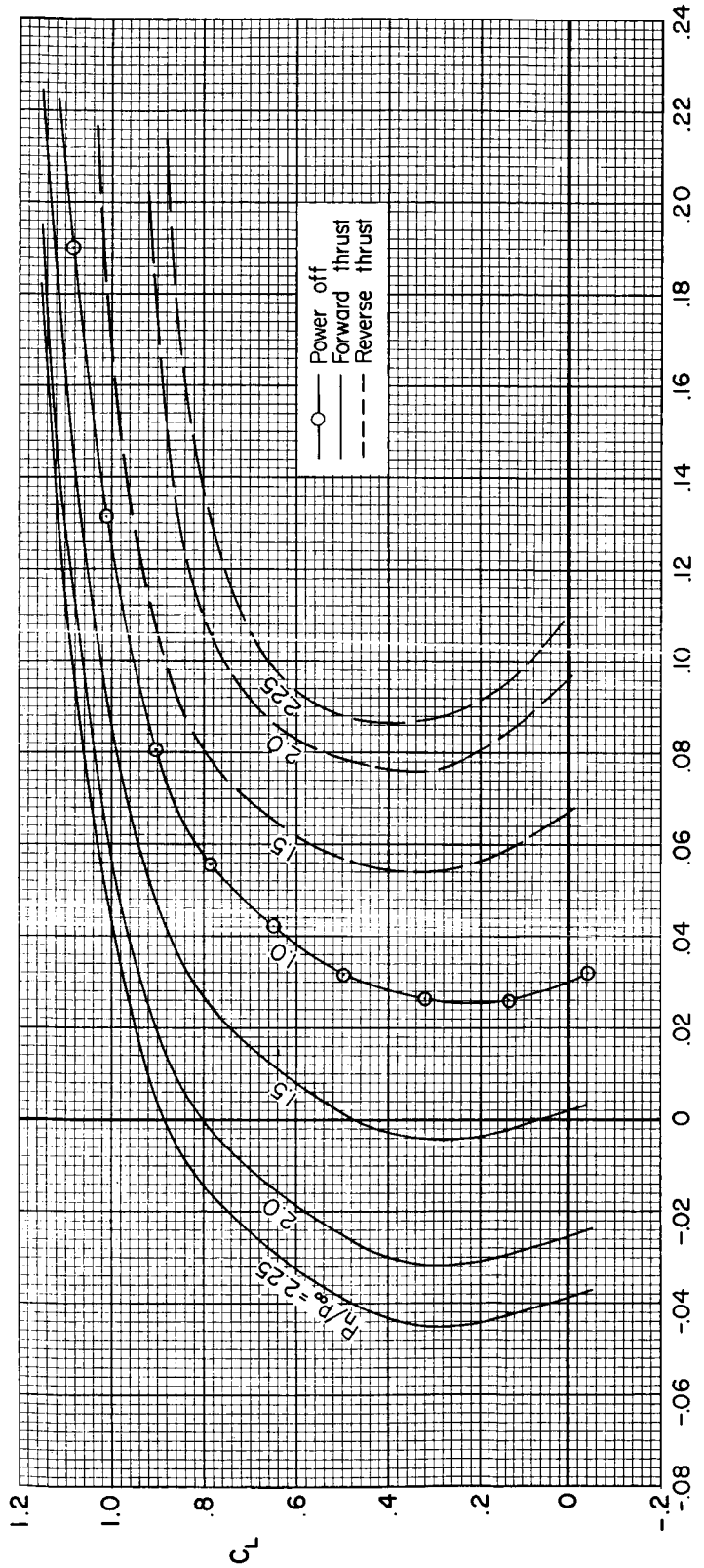

(b) C_X vs. C_L

Figure 10.- Continued.

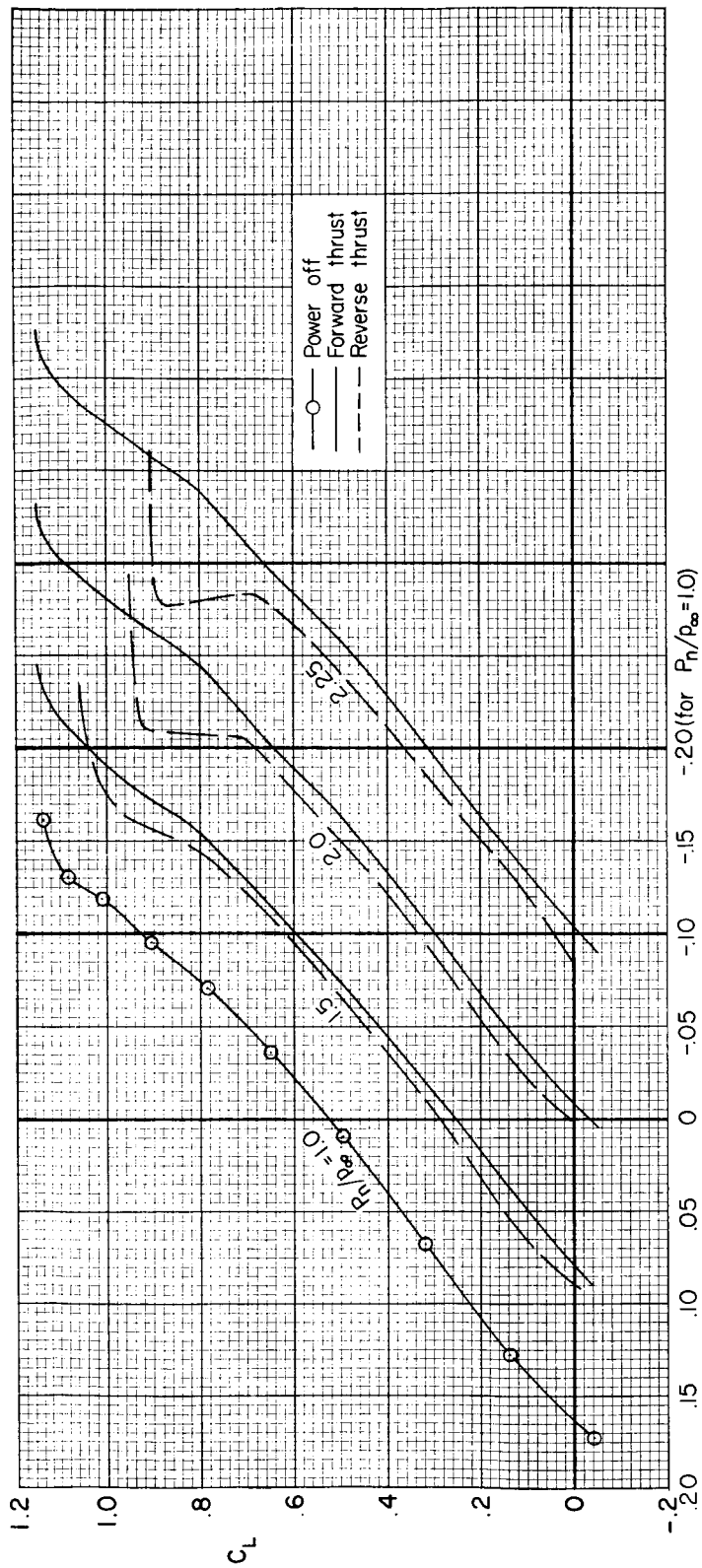

(c) C_m vs. C_L

Figure 10.- Concluded.

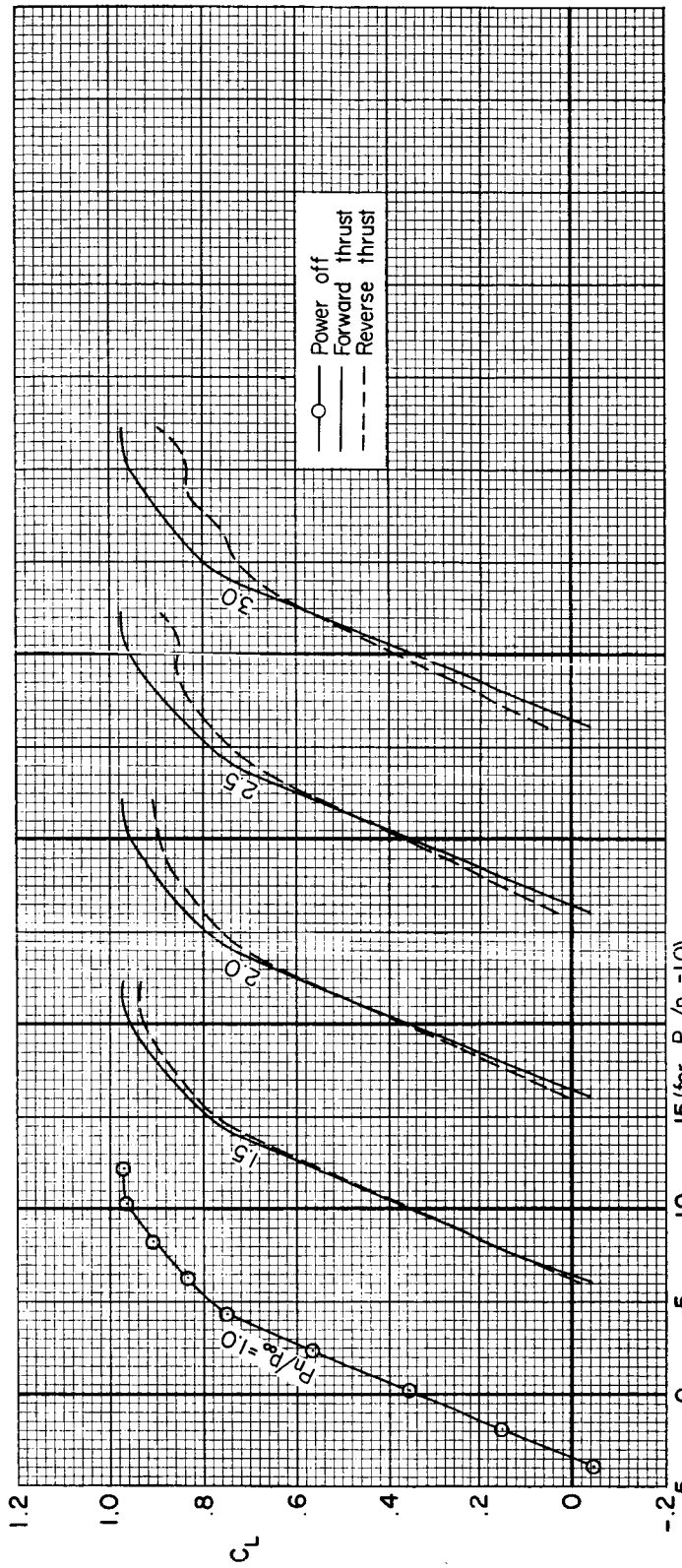

(a) C_L vs. α

Figure 11.- The effect of forward and reverse thrust on the longitudinal characteristics of the model; $i_t = -4^\circ$, M = 0.70.

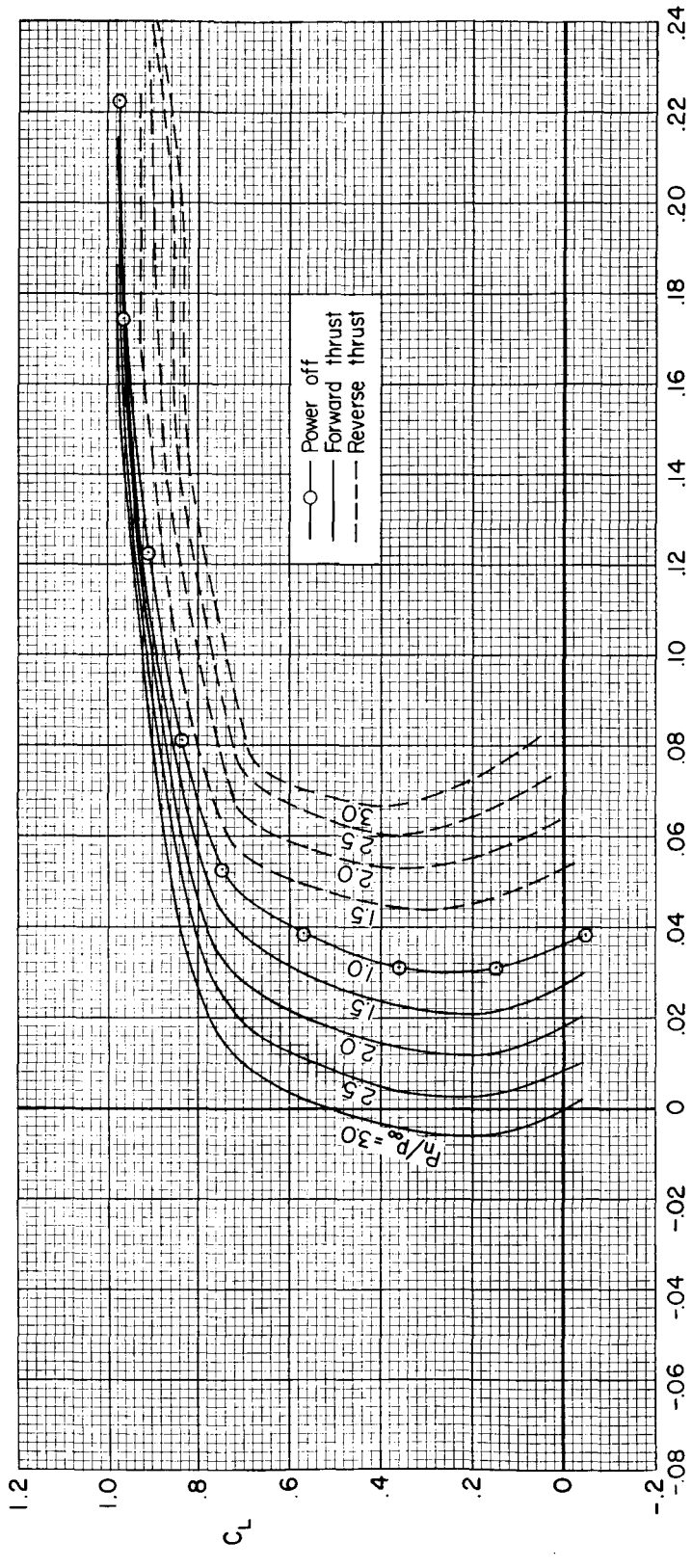

(b) C_X vs. C_L

Figure 11.- Continued.

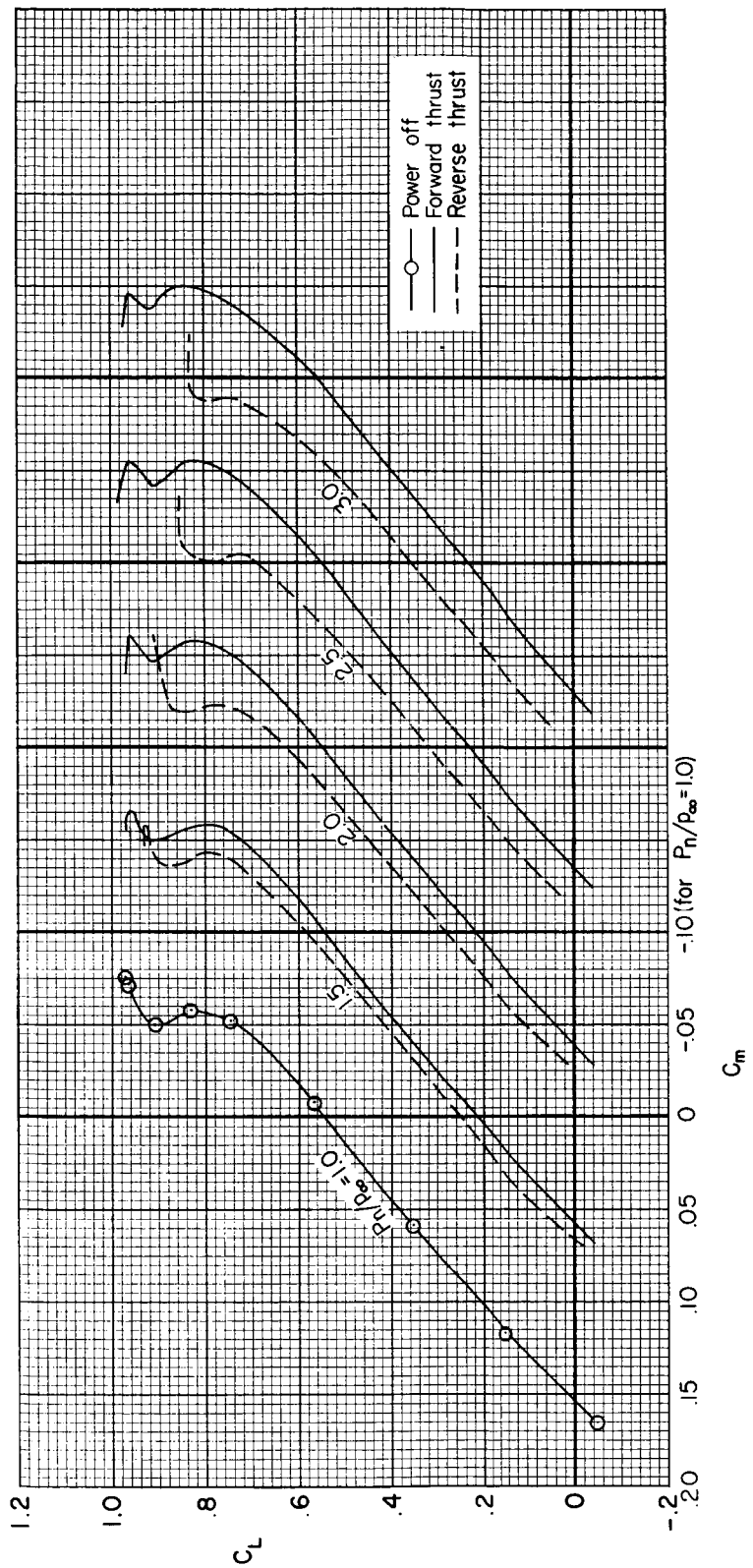

(c) C_m vs. C_L

Figure 11.- Concluded.

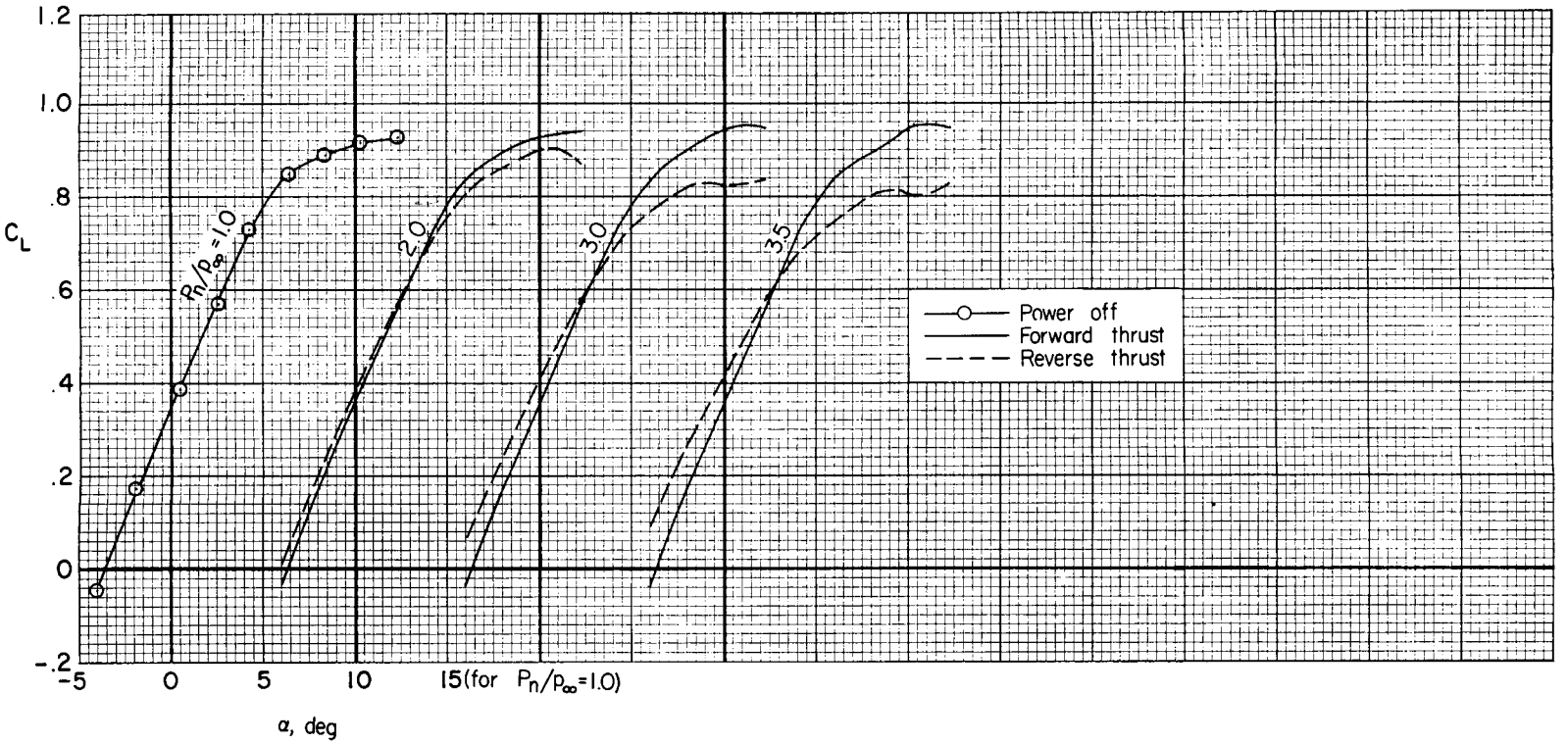

(a) C_L vs. α

Figure 12.- The effect of forward and reverse thrust on the longitudinal characteristics of the model; $i_t = -4^o$, M = 0.80.

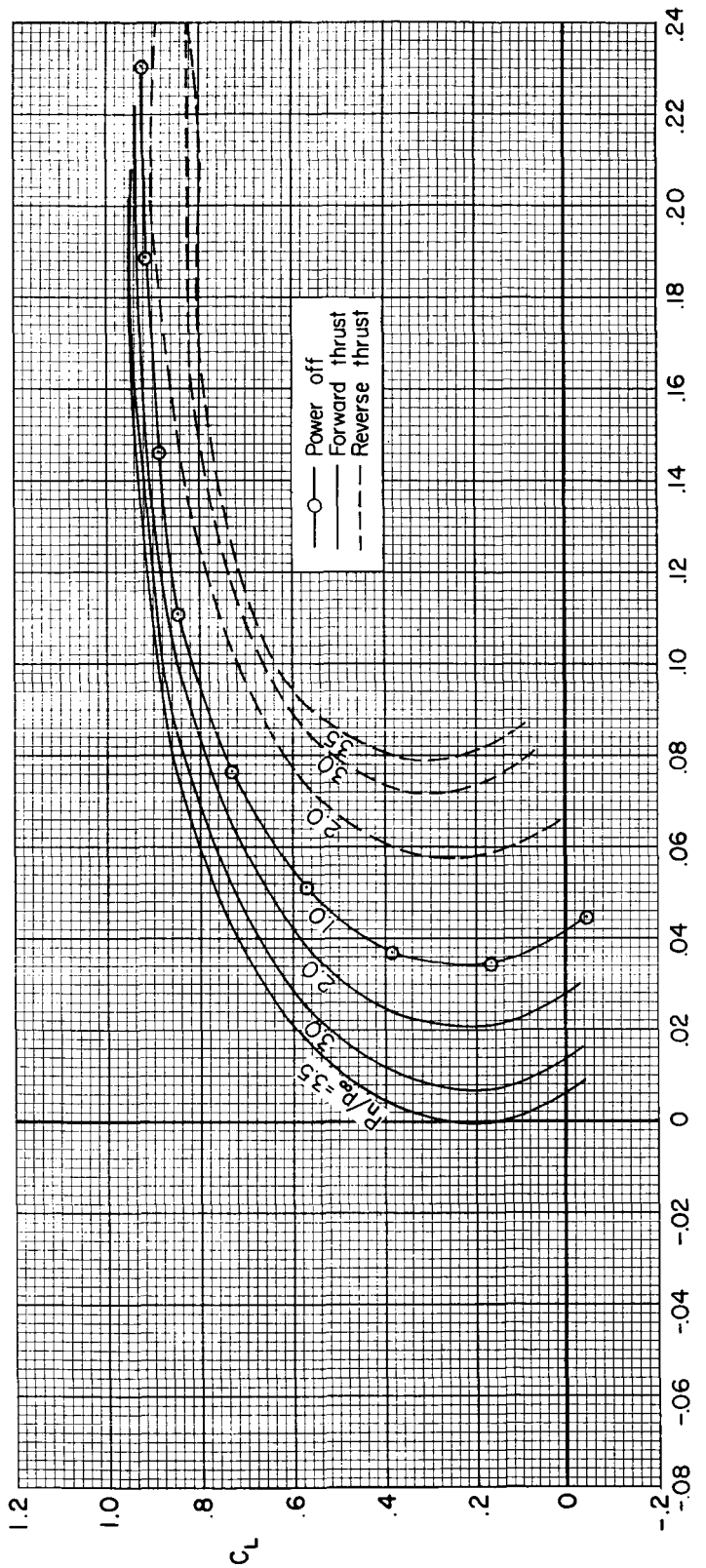

(b) C_X vs. C_L

Figure 12.- Continued.

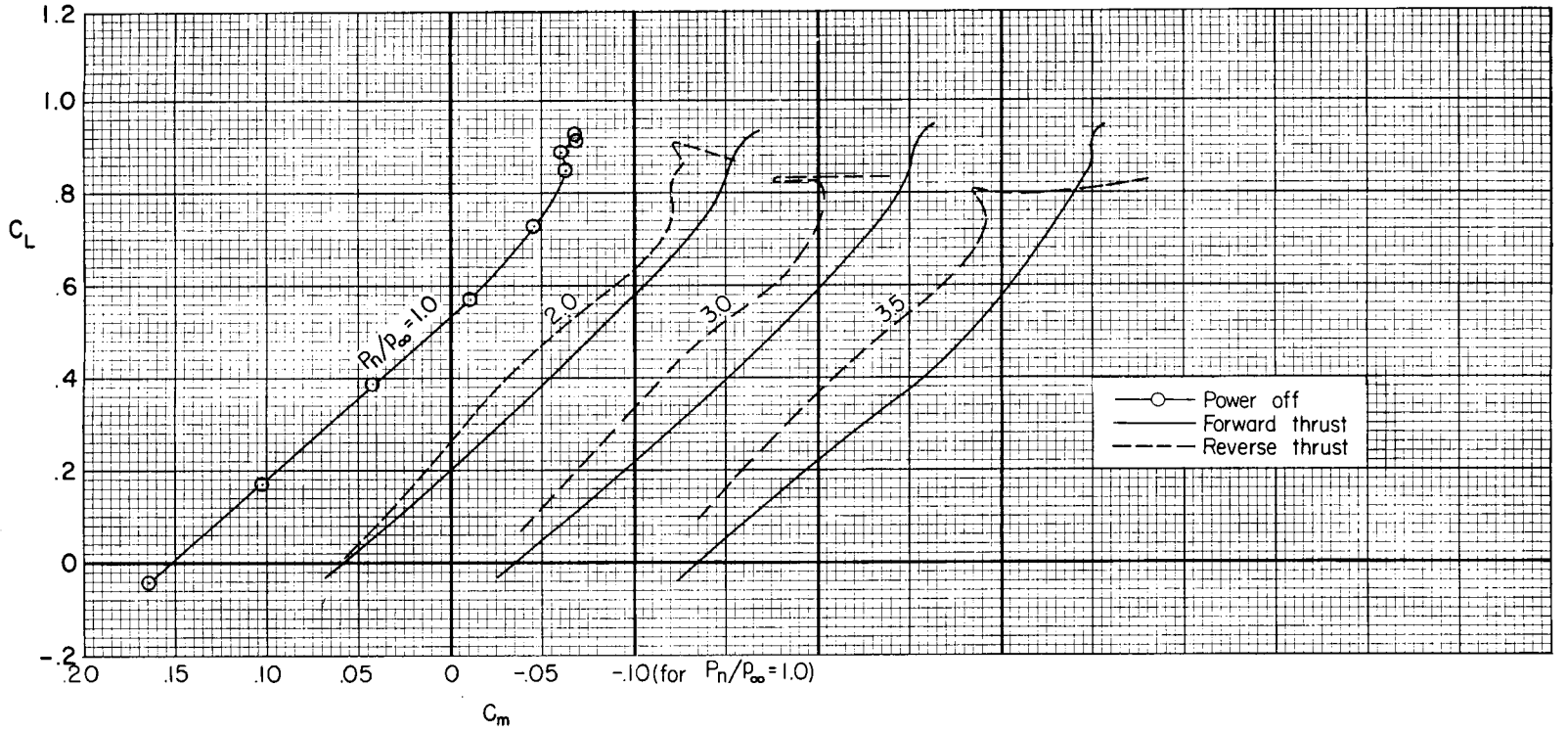

(c) C_m vs. C_L

Figure 12.- Concluded.

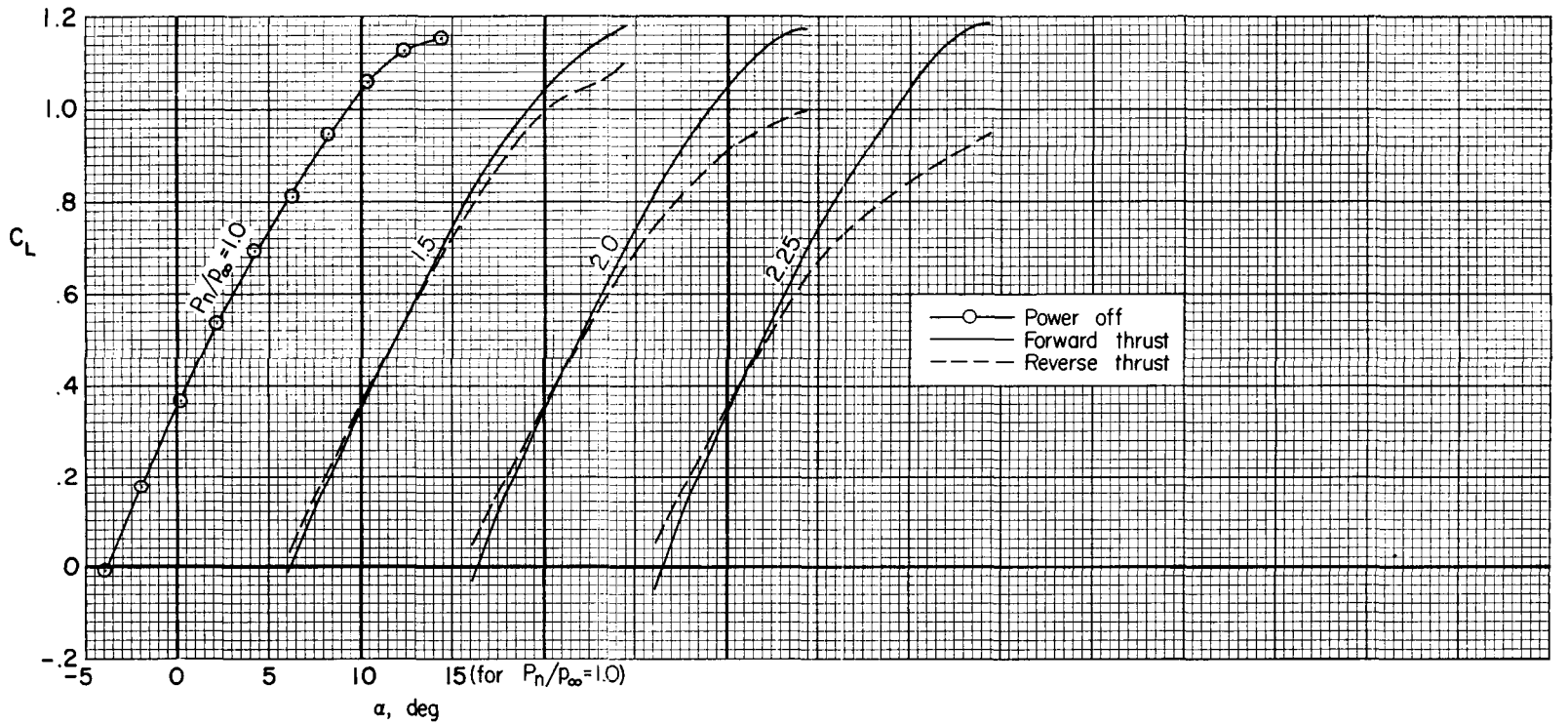

(a) C_L vs. α

Figure 13.- The effect of forward and reverse thrust on the longitudinal characteristics of the model; $i_t = 0^\circ$, M = 0.40.

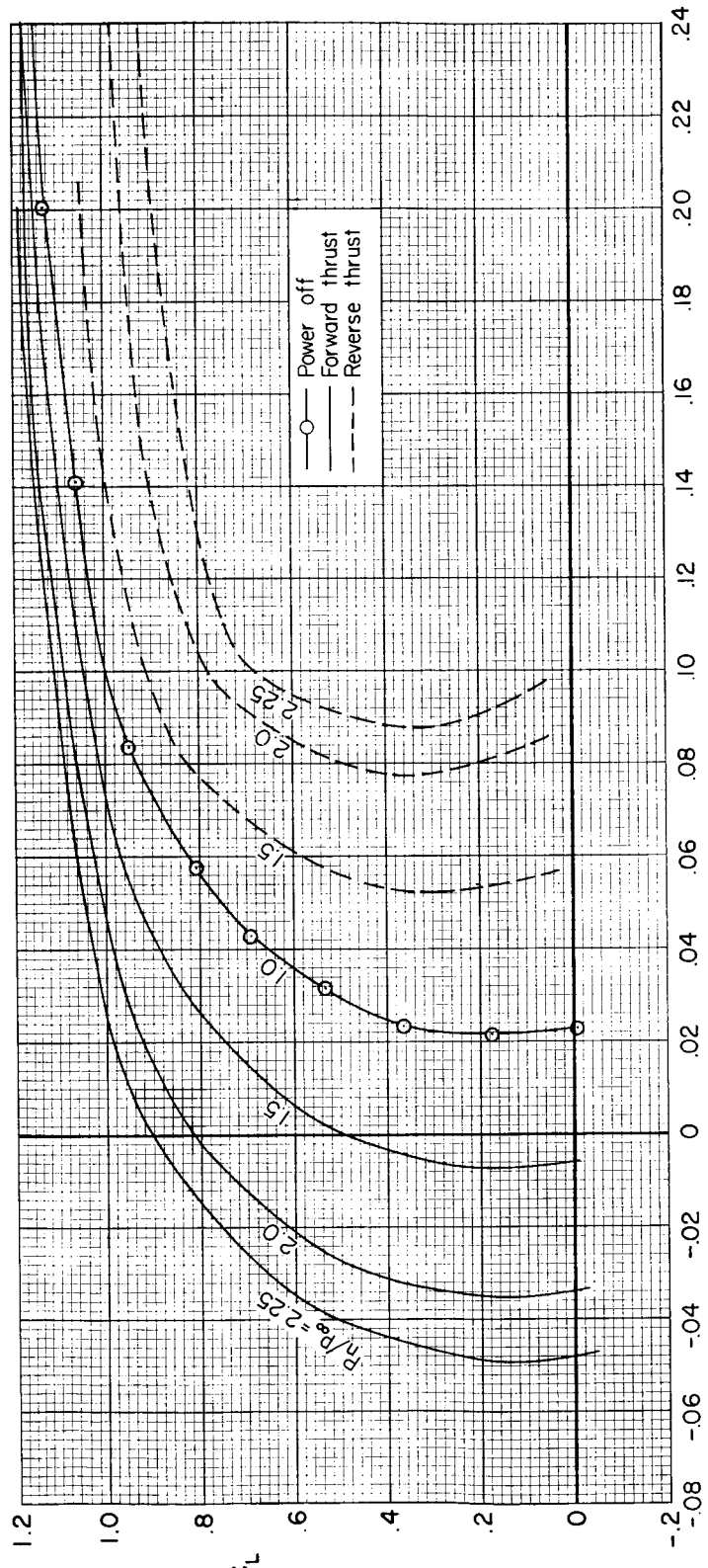

(b) C_X vs. C_L

Figure 13.- Continued.

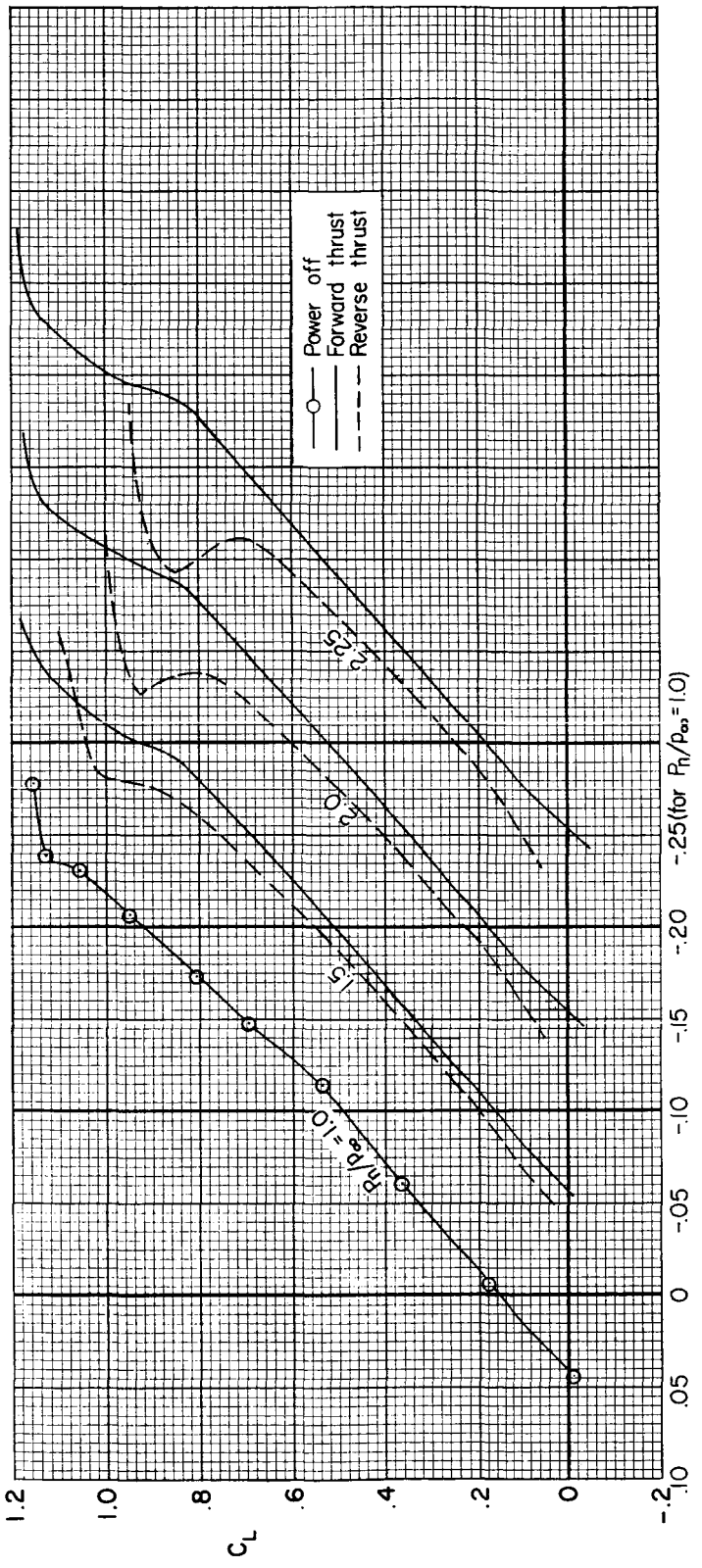

(c) C_m vs. C_L

Figure 13.- Concluded.

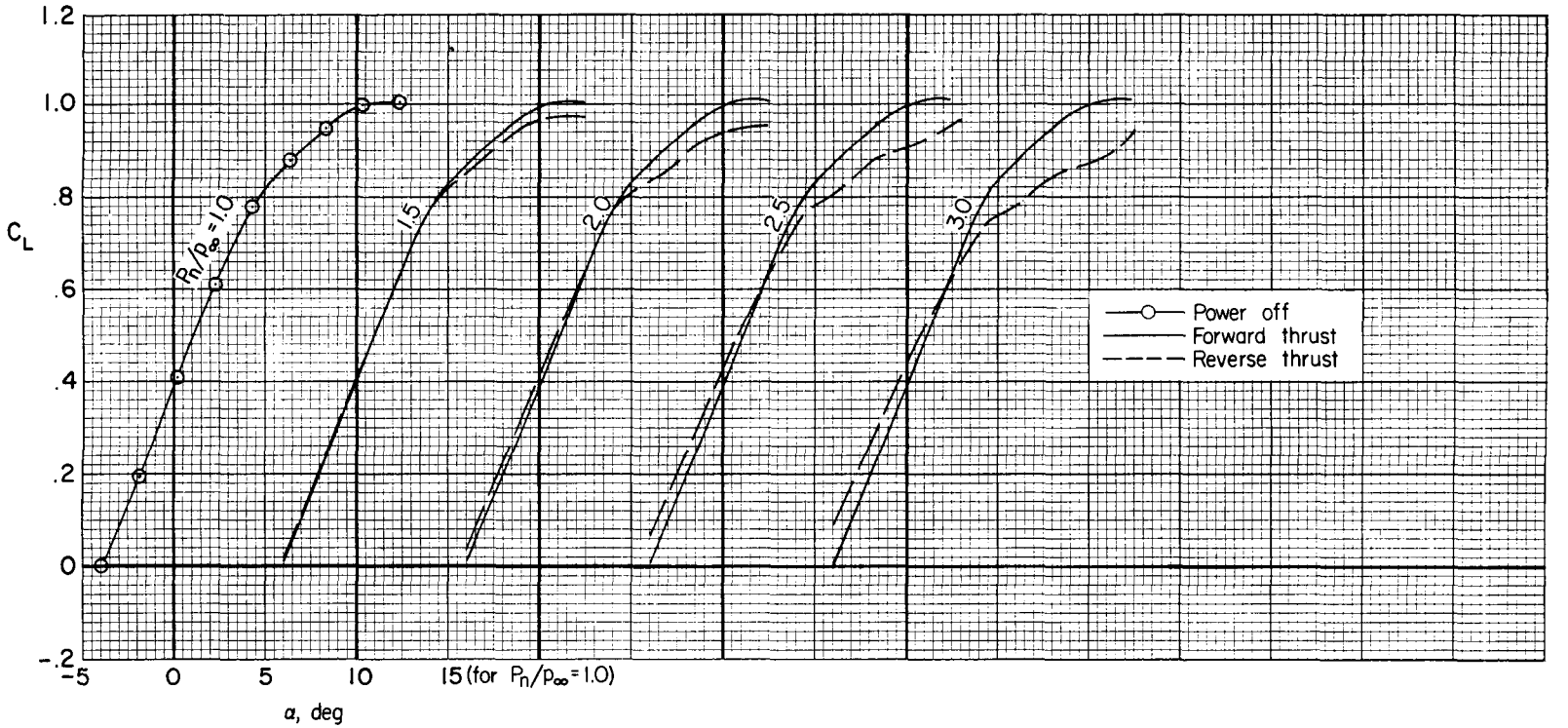

(a) C_L vs. α

Figure 14.- The effect of forward and reverse thrust on the longitudinal characteristics of the model; $i_t = 0^o$, M = 0.70.

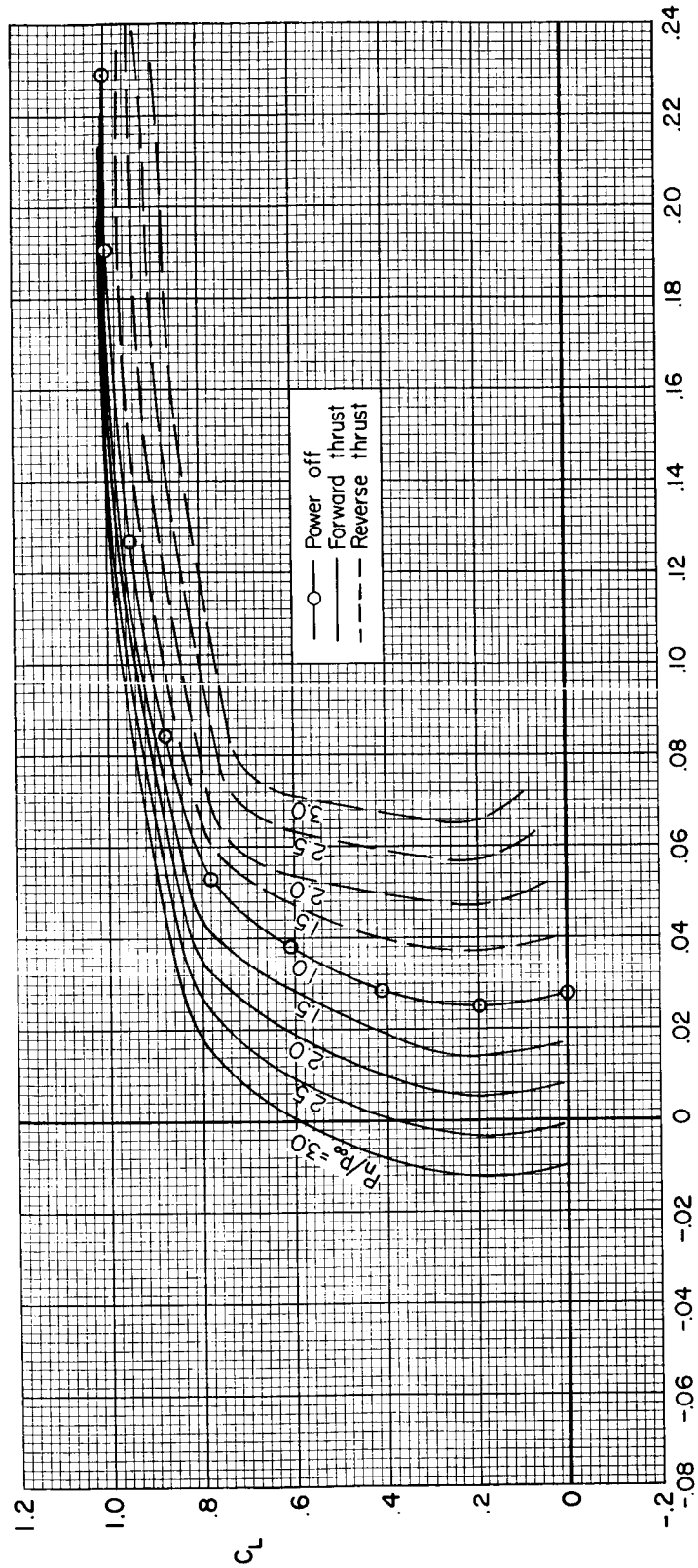

(b) C_X vs. C_L

Figure 14.- Continued.

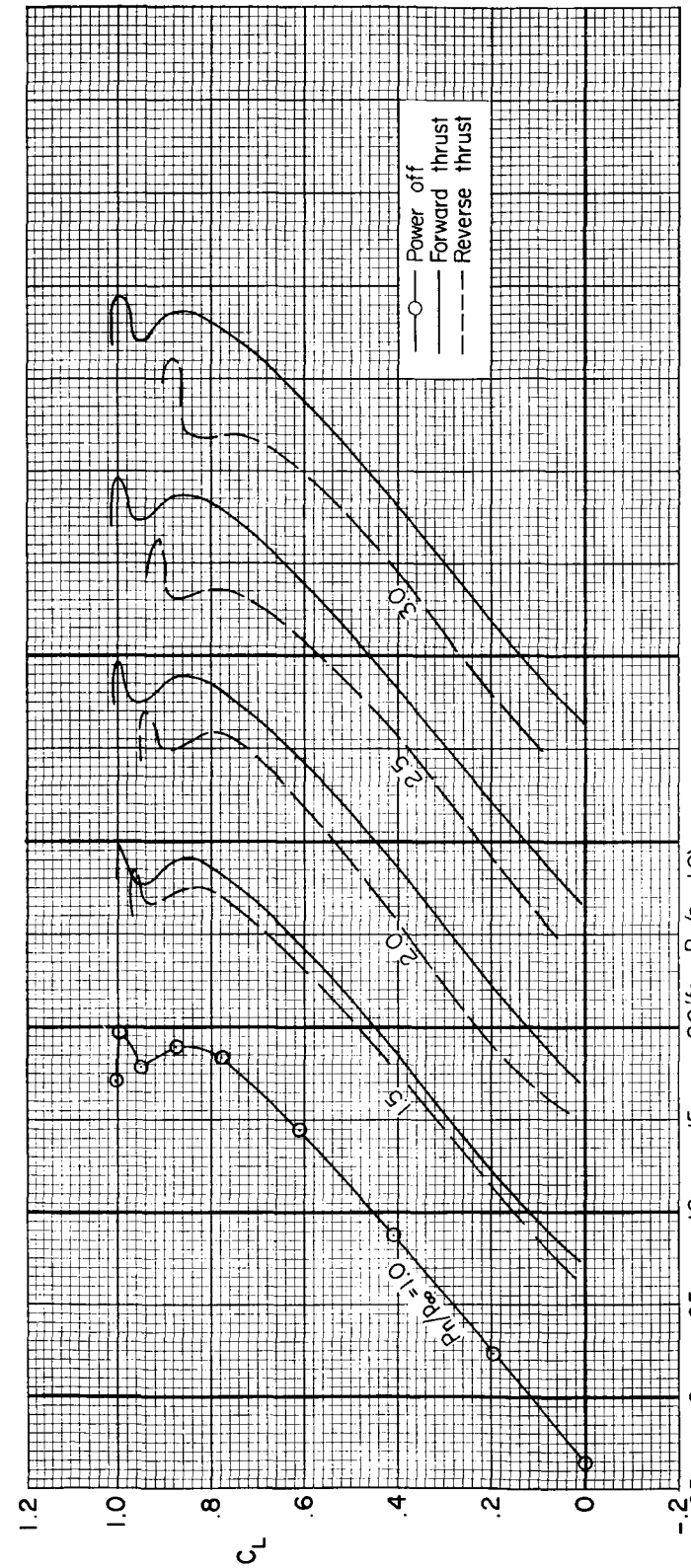

(c) C_m vs. C_L

Figure 14.- Concluded.

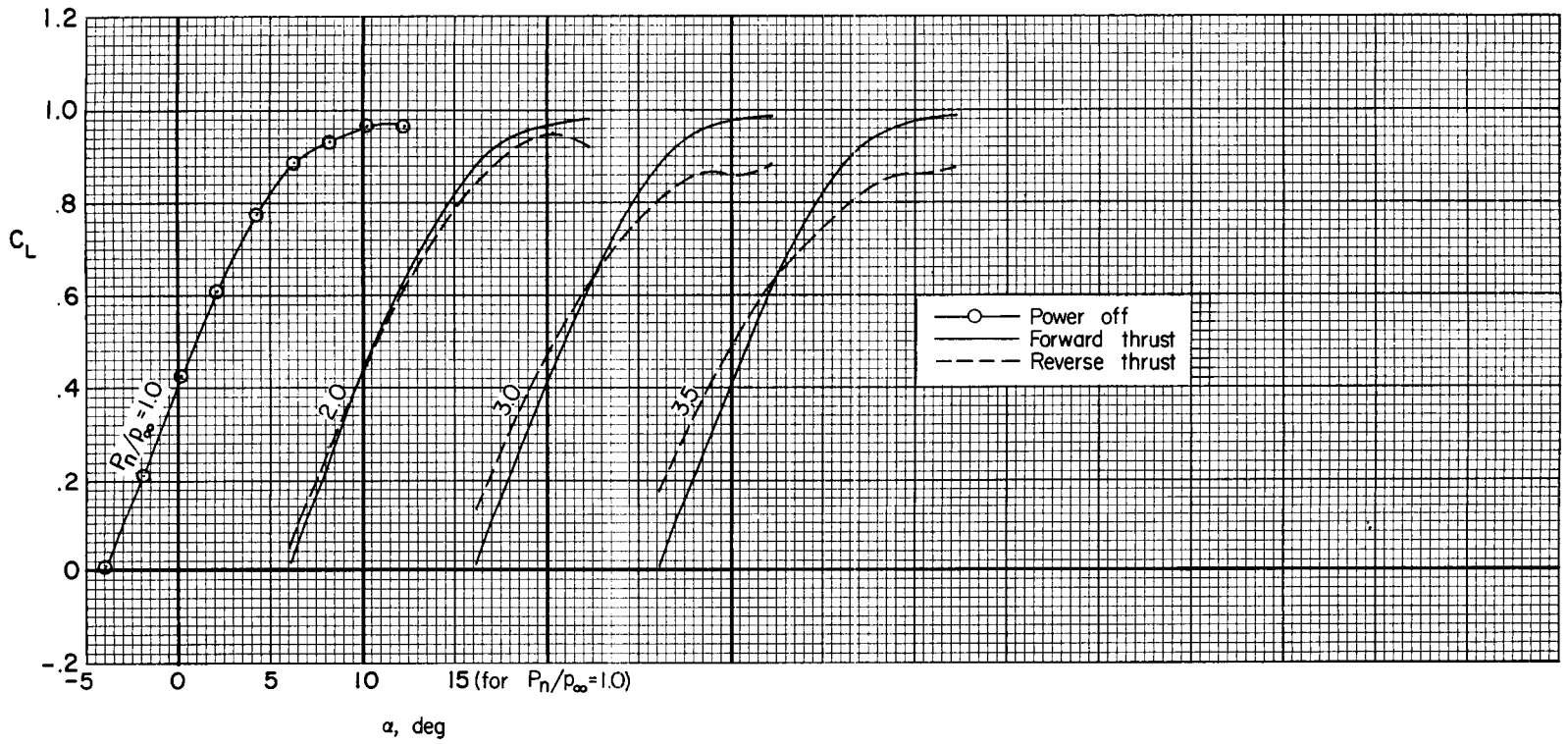

(a) C_L vs. α

Figure 15.- The effect of forward and reverse thrust on the longitudinal characteristics of the model; $i_t = 0^\circ$, M = 0.80.

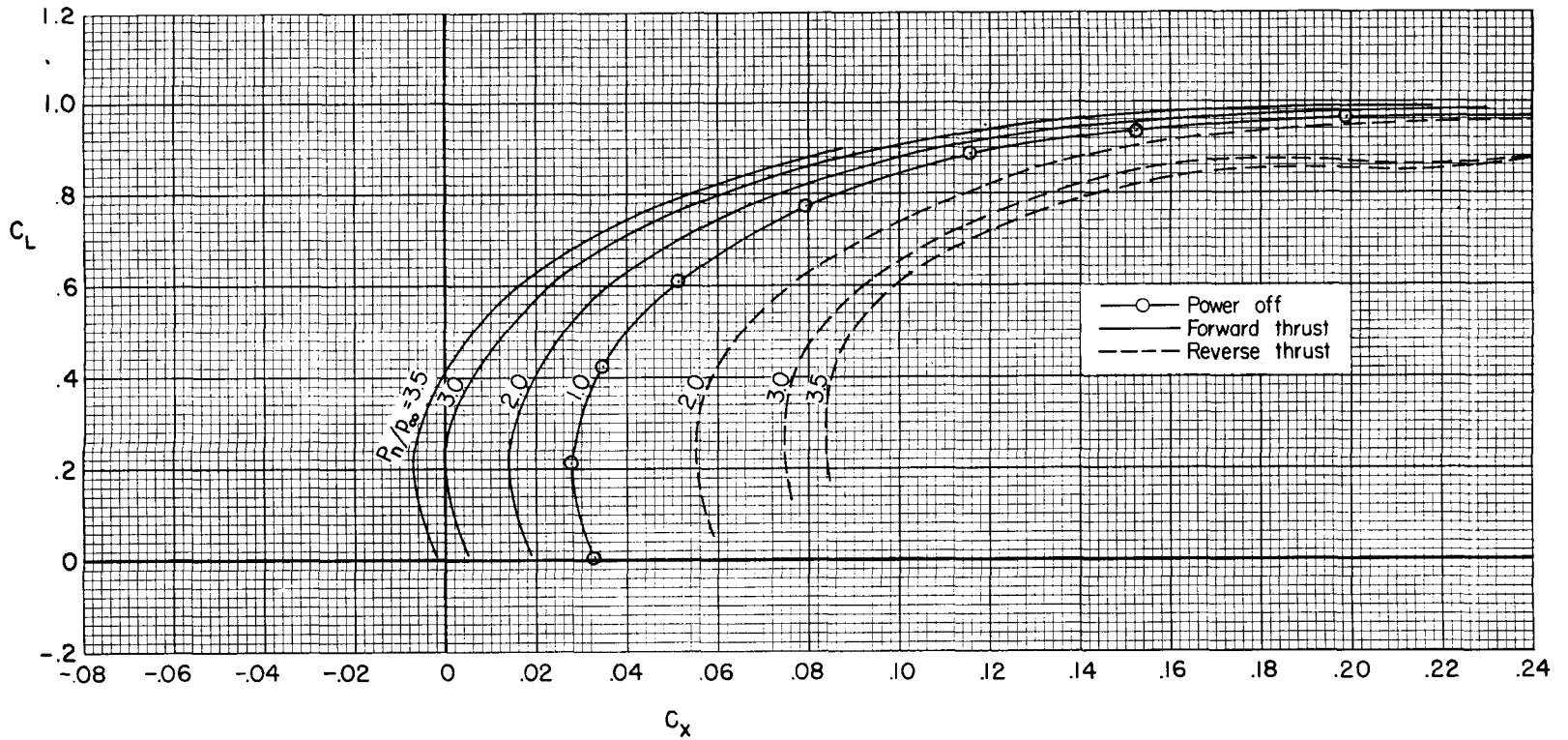

(b) C_X vs. C_L

Figure 15.- Continued.

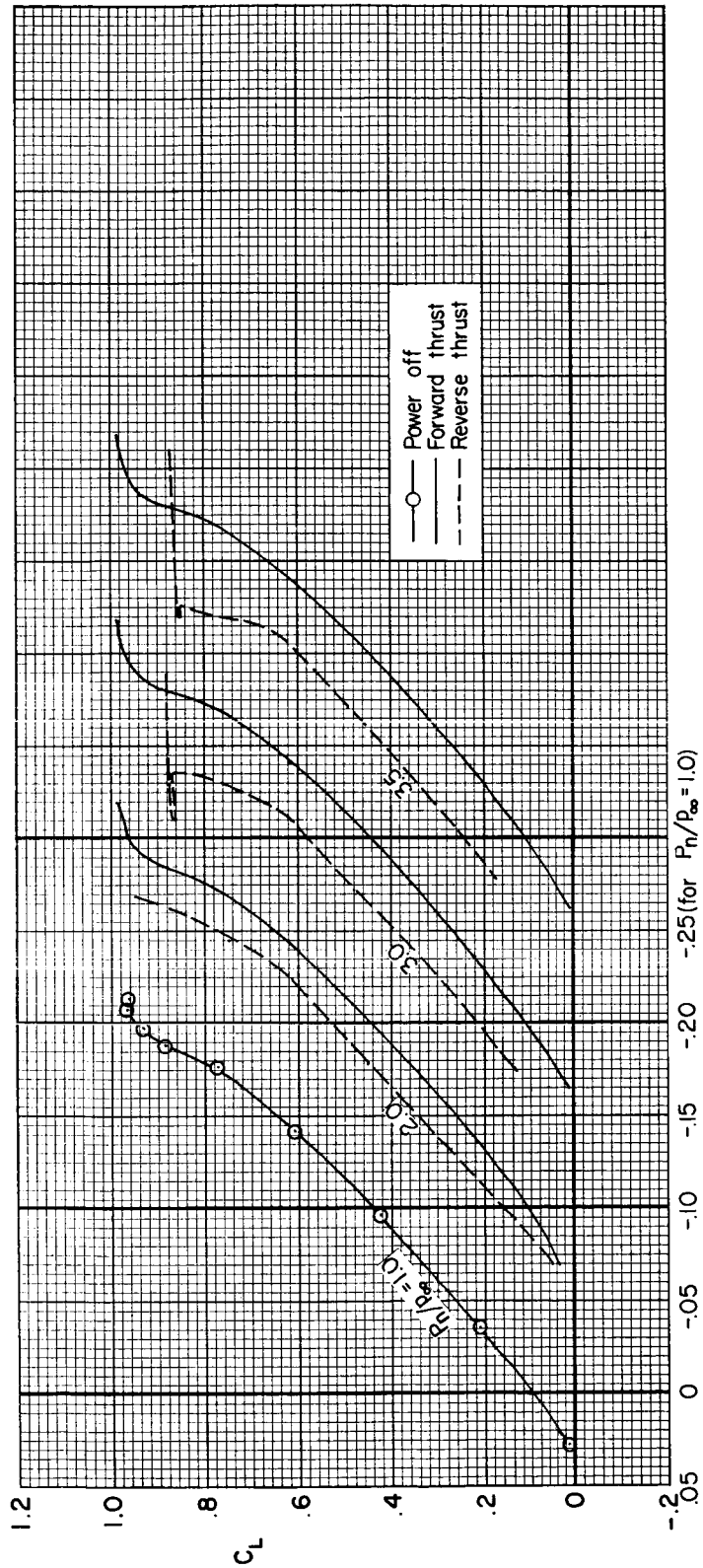

(c) C_m vs. C_L

Figure 15.- Concluded.

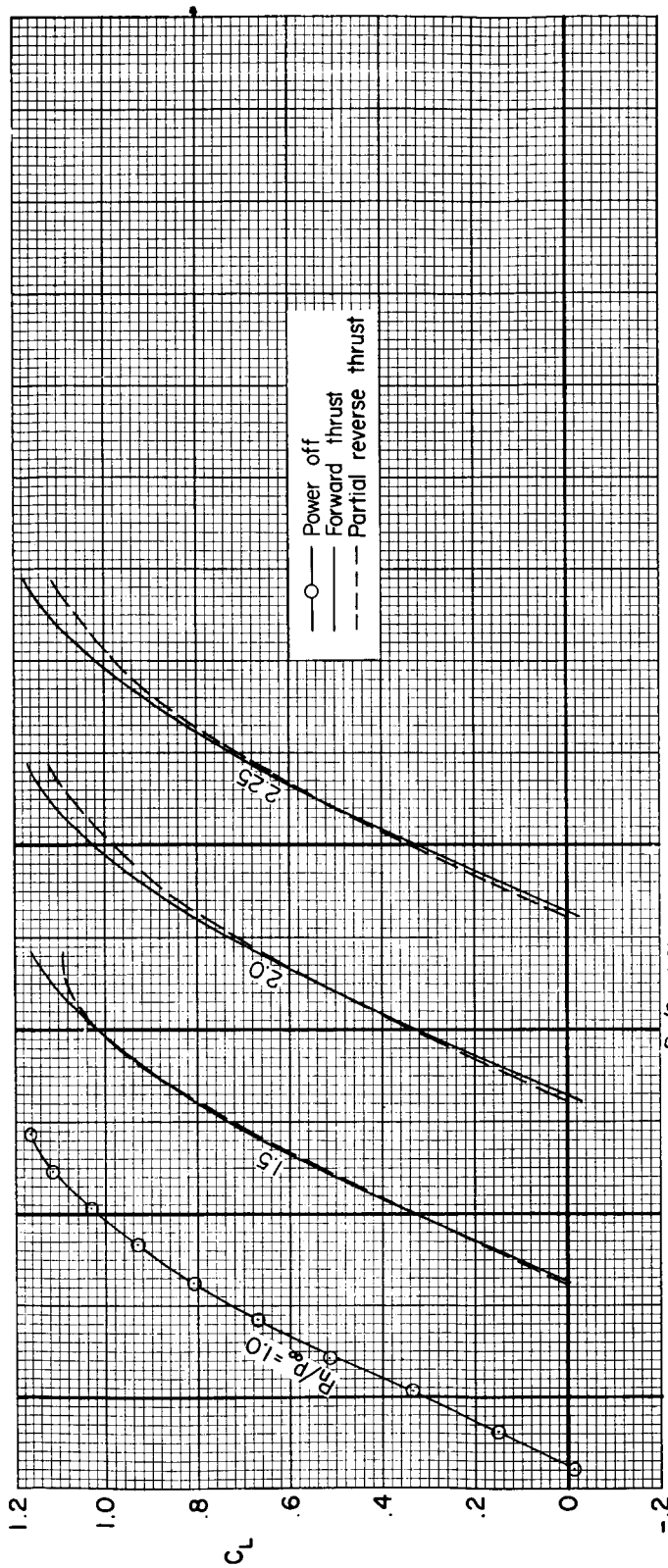

(a) C_L vs. α

Figure 16.- The effect of partial operation of thrust reversers on the longitudinal characteristics of the model; $i_t = -2^0$, M = 0.40.

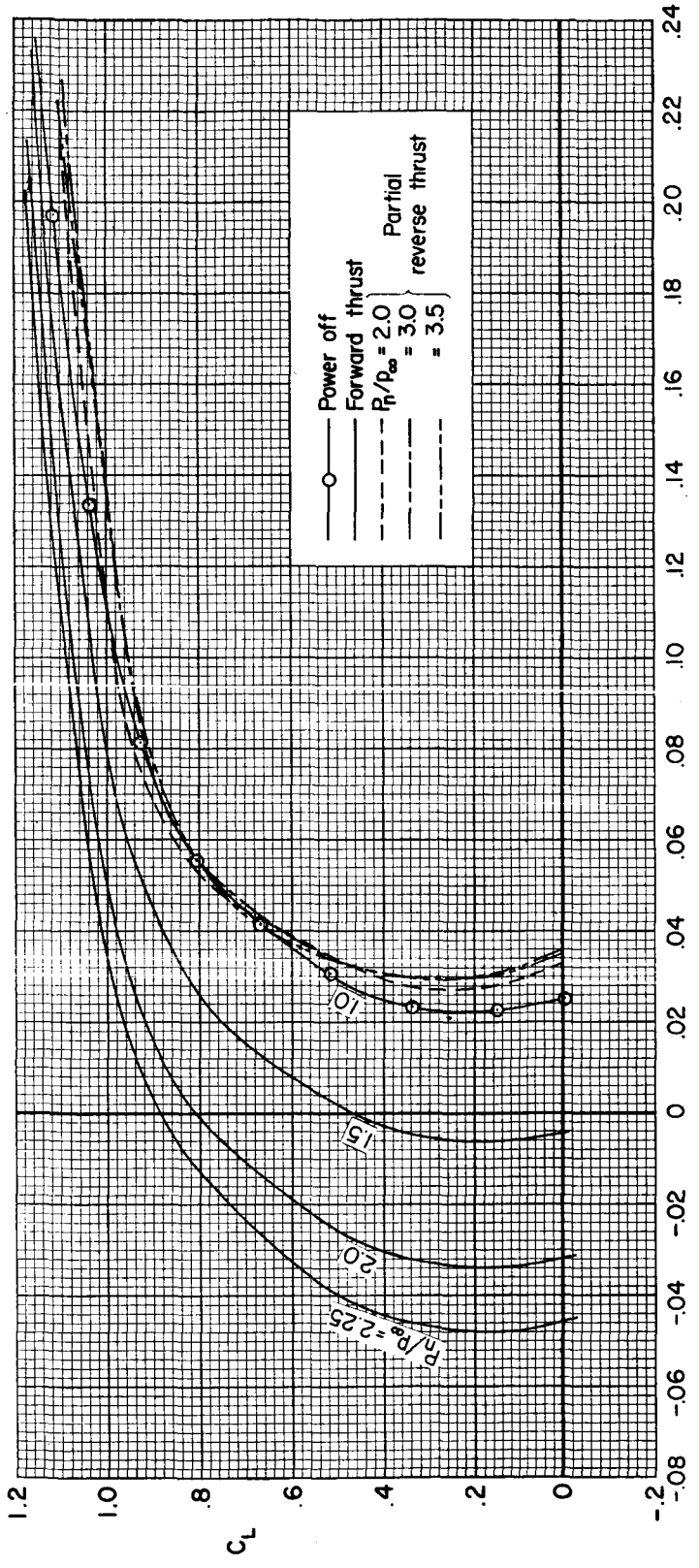

(b) C_X vs. C_L

Figure 16.- Continued.

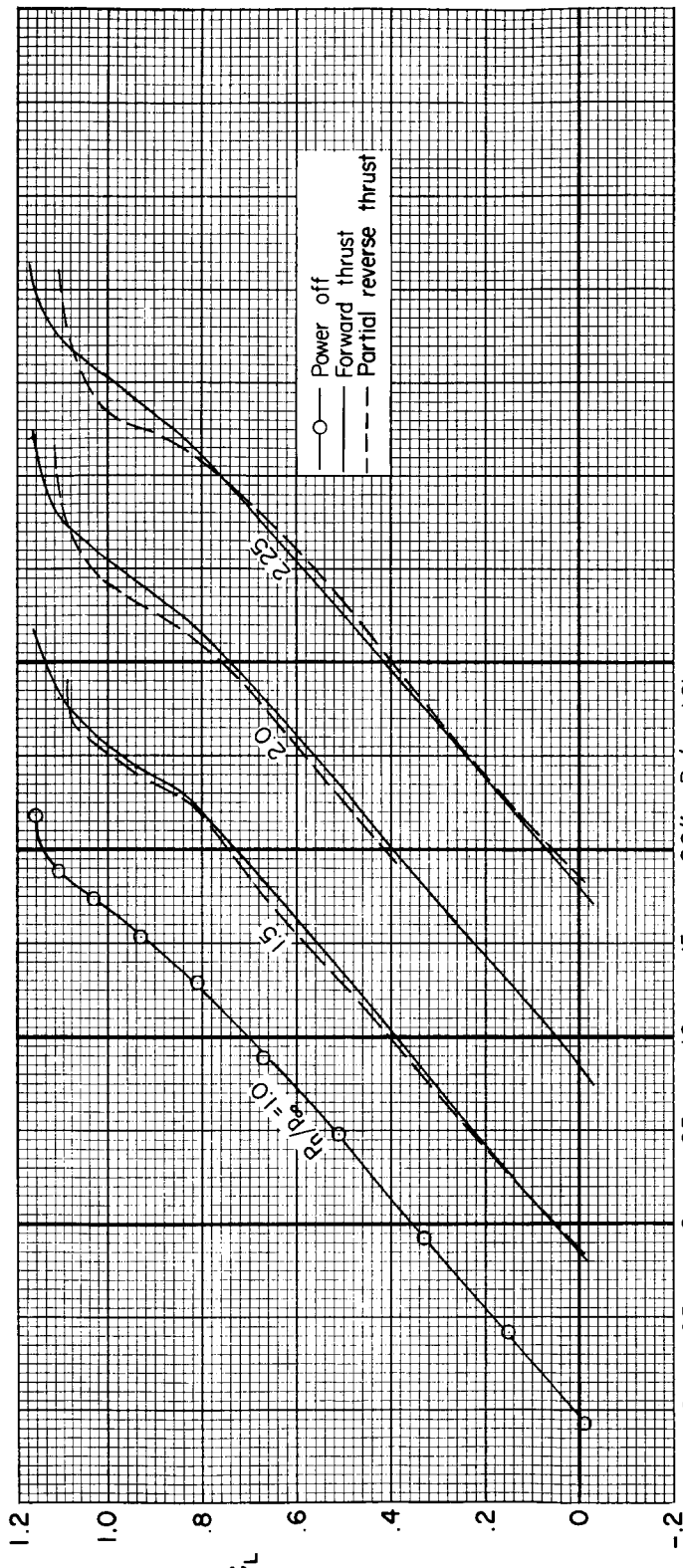

(c) C_m vs. C_L

Figure 16.- Concluded.

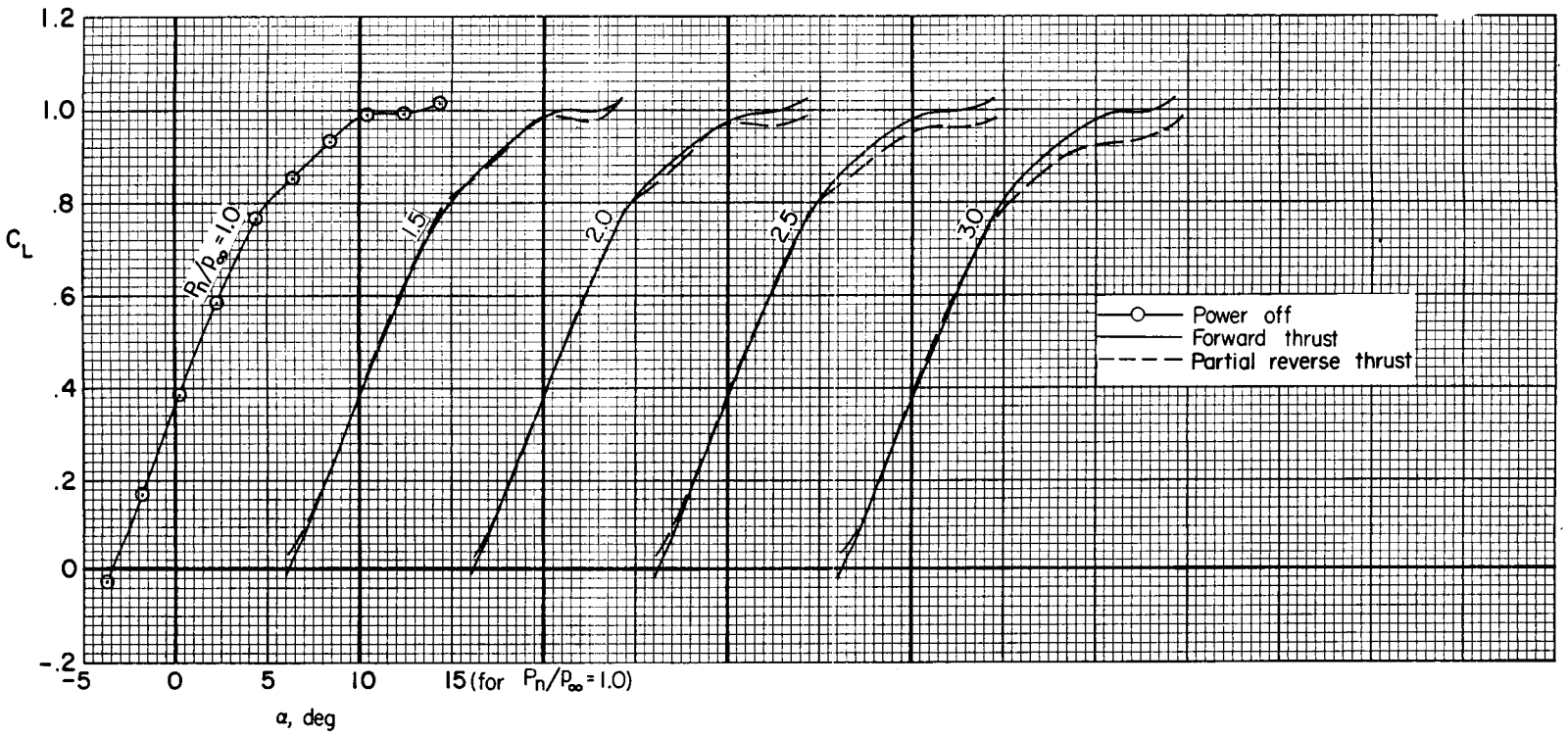

(a) C_L vs. α

Figure 17.- The effect of partial operation of thrust reversers on the longitudinal characteristics of the model; $i_t = -2^\circ$, M = 0.70.

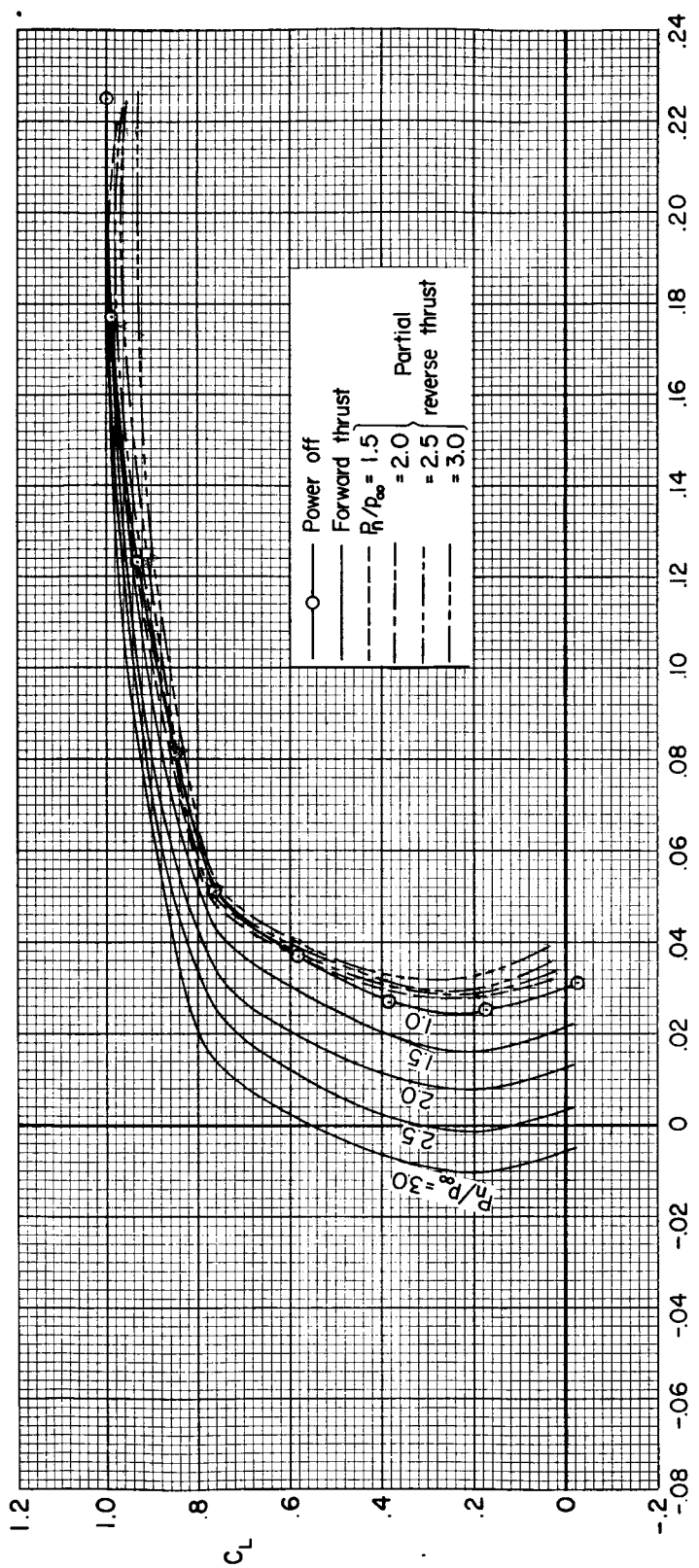

(b) C_X vs. C_L

Figure 17.- Continued.

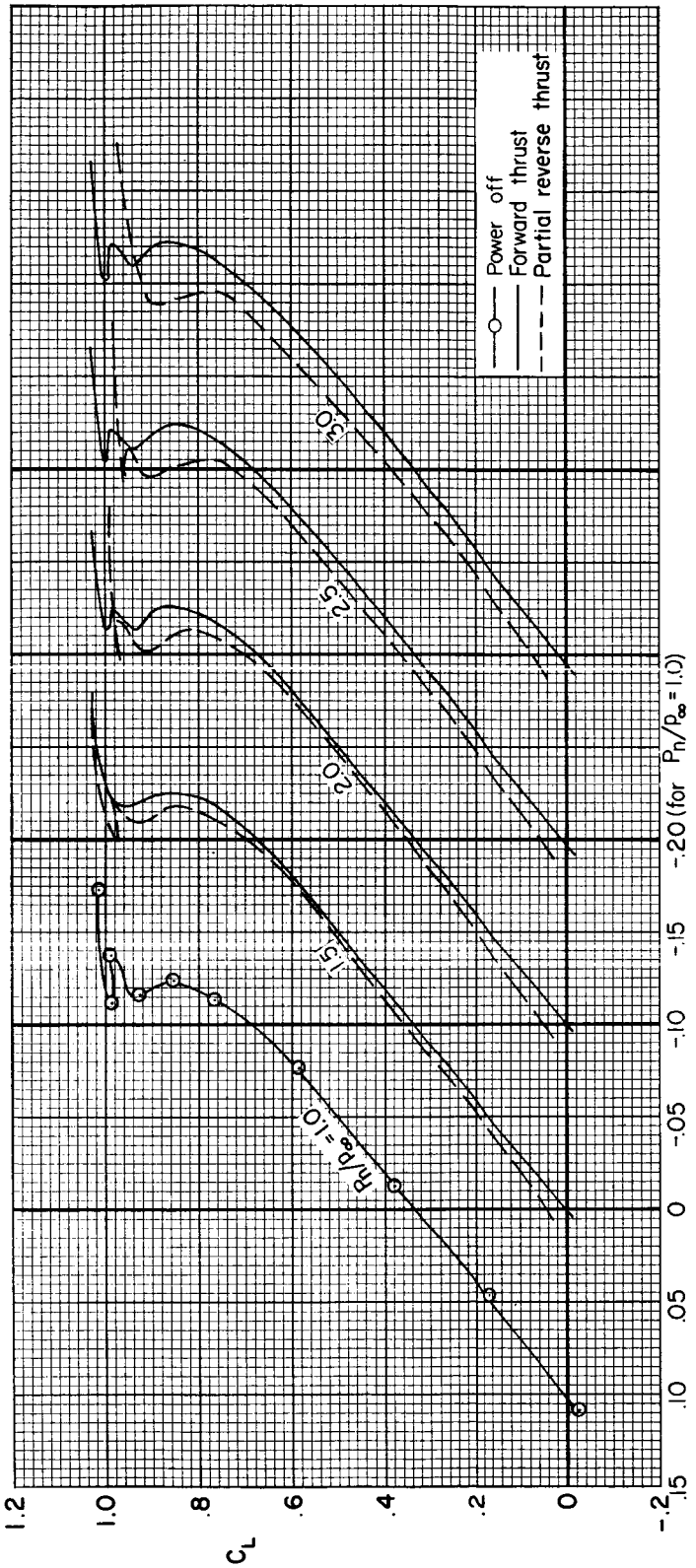

(c) C_m vs. C_L

Figure 17.- Concluded.

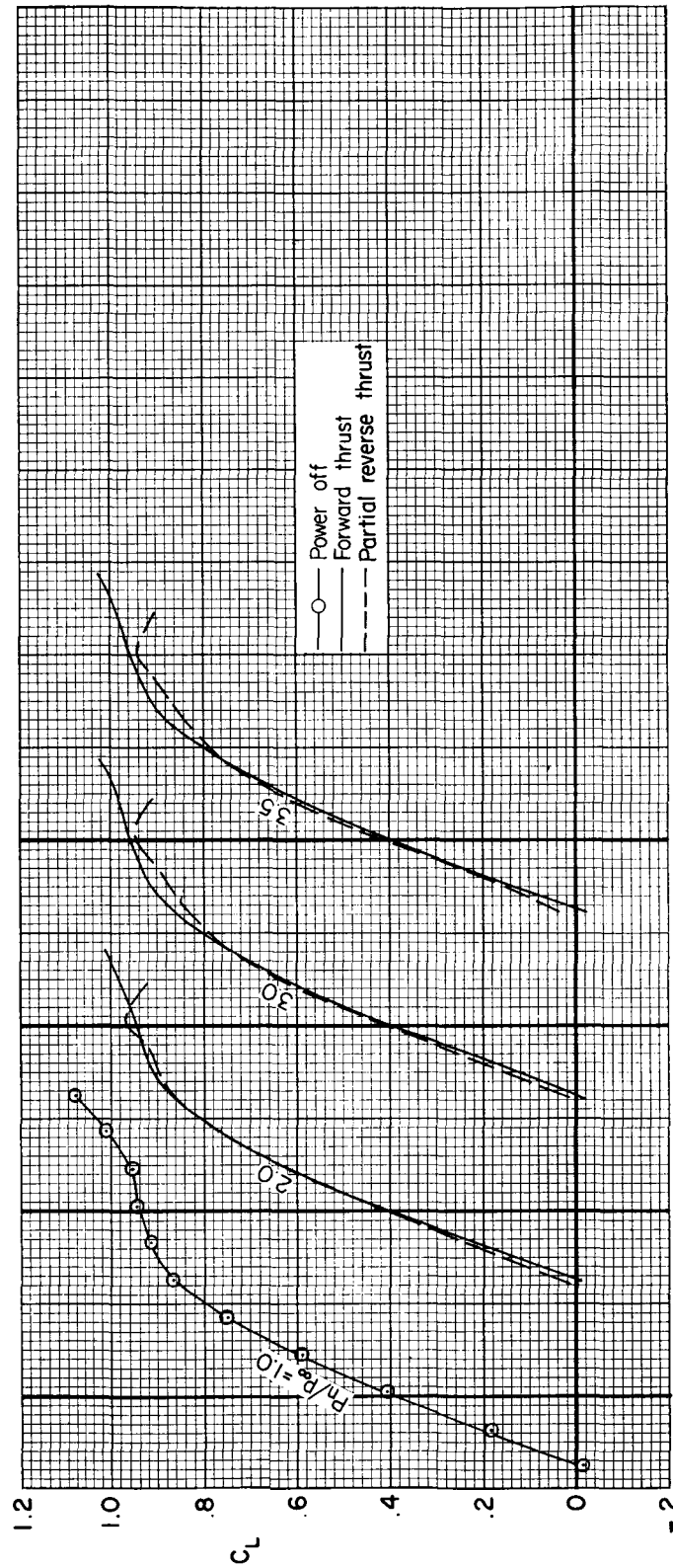

(a) C_L vs. α

Figure 18.- The effect of partial operation of thrust reversers on the longitudinal characteristics of the model; $i_t = -2^o$, M = 0.80.

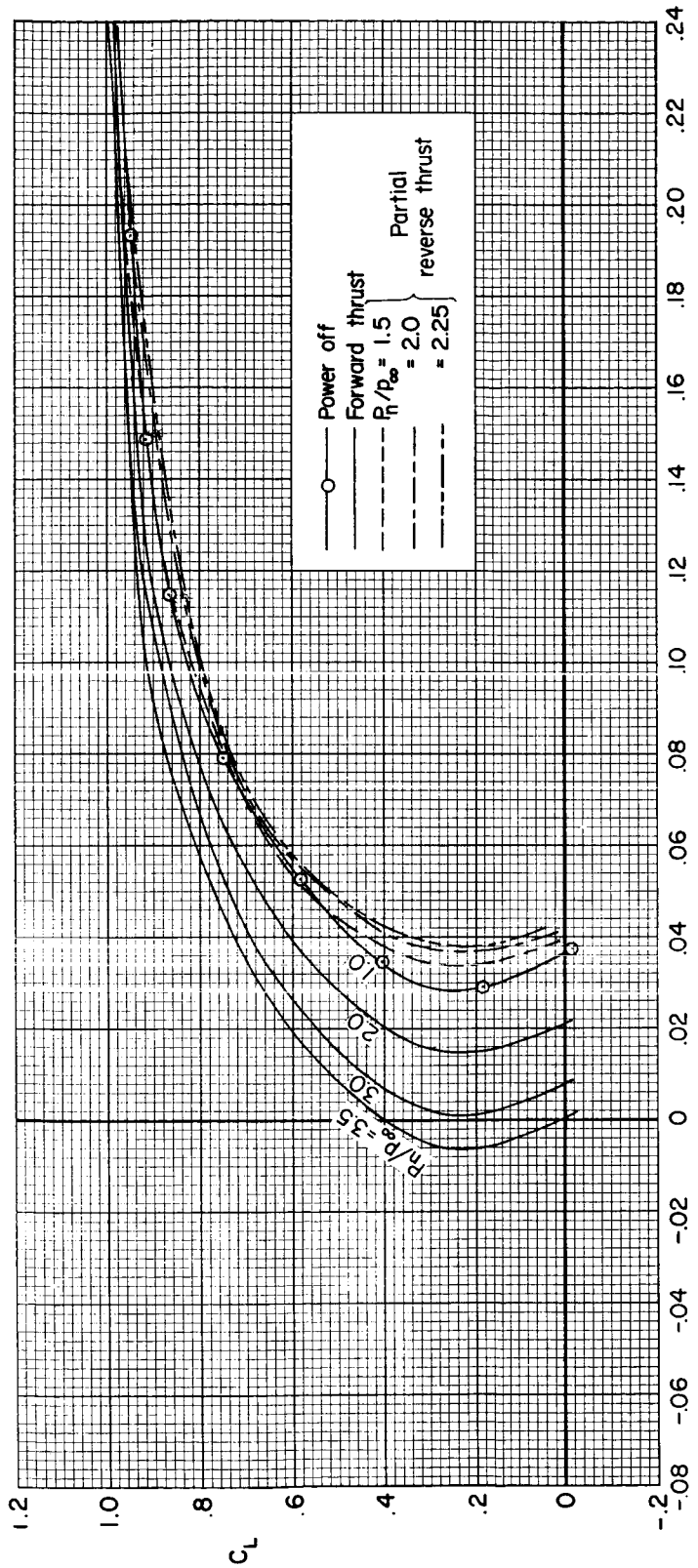

(b) C_X vs. C_L

Figure 18.- Continued.

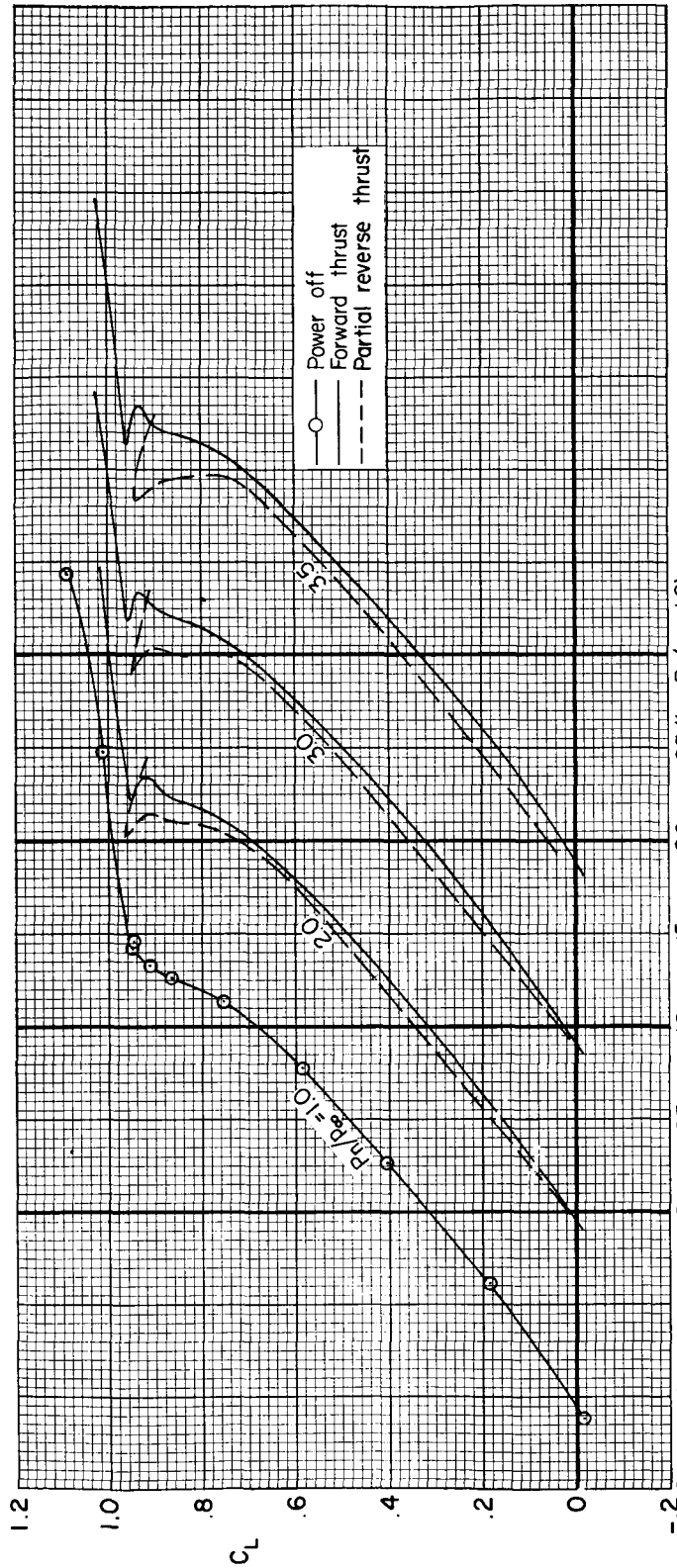

(c) C_m vs. C_L

Figure 18.- Concluded.

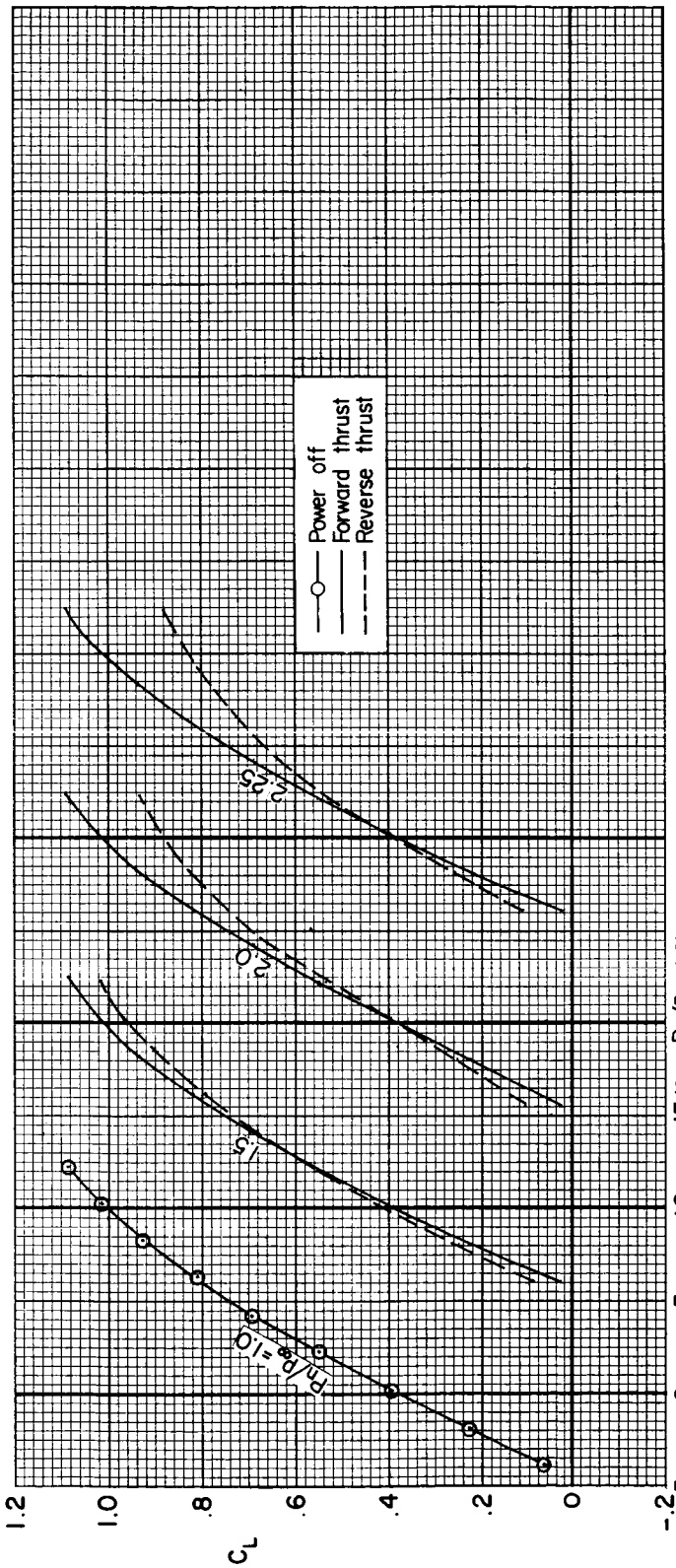

(a) C_L vs. α

Figure 19.- The effect of forward and reverse thrust on the longitudinal characteristics of the model; tail off, M = 0.40.

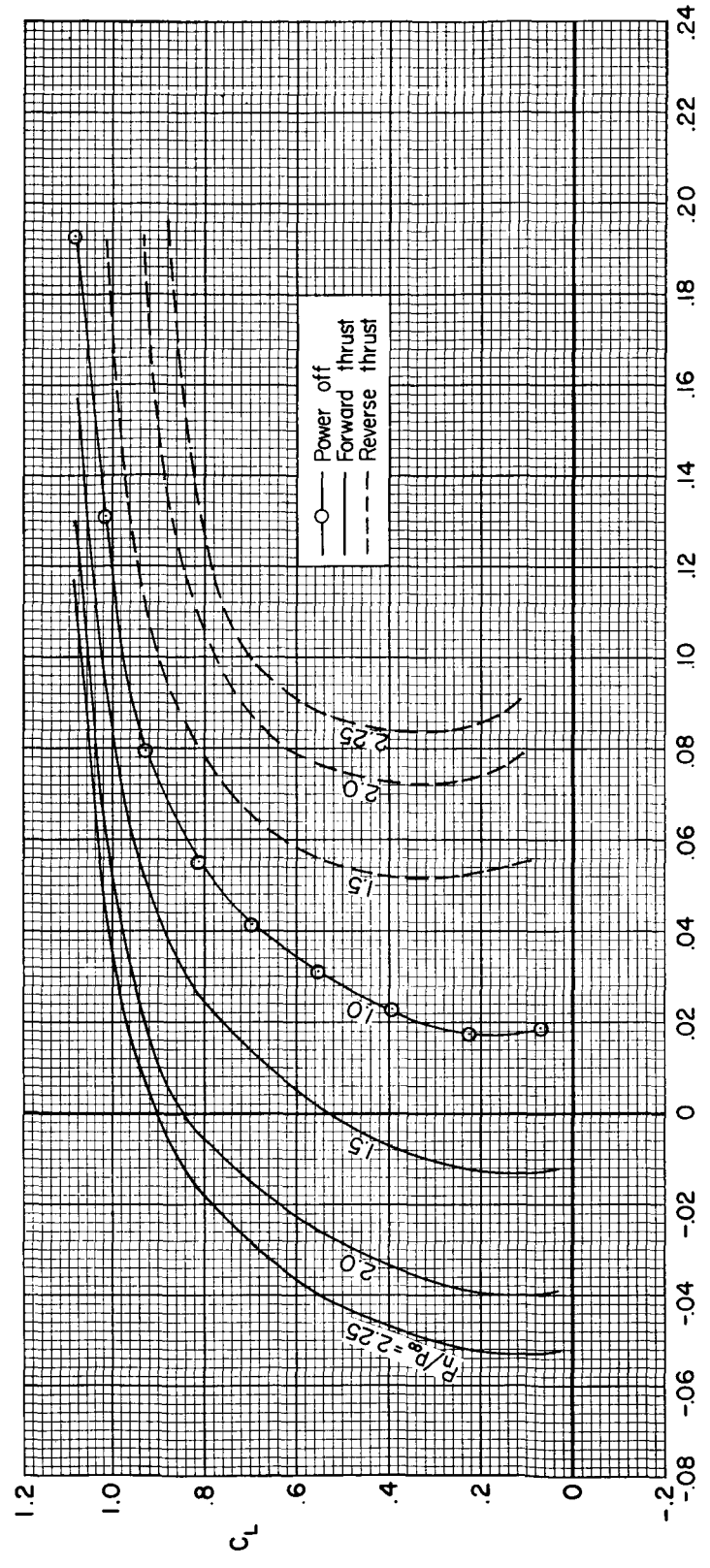

(b) C_X vs. C_L

Figure 19.- Continued.

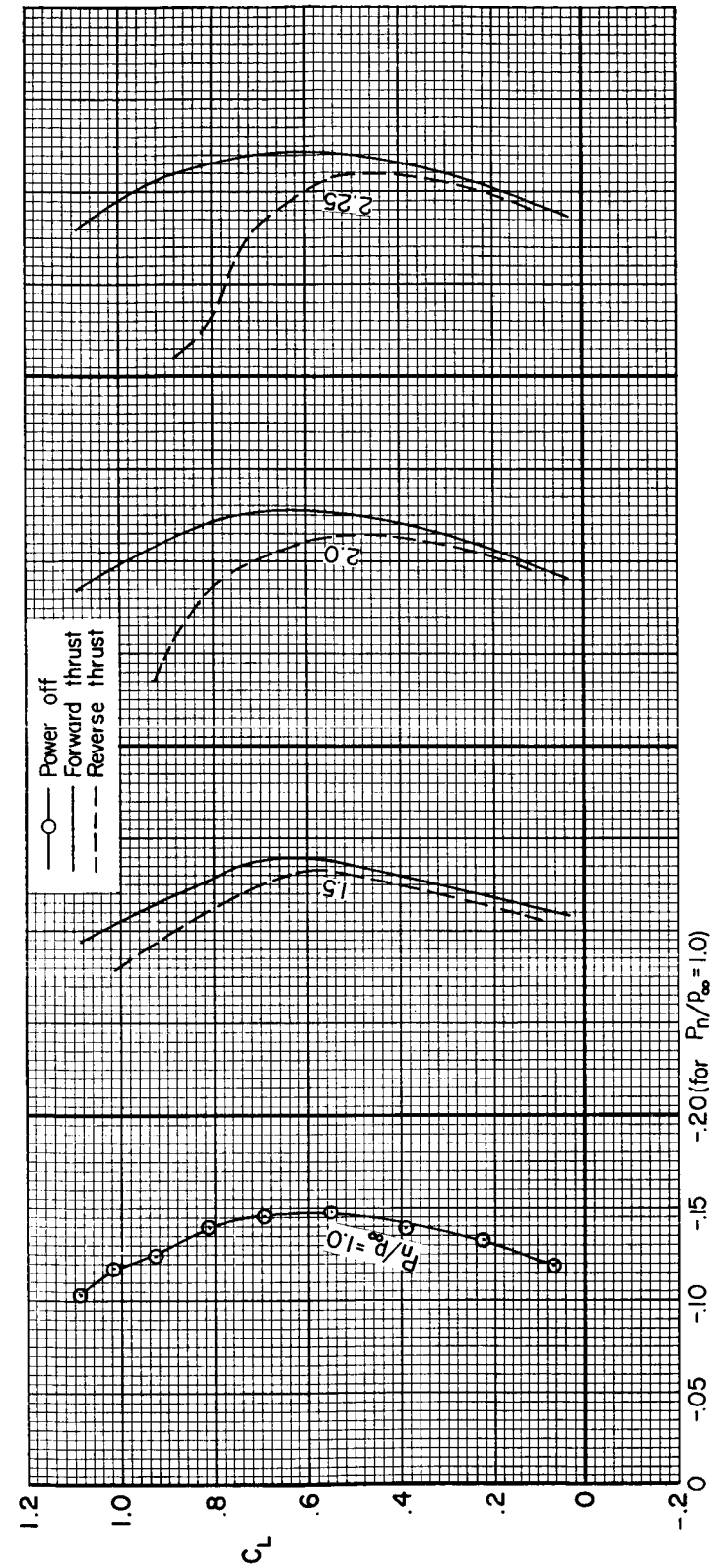

(c) C_m vs. C_L

Figure 19.- Concluded.

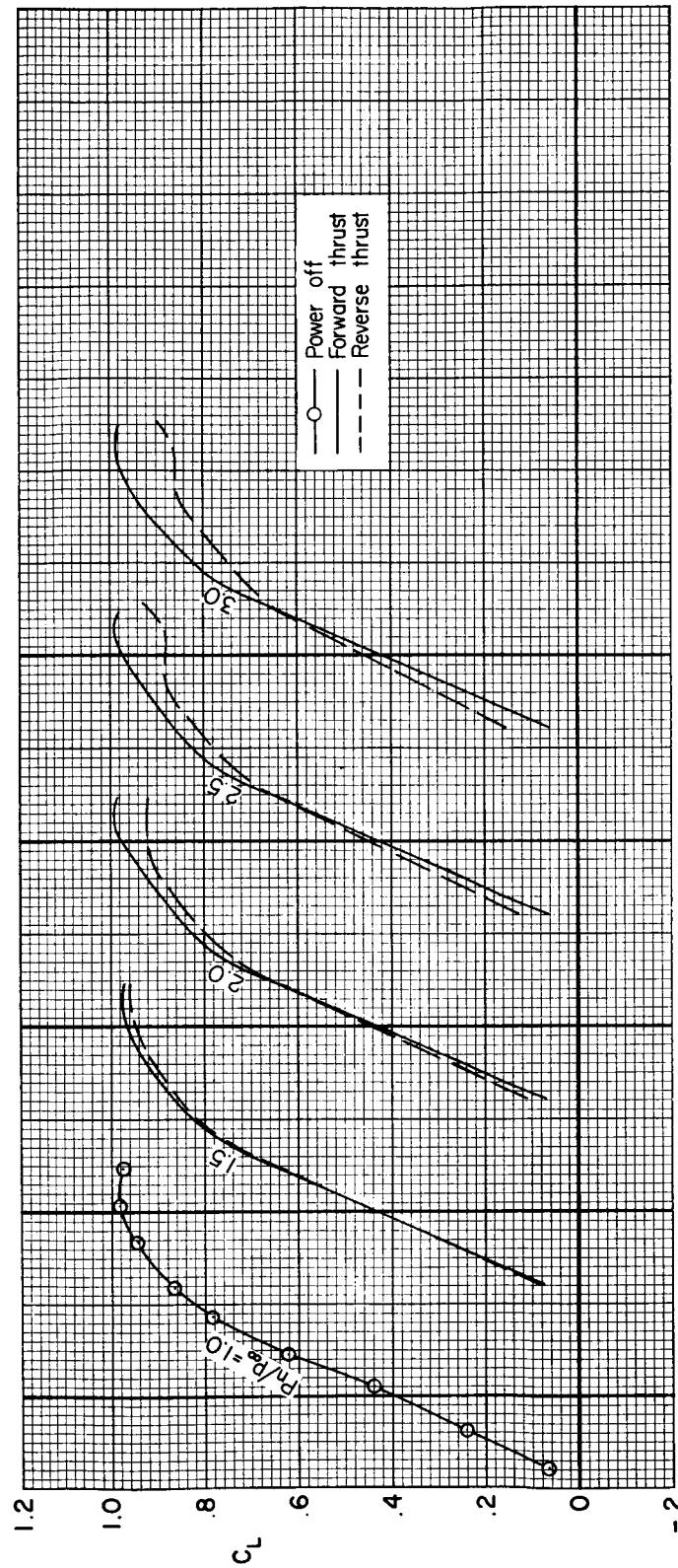

(a) C_L vs. α

Figure 20.- The effect of forward and reverse thrust on the longitudinal characteristics of the model; tail off, M = 0.70.

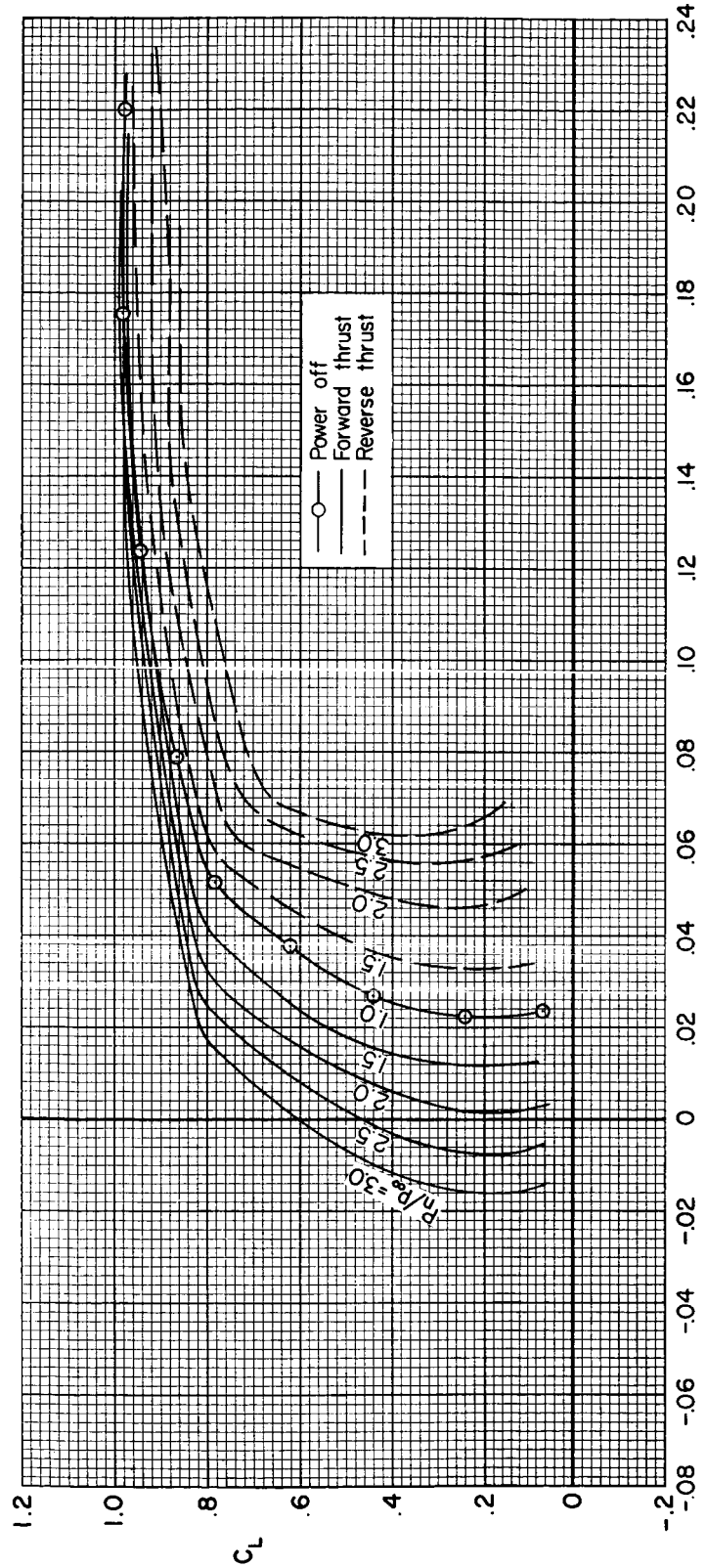

(b) C_X vs. C_L

Figure 20.- Continued.

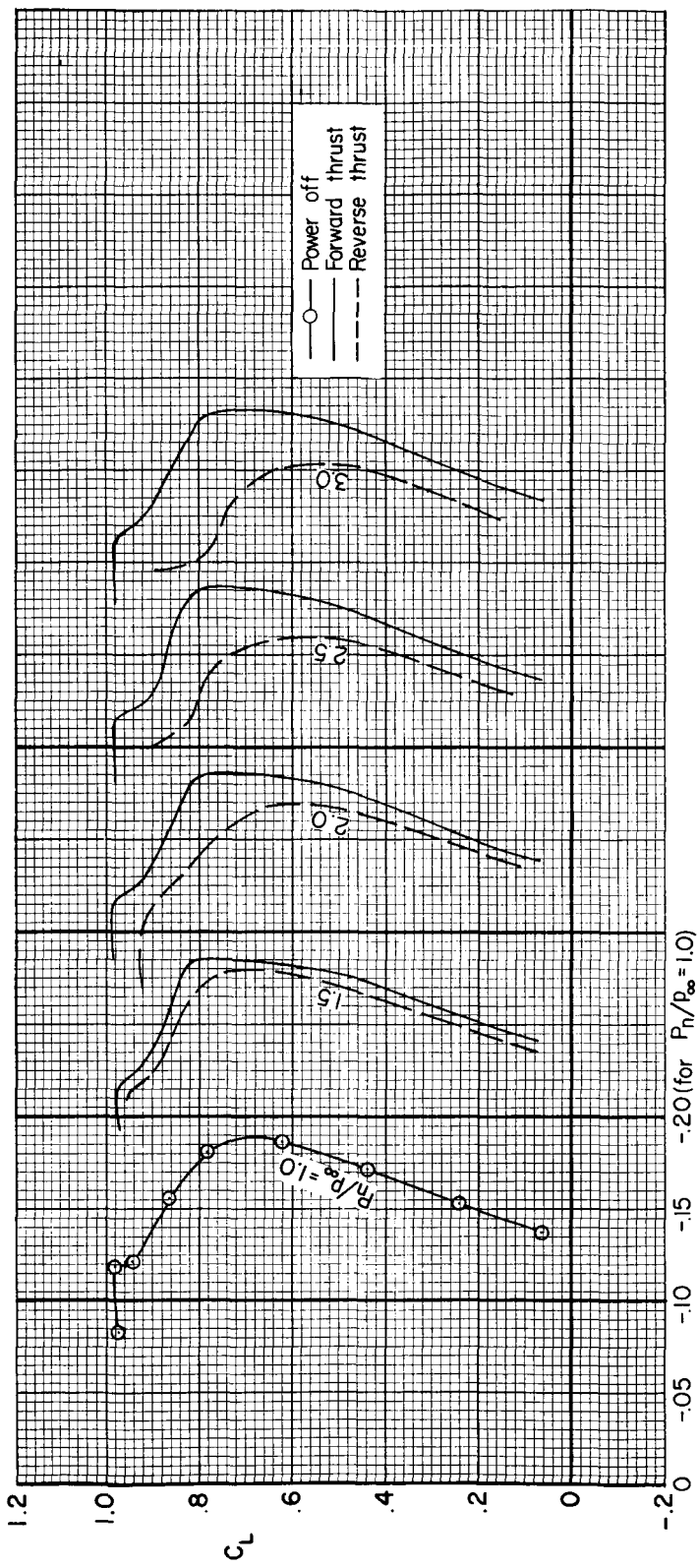

(c) C_m vs. C_L

Figure 20.- Concluded.

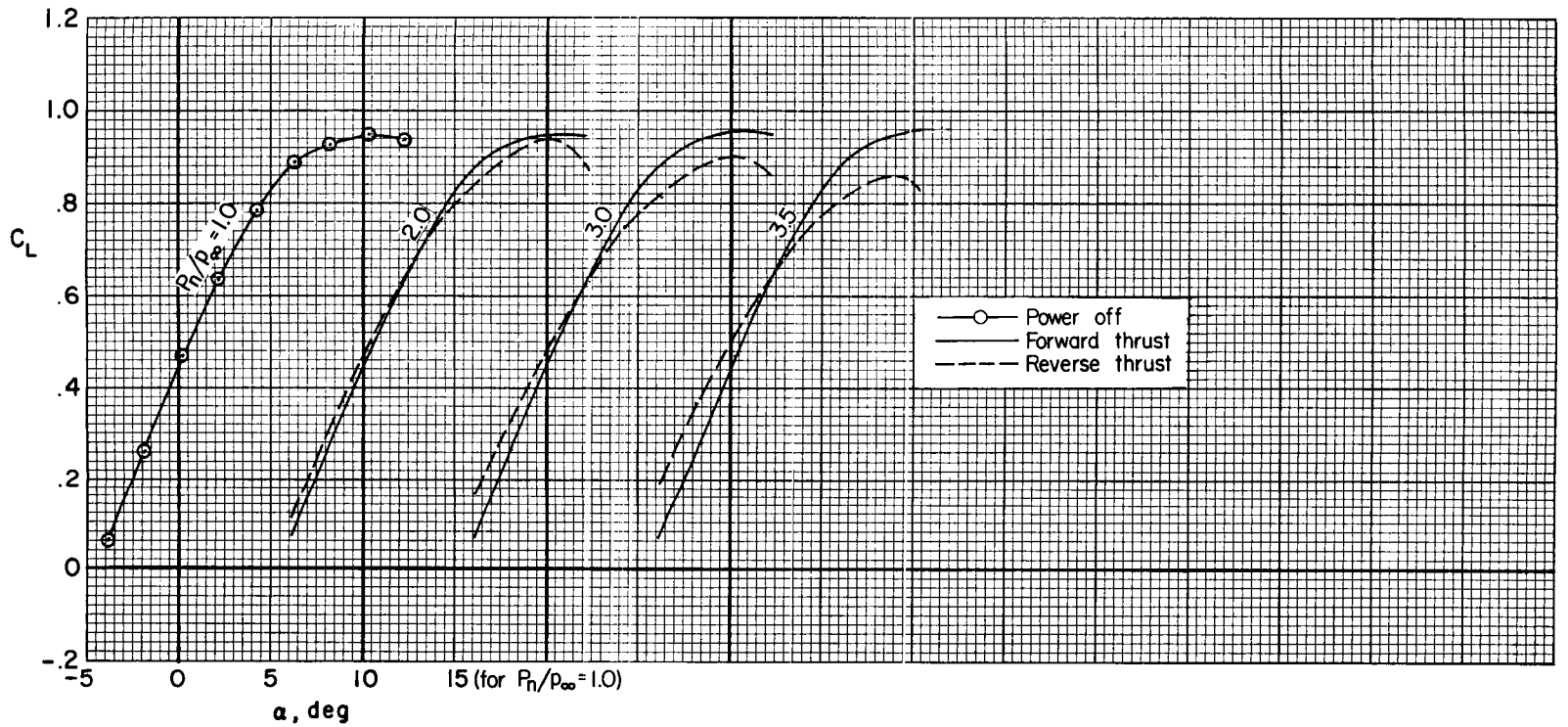

(a) C_L vs. α

Figure 21.- The effect of forward and reverse thrust on the longitudinal characteristics of the model; tail off, M = 0.80.

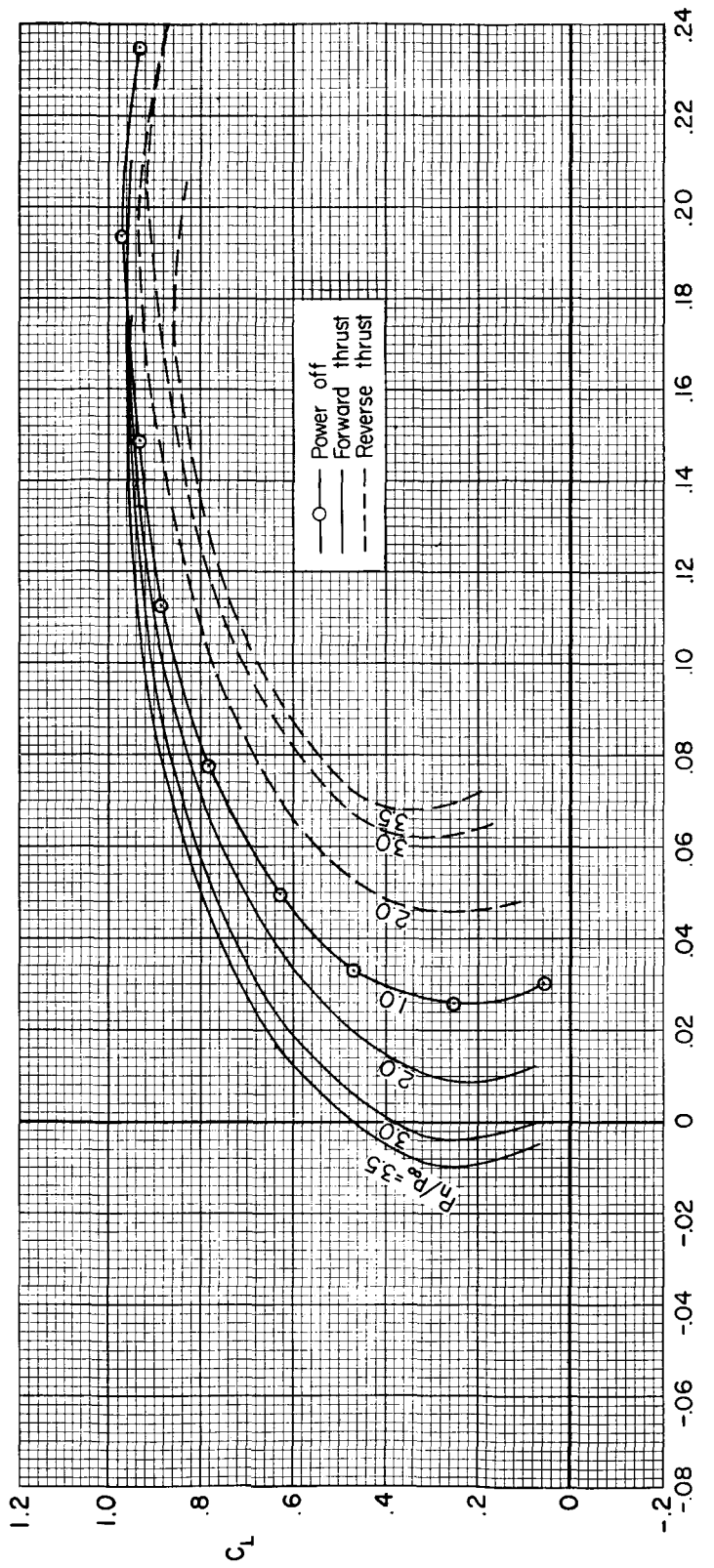

(b) C_X vs. C_L

Figure 21.- Continued.

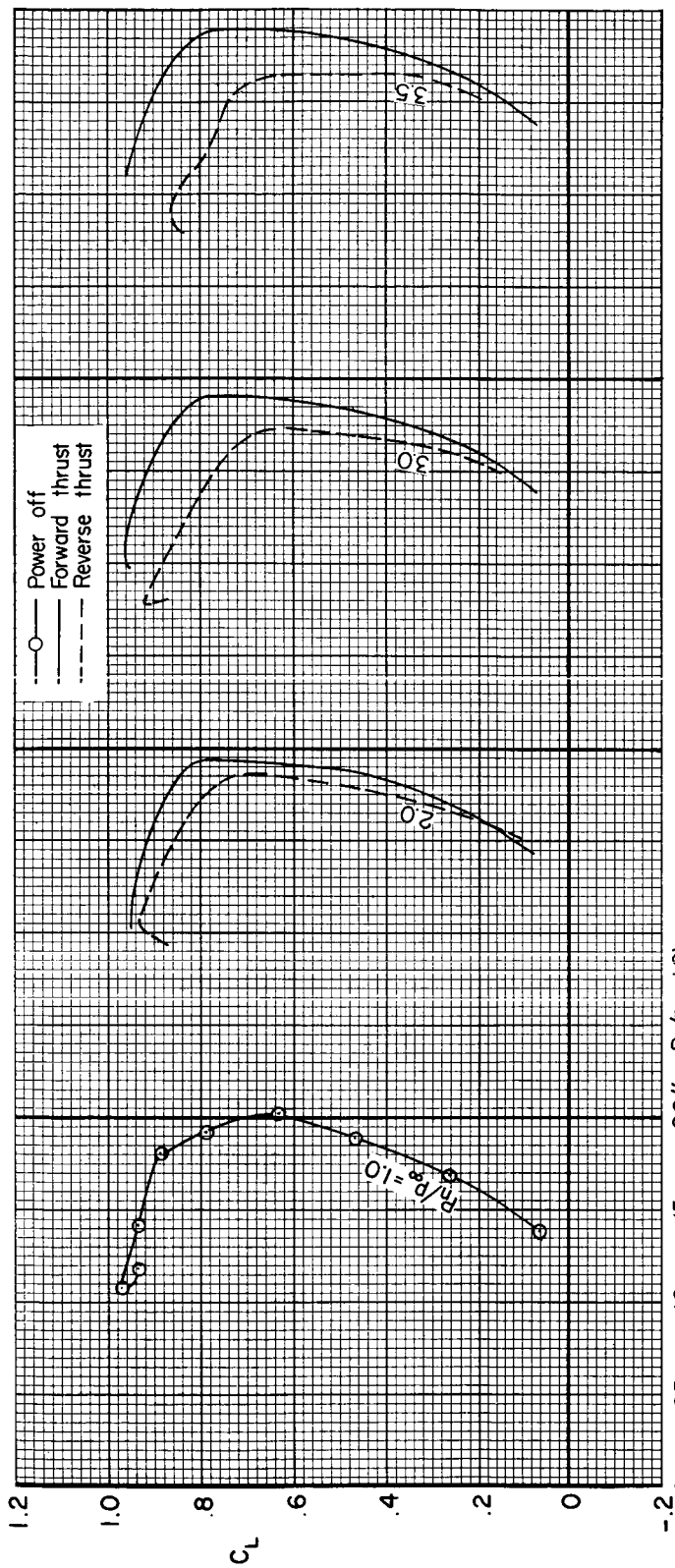

(c) C_m vs. C_L

Figure 21.- Concluded.

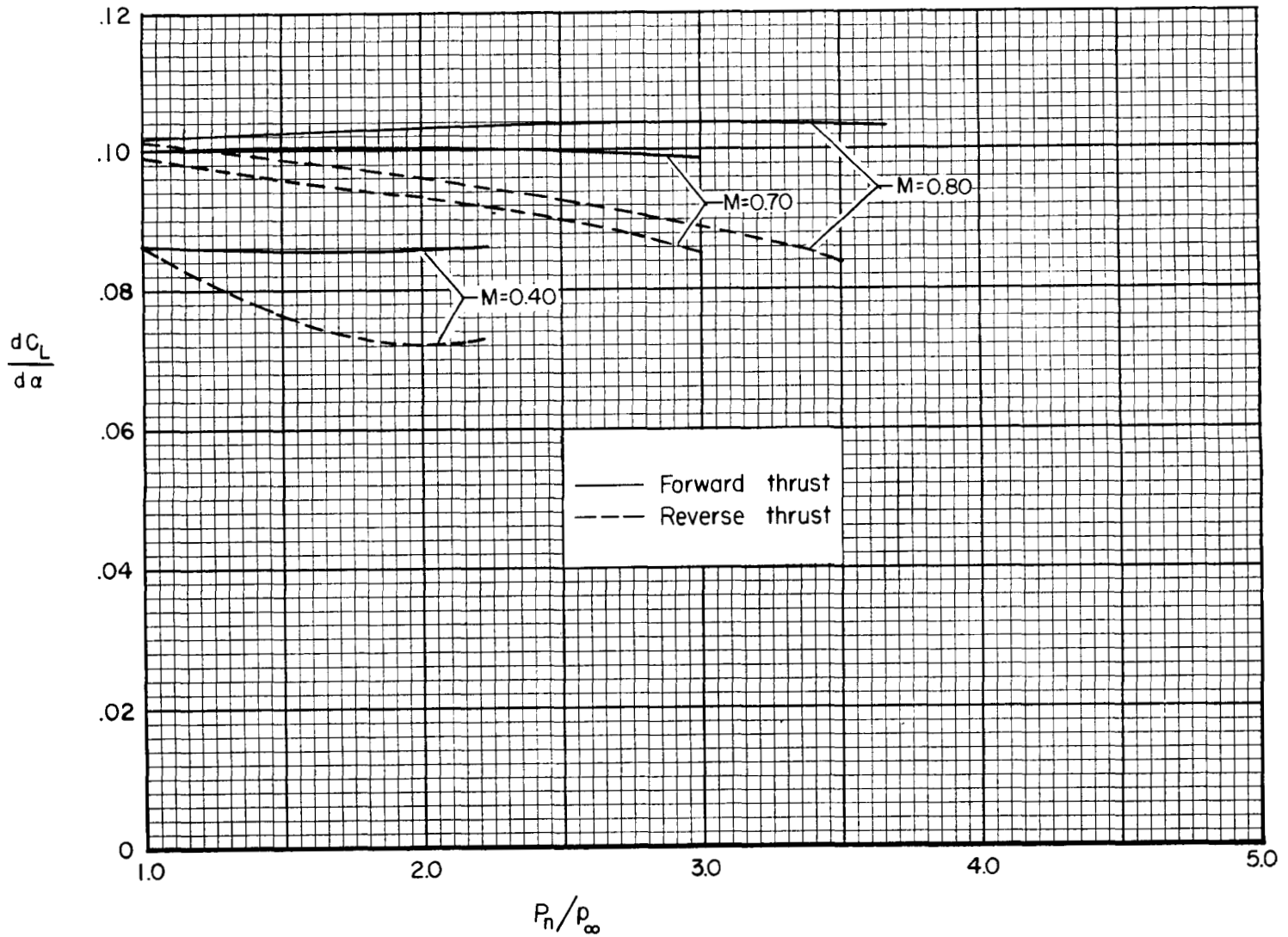

Figure 22.- The effect of forward and reverse thrust at several Mach numbers on the lift-curve slopes of the model; $C_L = 0.30$.

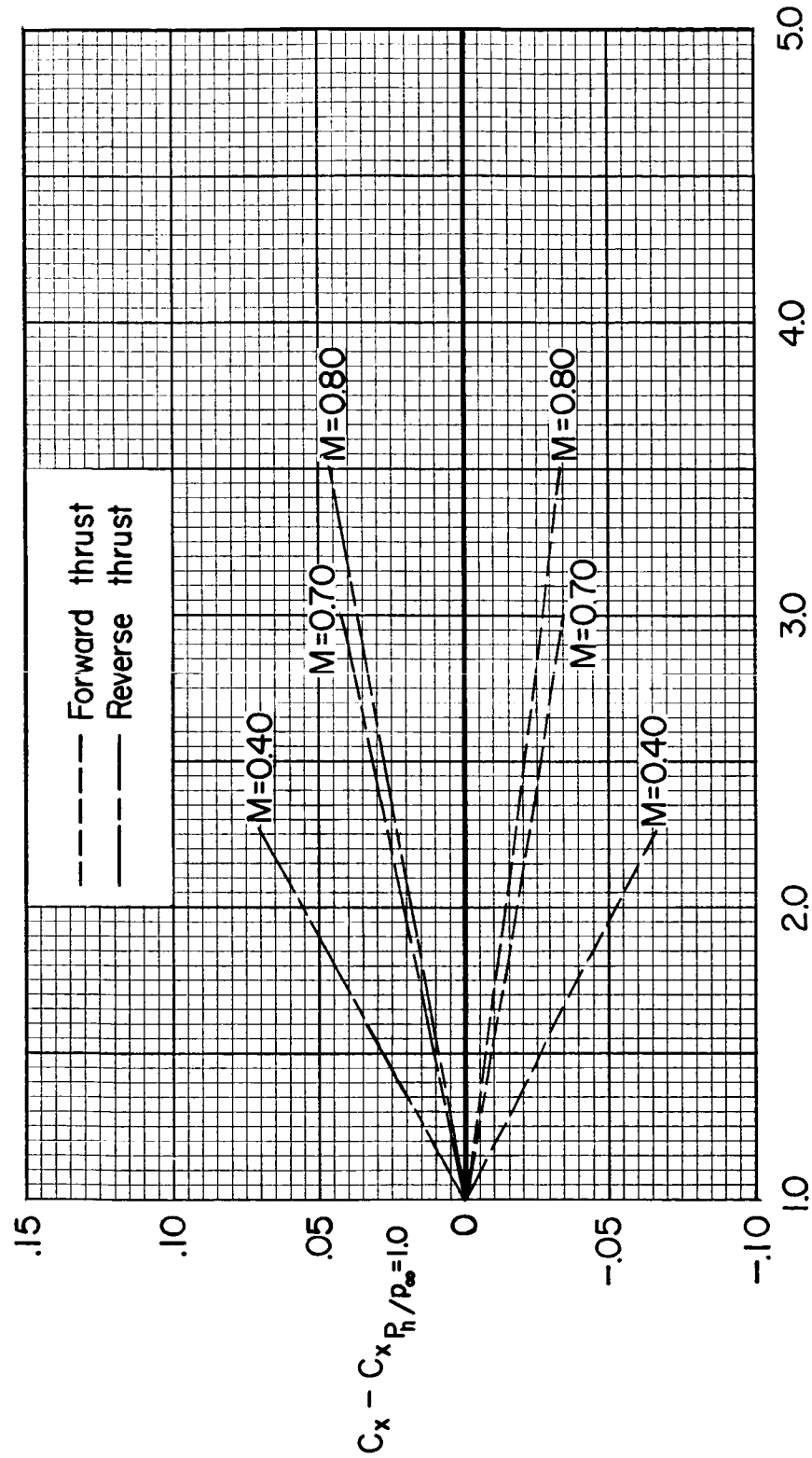

Figure 23.- The effect of forward and reverse thrust at several Mach numbers on the longitudinal-force coefficients of the model; $C_L = 0.30$.

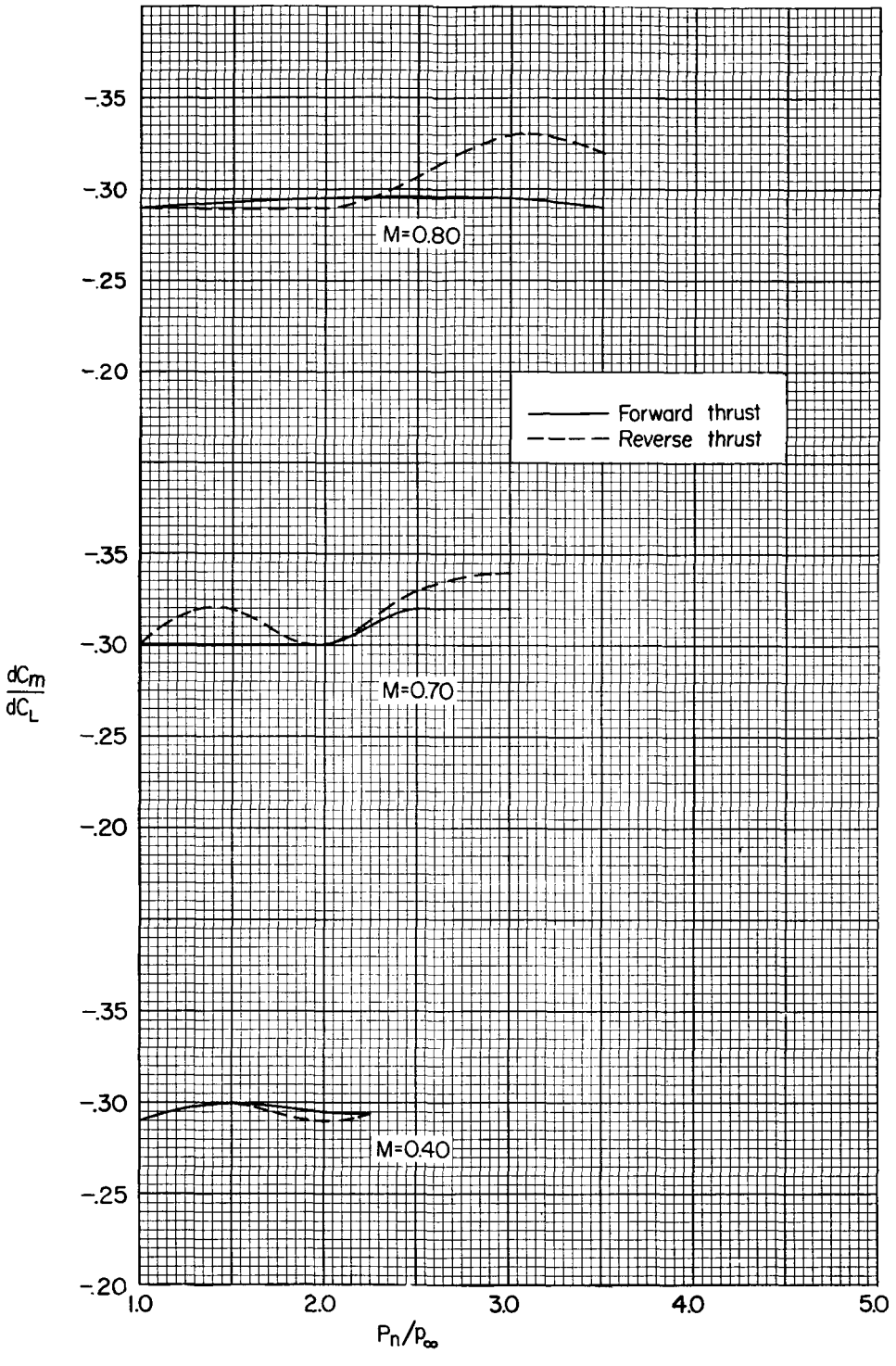

Figure 24.- The effect of forward and reverse thrust at several Mach numbers on the pitching-moment curve slopes of the model; $C_L = 0.30$.

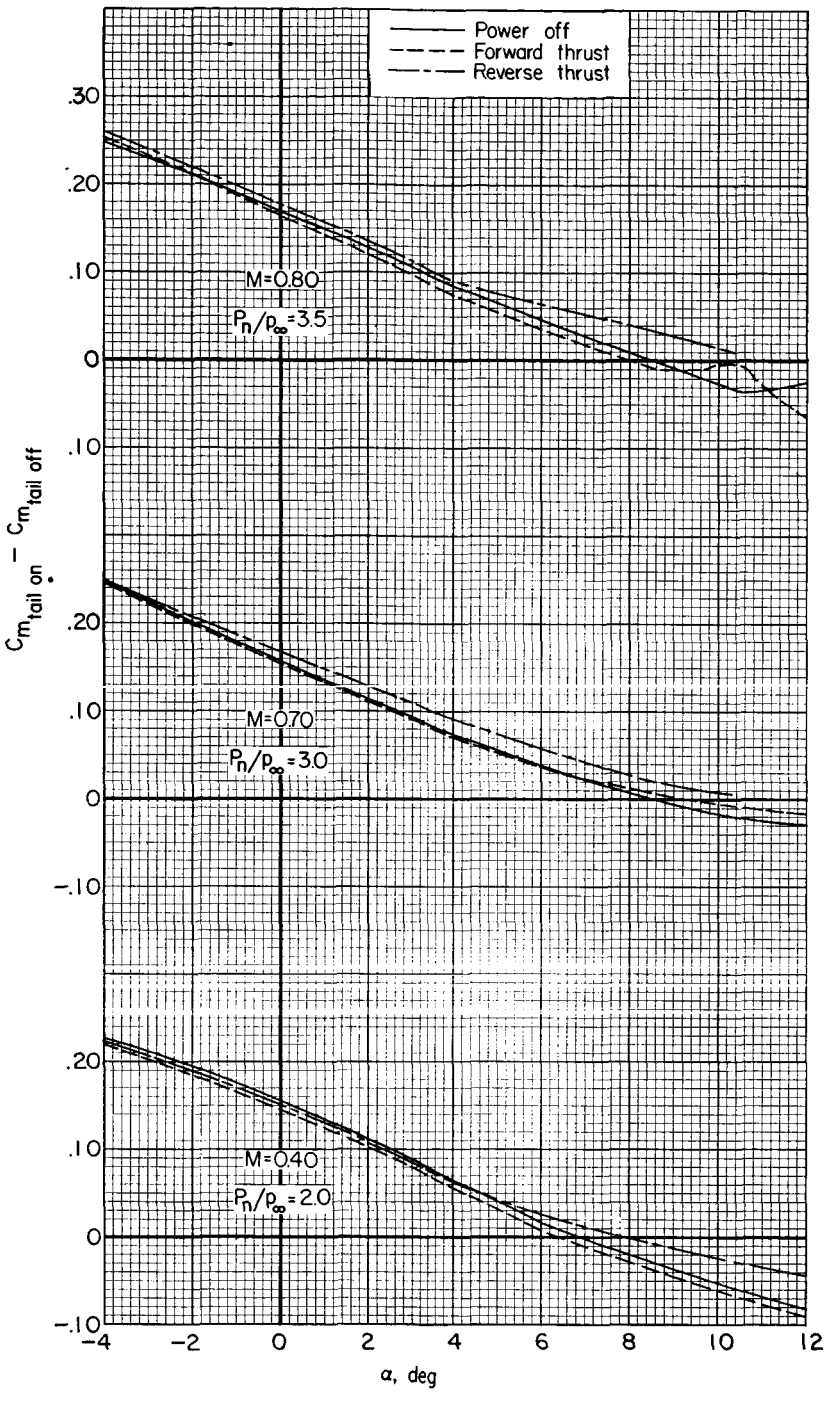

Figure 25.- The effect of forward and reverse thrust at several Mach numbers on the variation of the pitching-moment contribution of the horizontal tail with angle of attack; $i_t = -2^\circ$.

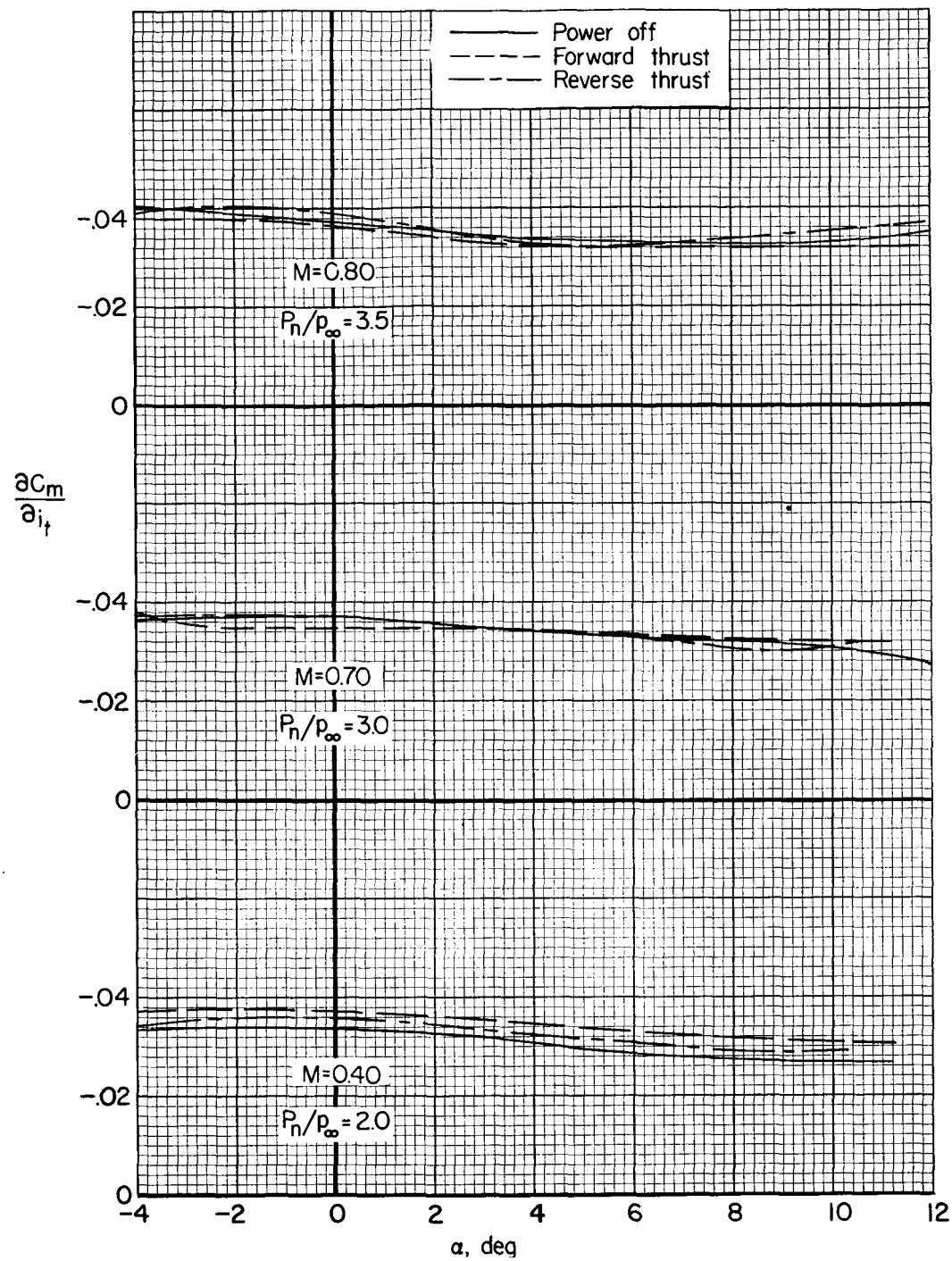

Figure 26.- The effect of forward and reverse thrust at several Mach numbers on the variation of tail-effectiveness parameter, $\partial C_m/\partial i_t$, with angle of attack.

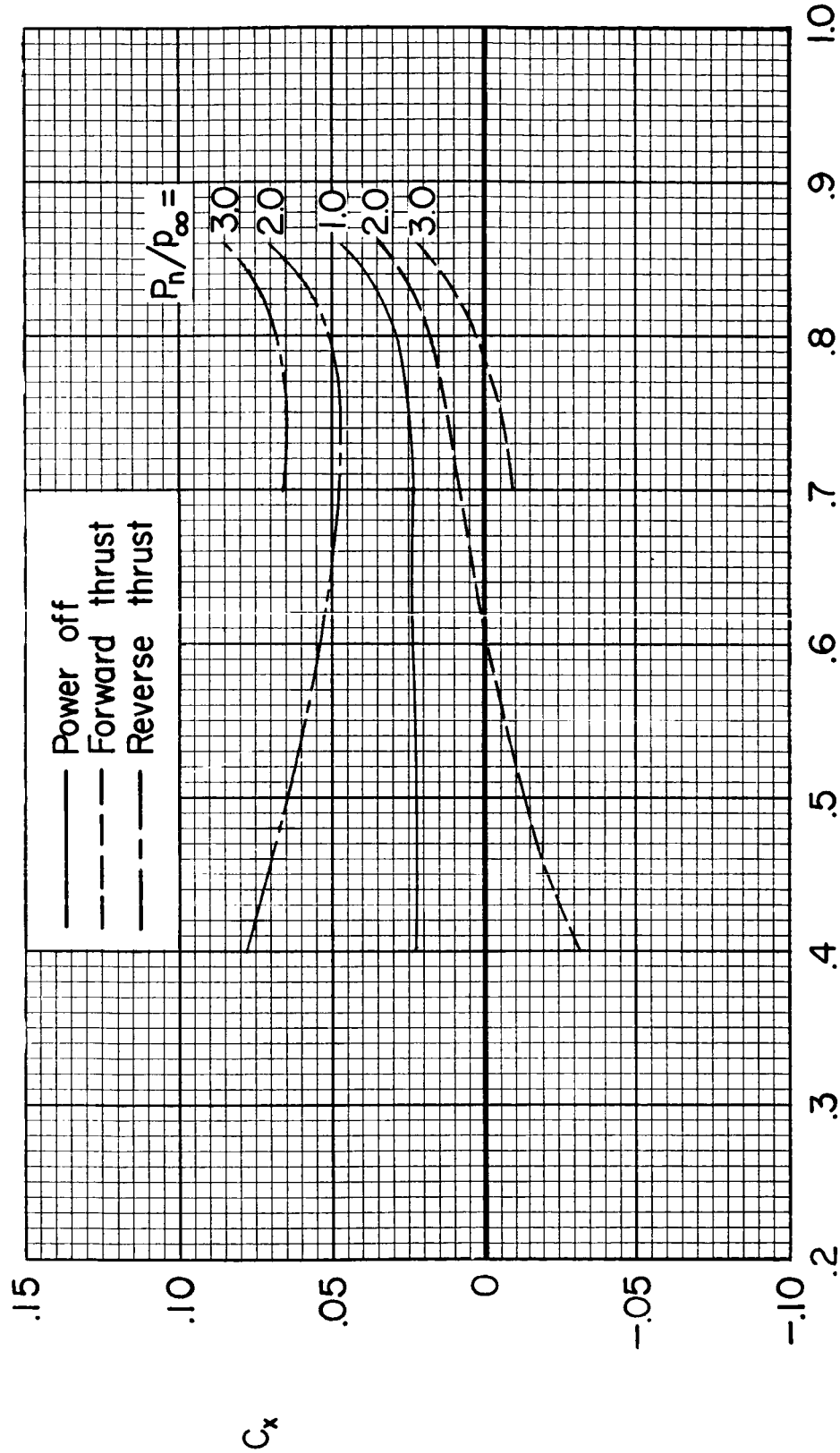

Figure 27.- The effect of Mach number at constant jet-pressure ratio on the longitudinal-force coefficients of the model for forward and reverse thrust; C_L = 0.30.

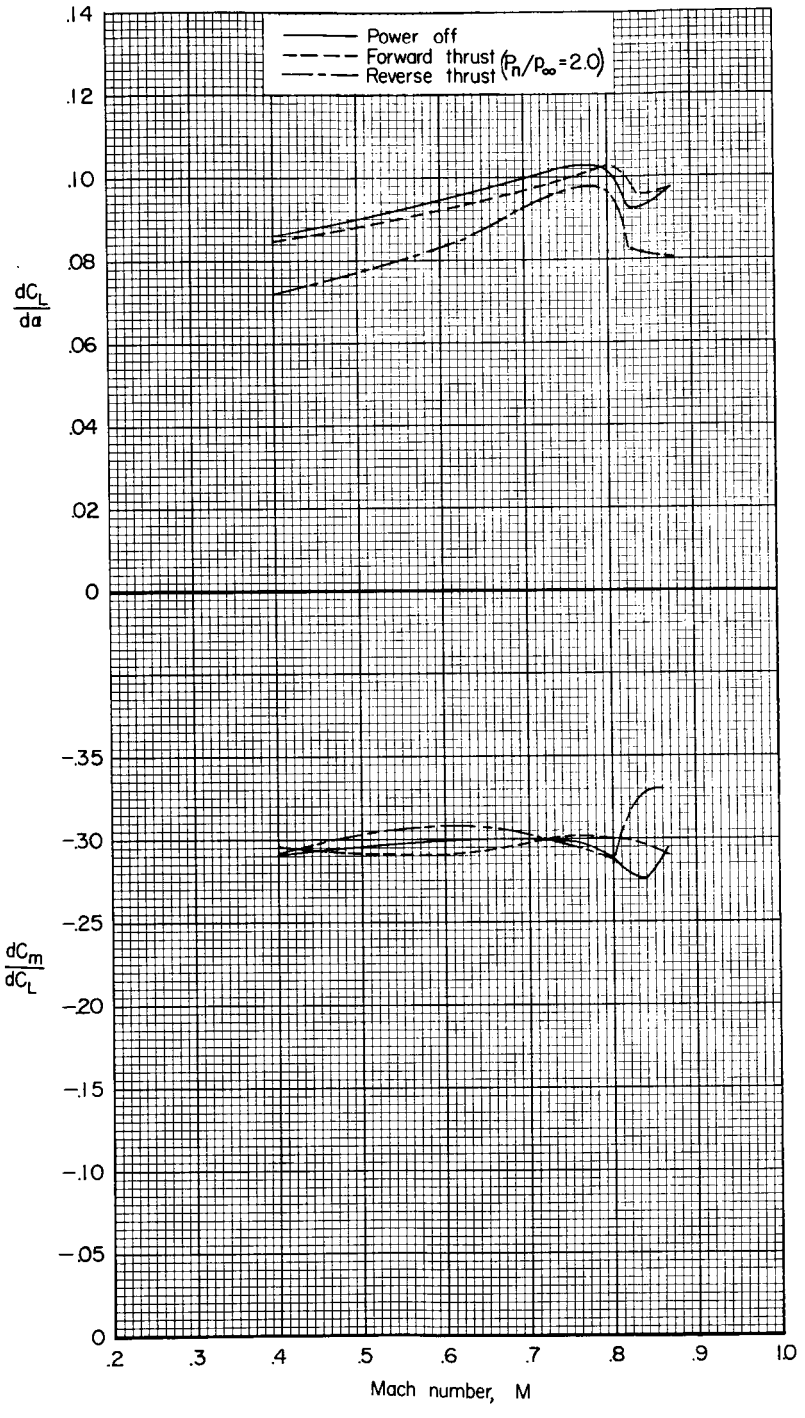

Figure 28.- The effect of Mach number at constant jet-pressure ratio on the slopes of the lift and pitching-moment curves for forward and reverse thrust; C_L = 0.30.

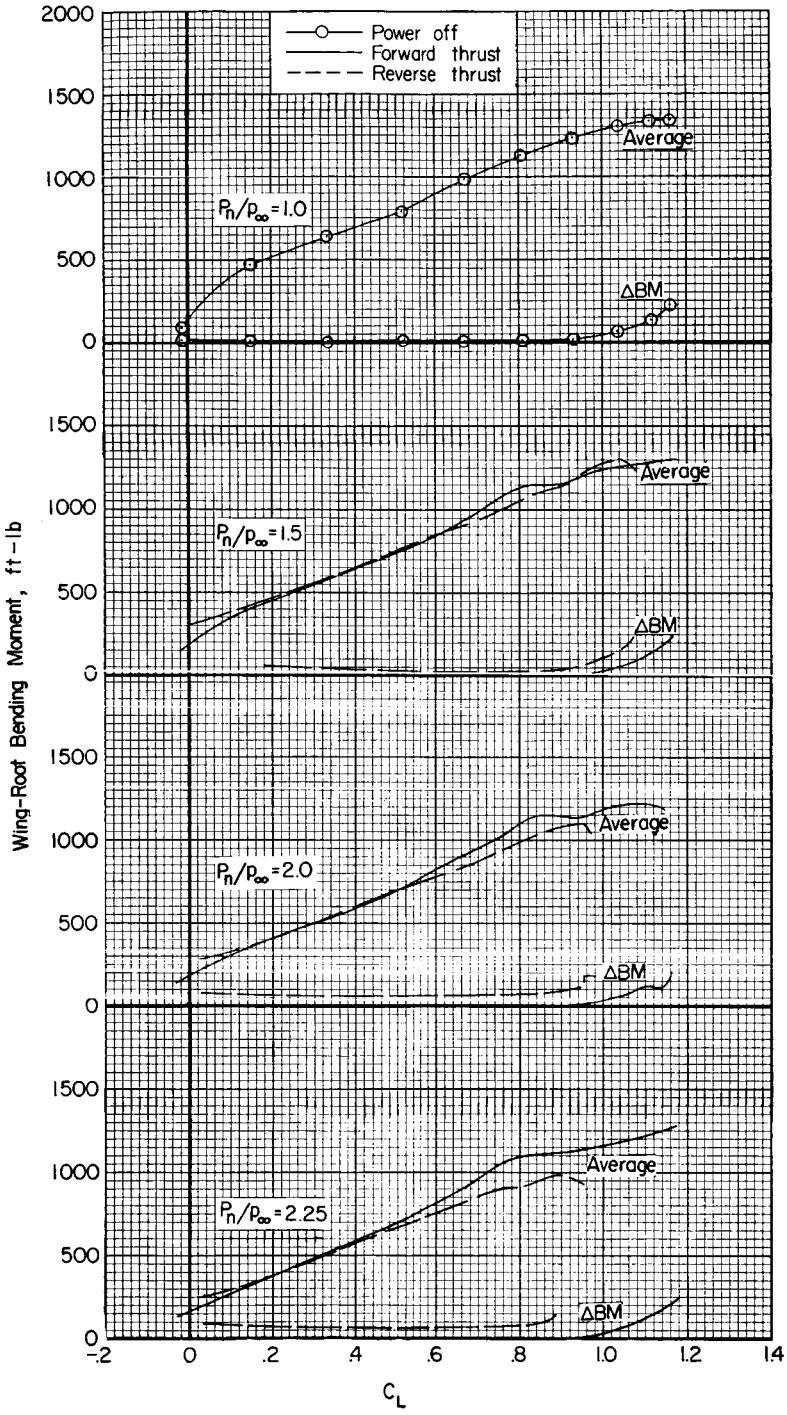

Figure 29.- The effect of forward and reverse thrust on the steady state and fluctuating bending moments of the wing; M = 0.40, q ≈ 126 psf.

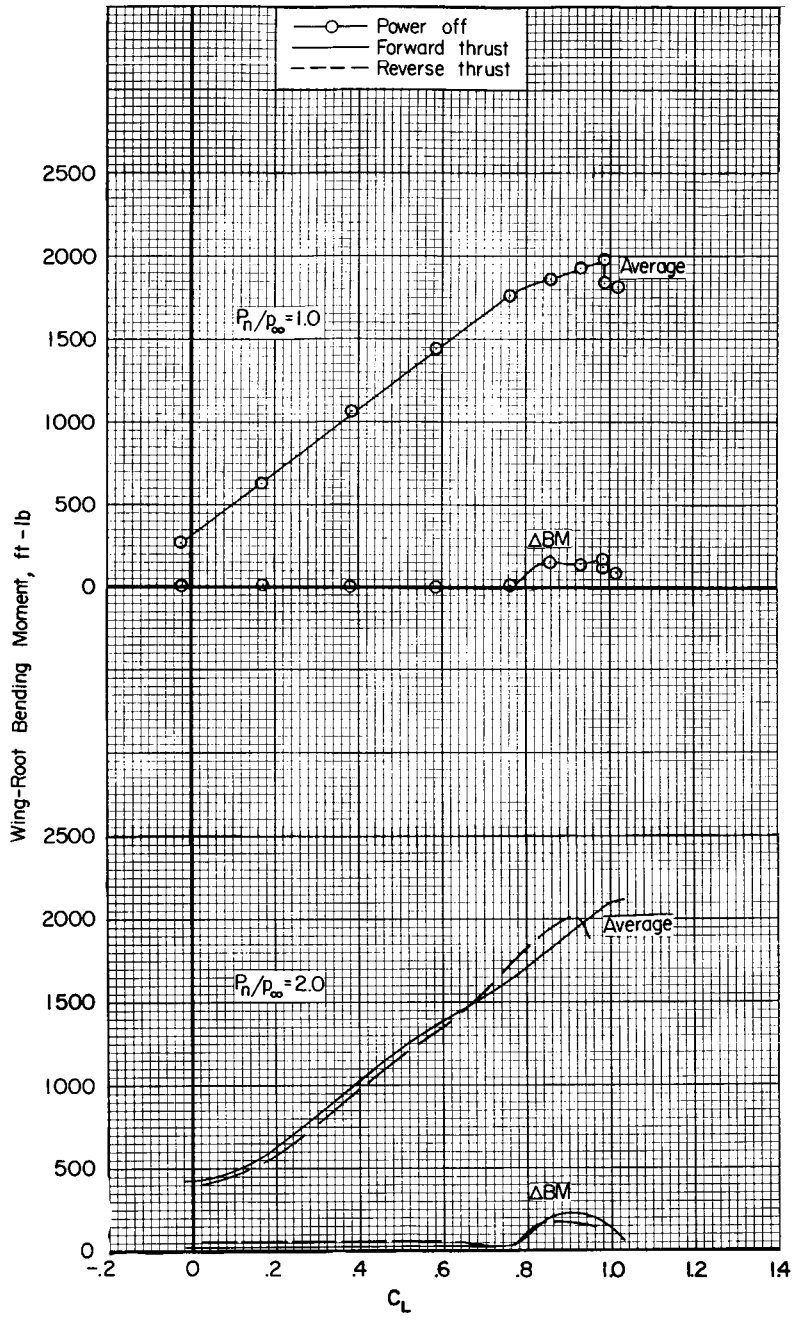

(a) P_n/p_∞ = 1.0, 2.0

Figure 30.- The effect of forward and reverse thrust on the steady state and fluctuating bending moments of the wing; M = 0.70, q ≈ 225 psf.

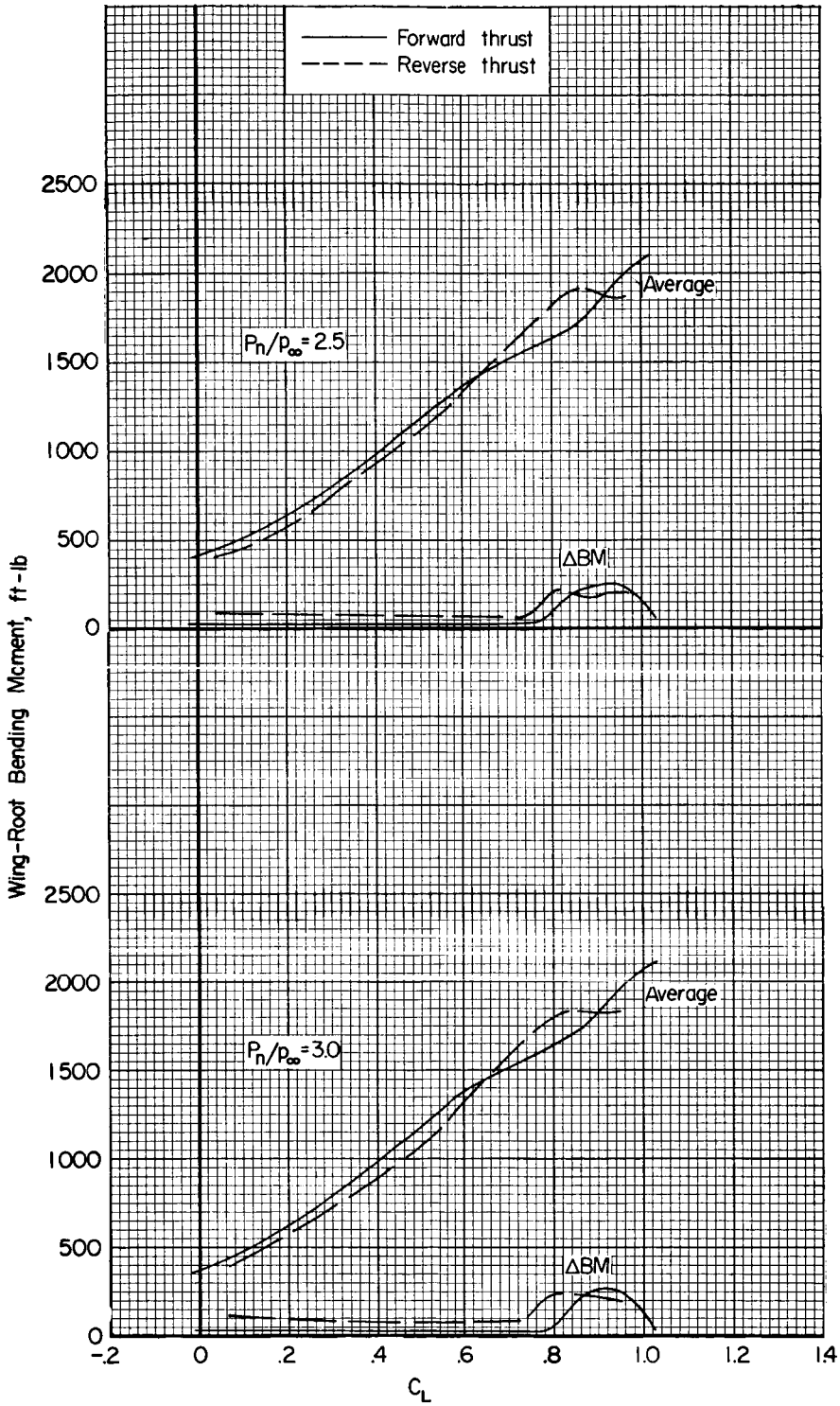

(b) $P_n/p_\infty = 2.5, 3.0$

Figure 30.- Concluded.

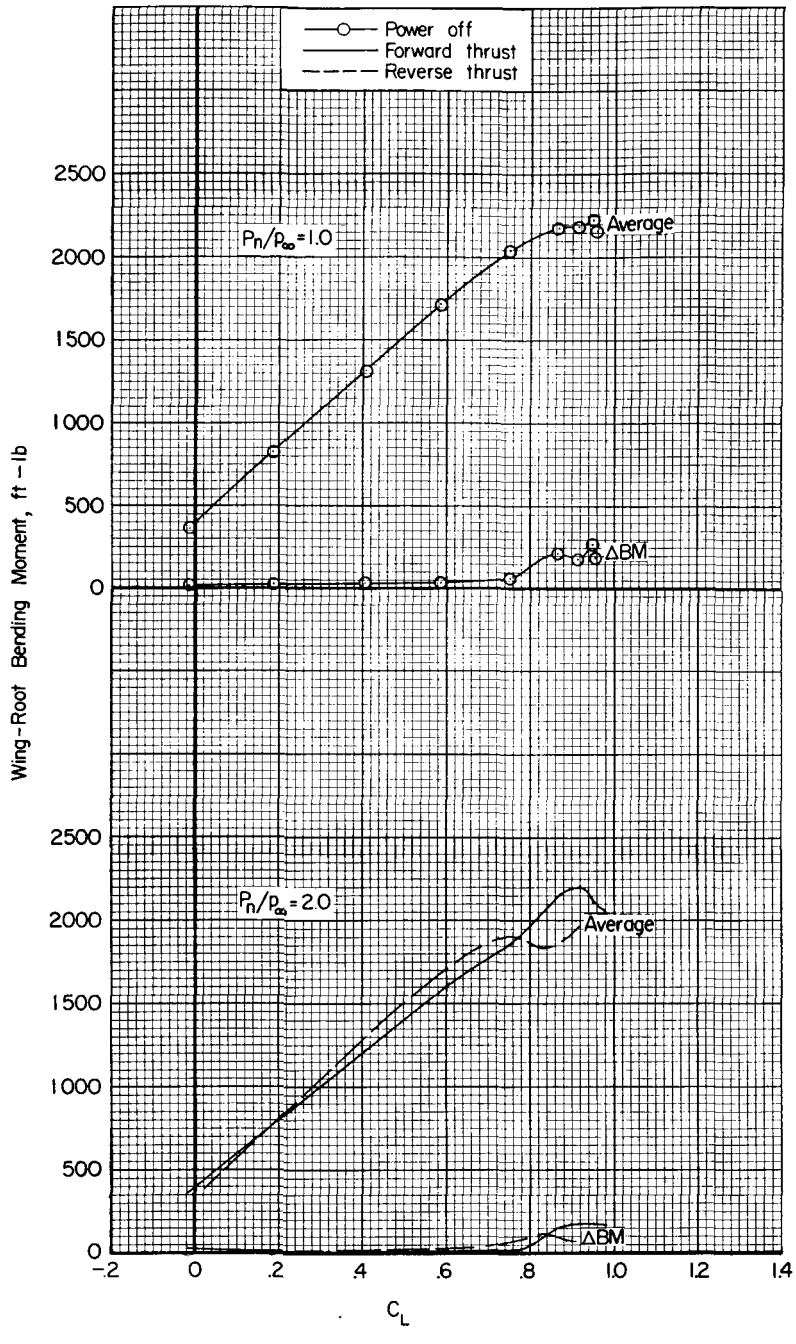

(a) P_n/p_∞ = 1.0, 2.0

Figure 31.- The effect of forward and reverse thrust on the steady state and fluctuating bending moments of the wing; M = 0.80, q ≈ 260 psf.

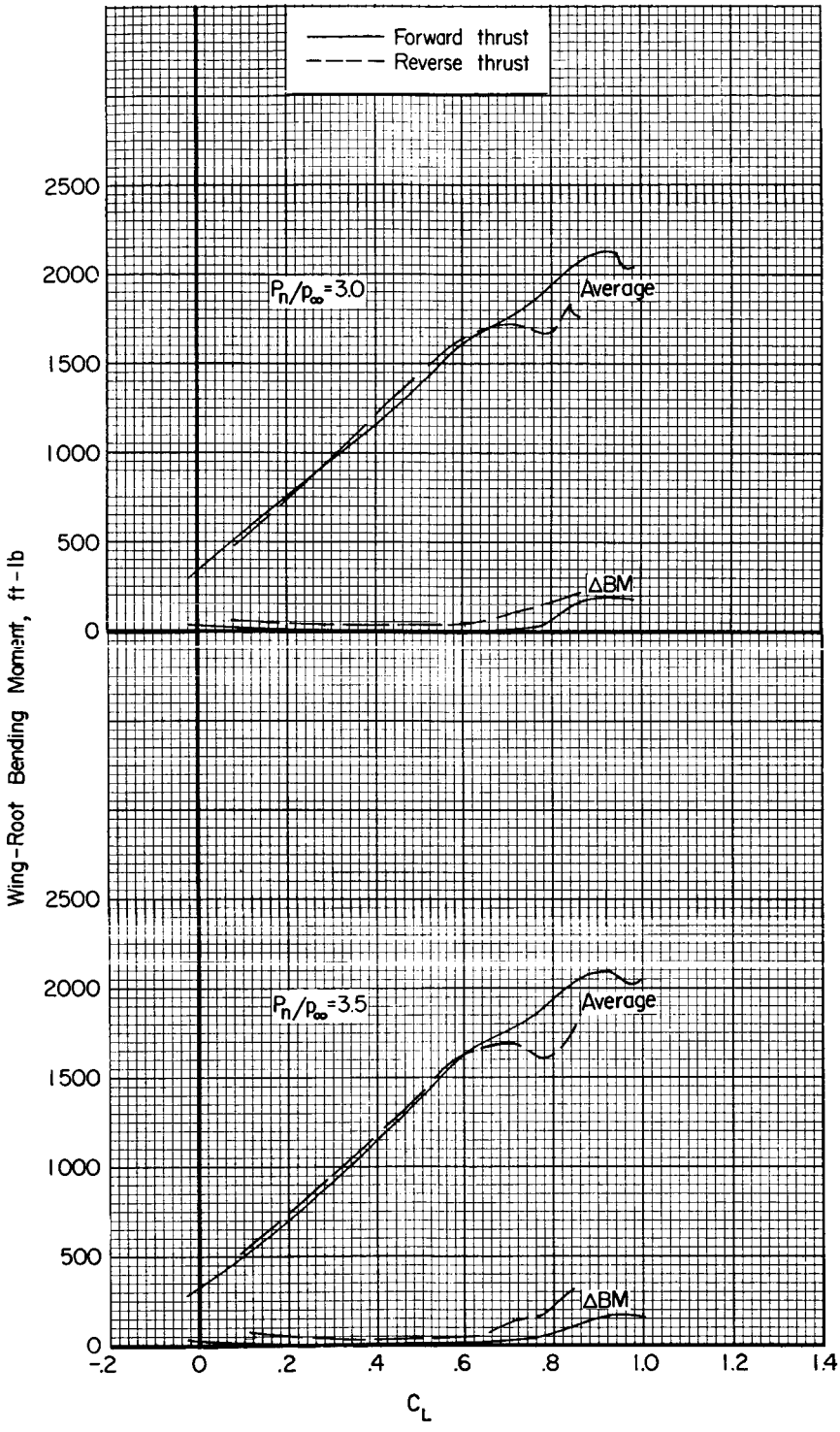

(b) P_n/p_∞ = 3.0, 3.5

Figure 31.- Concluded.

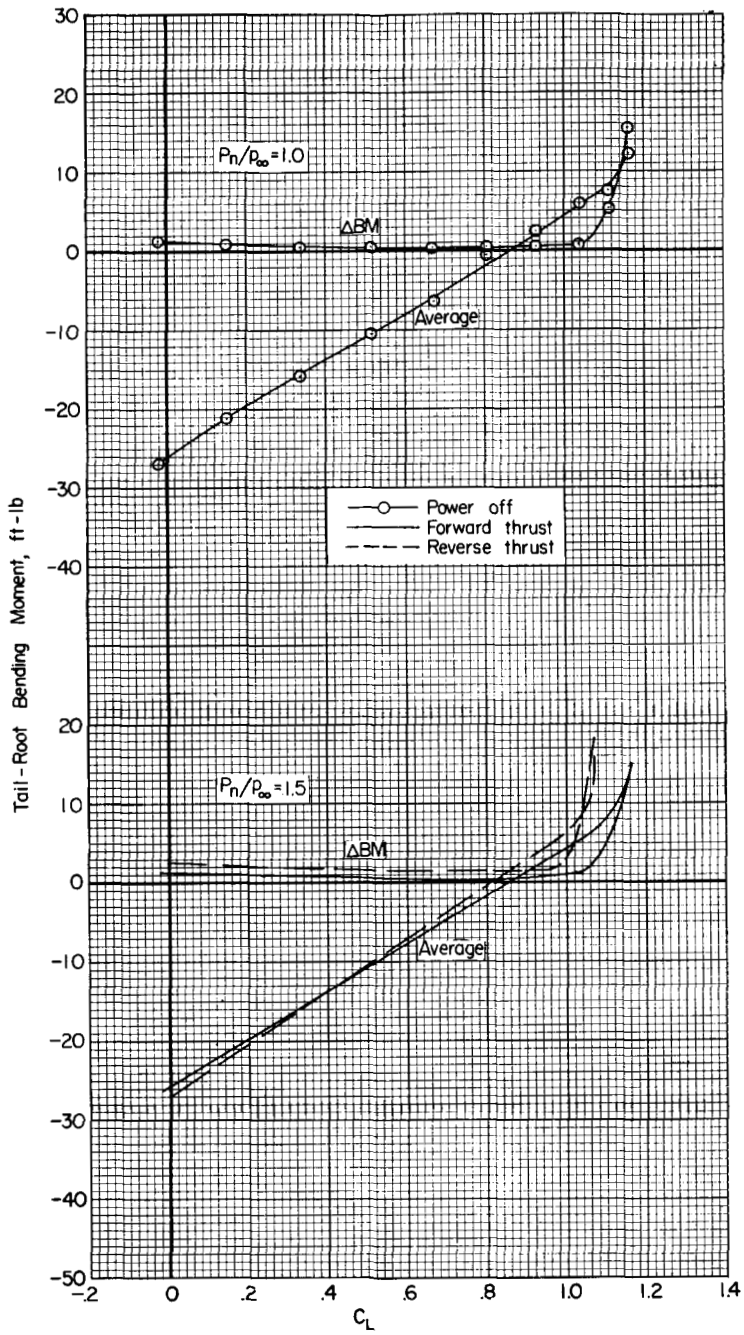

(a) P_n/p_∞ = 1.0, 1.5

Figure 32.- The effect of forward and reverse thrust on the steady state and fluctuating bending moments of the horizontal tail; M = 0.40, q ≈ 125 psf, $i_t = -2^\circ$.

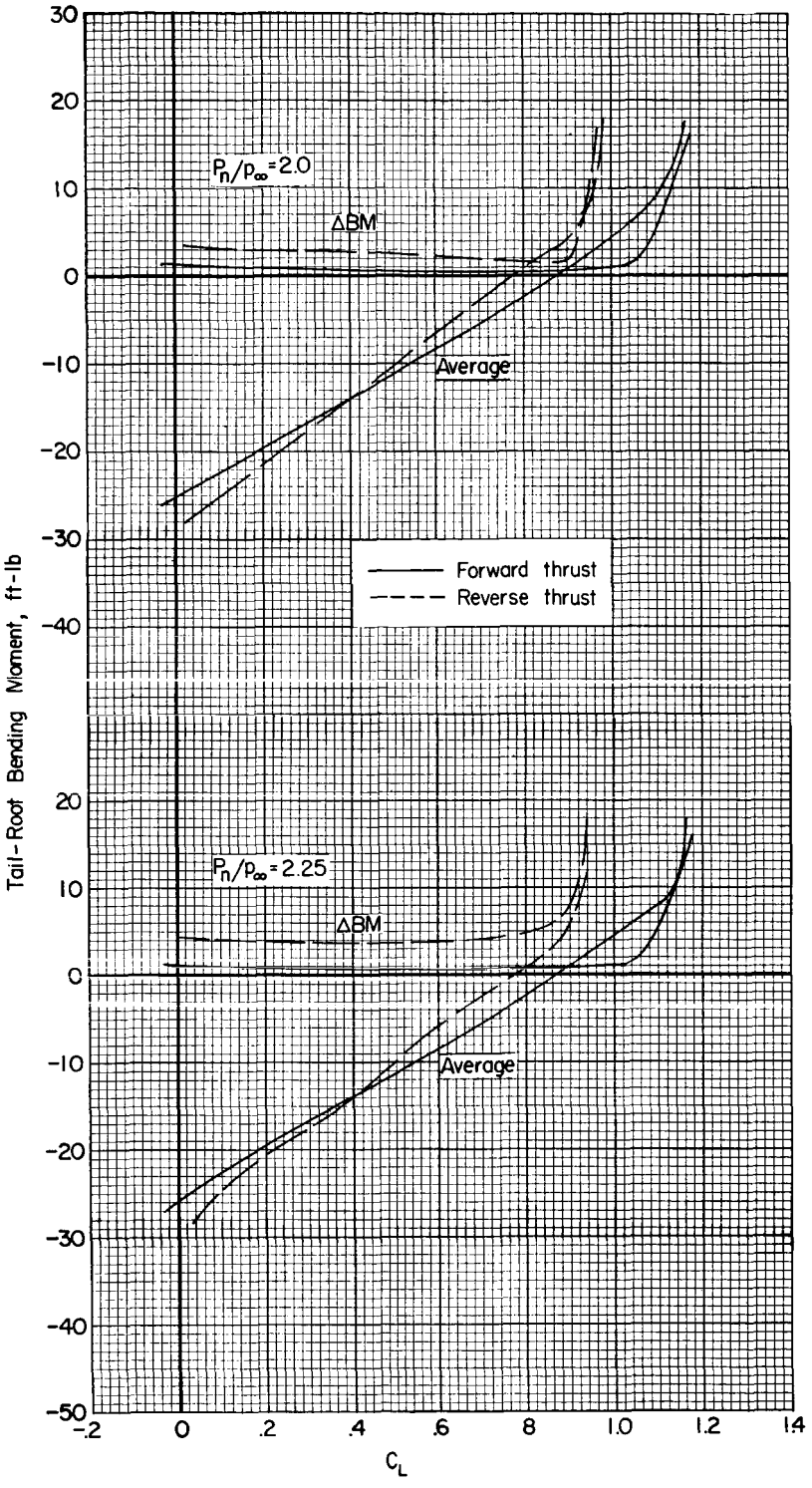

(b) P_n/p_∞ = 2.0, 2.25

Figure 32.- Concluded.

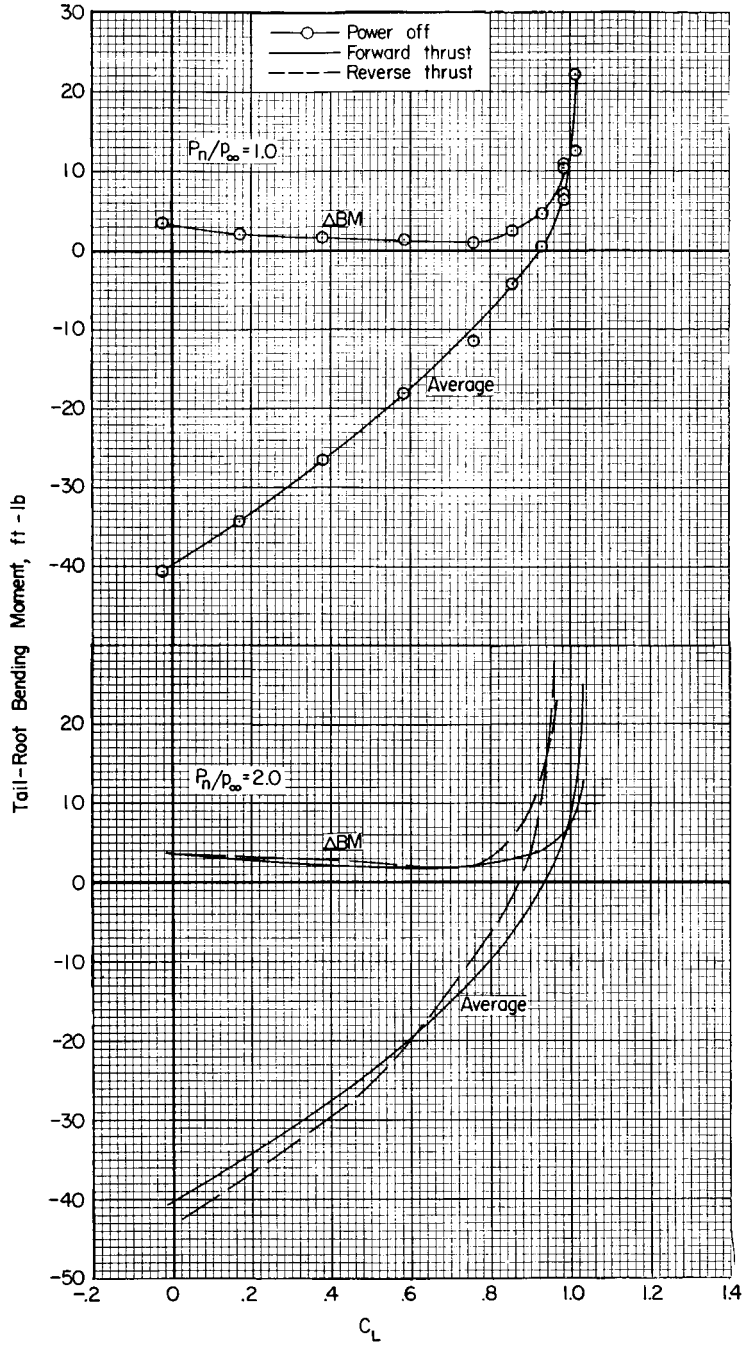

(a) P_n/P_∞ = 1.0, 2.0

Figure 33.- The effect of forward and reverse thrust on the steady state and fluctuating bending moments of the horizontal tail; M = 0.70, q ≈ 225 psf, $i_t = -2^\circ$.

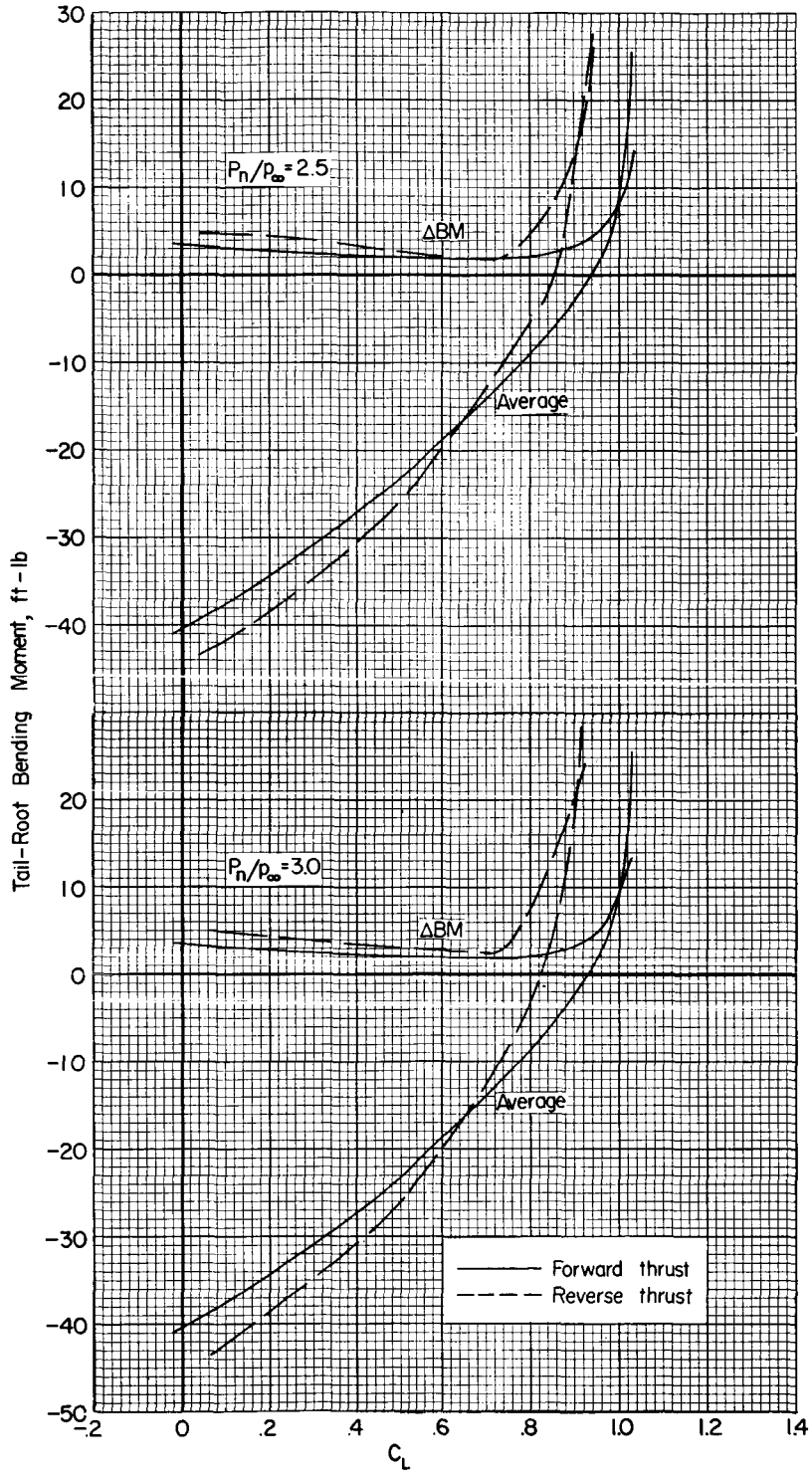

(b) P_n/p_∞ = 2.5, 3.0

Figure 33.- Concluded.

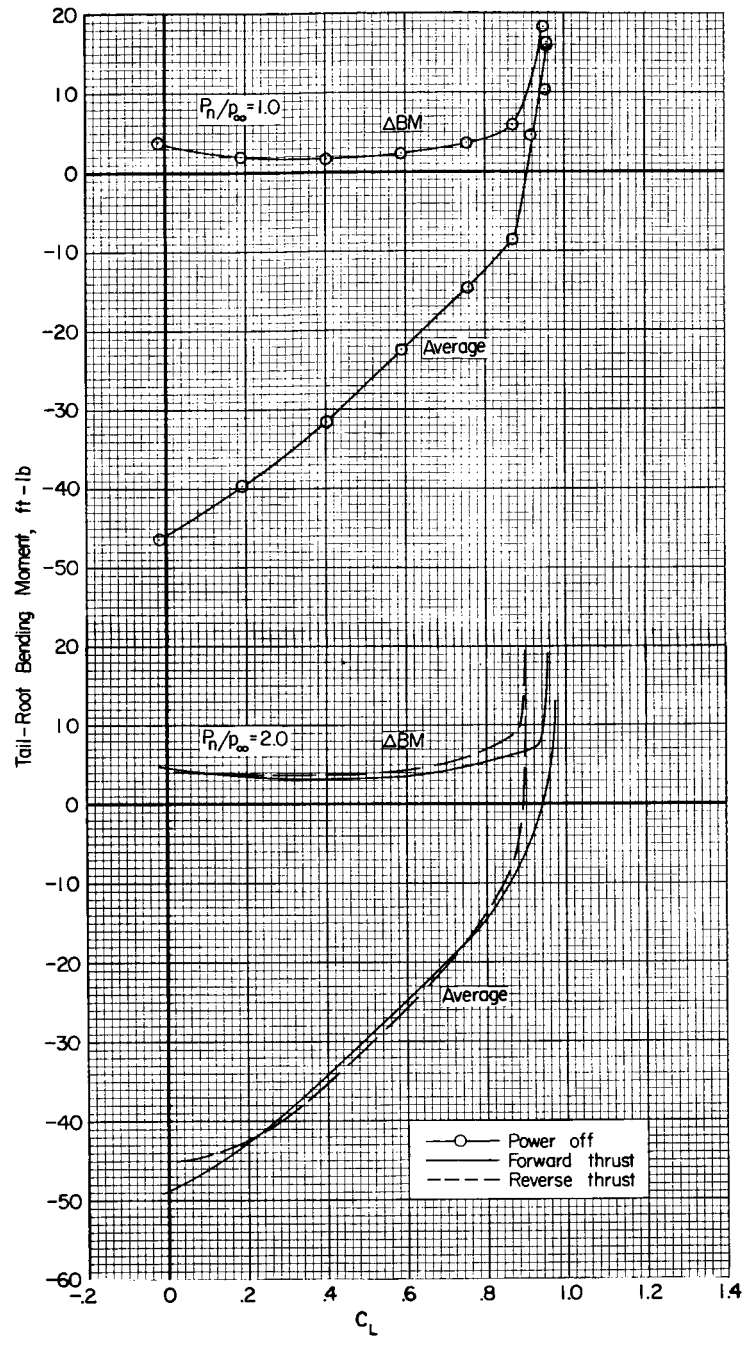

(a) P_n/p_∞ = 1.0, 2.0

Figure 34.- The effect of forward and reverse thrust on the steady state and fluctuating bending moments of the horizontal tail; M = 0.80, q ≈ 260 psf, i_t = -2°.

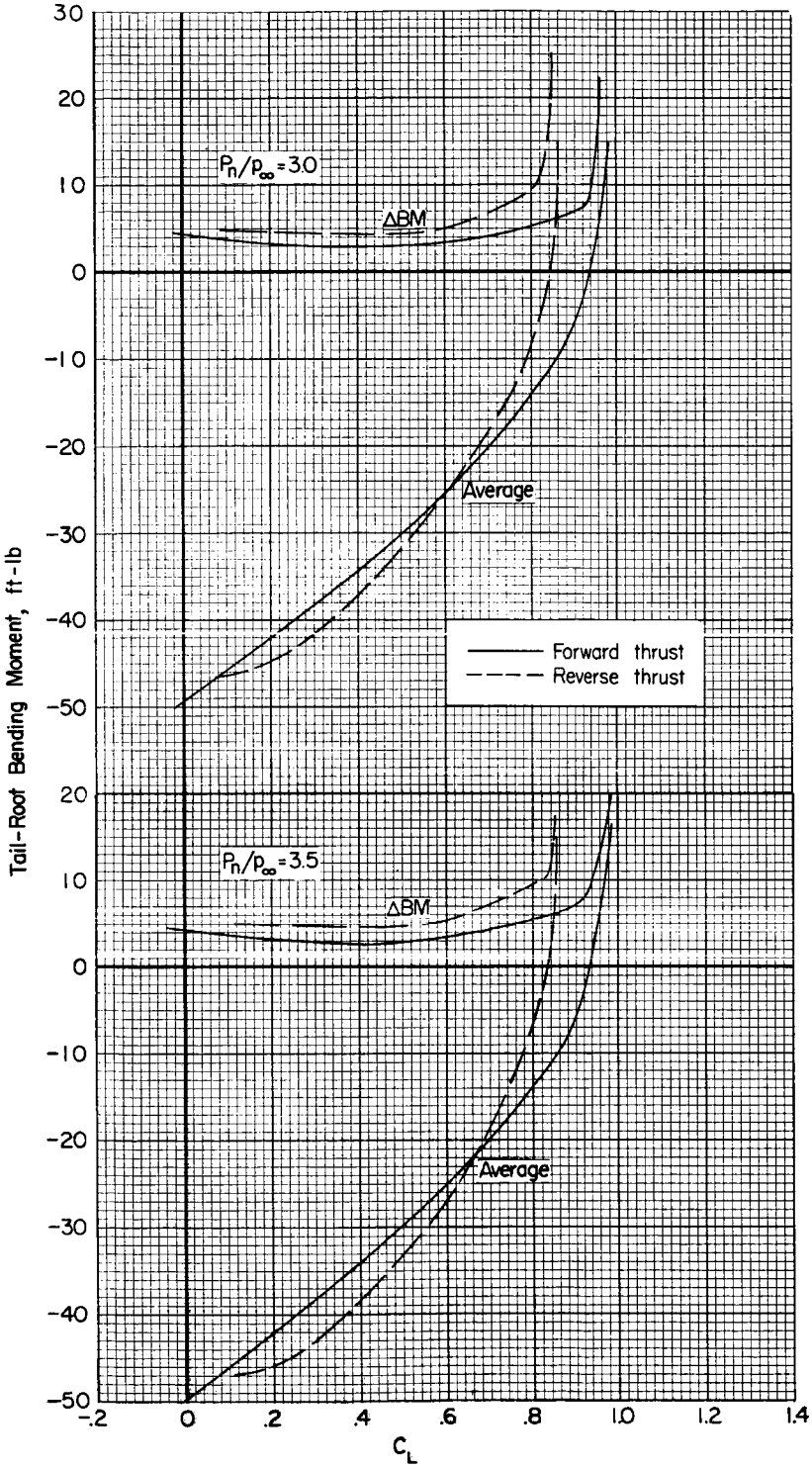

(b) P_n/p_∞ = 3.0, 3.5

Figure 34.- Concluded.

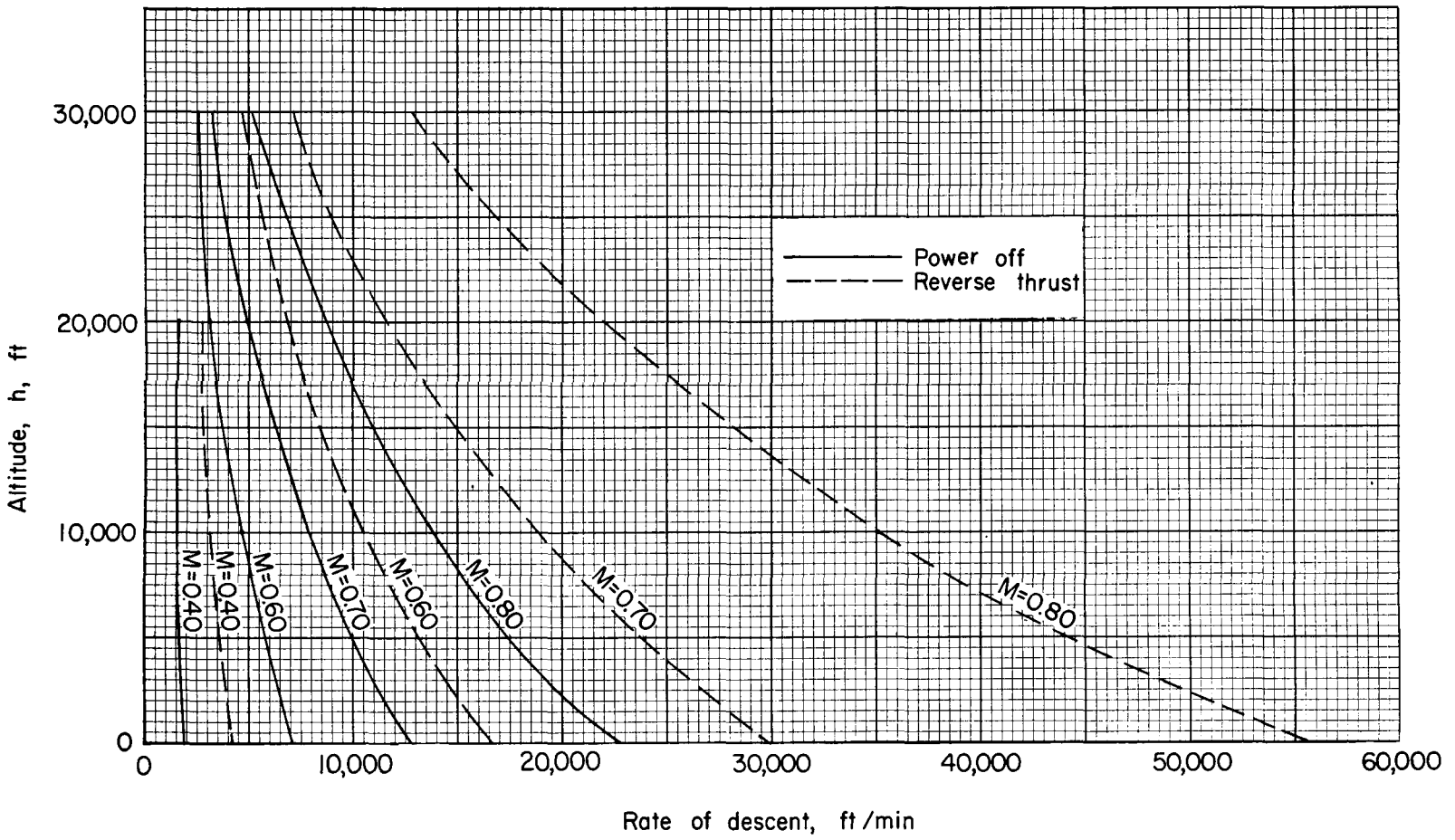

Figure 35.- The effect of reverse thrust on rates of descent at several constant Mach numbers for a hypothetical four-engine jet transport airplane; assumed weight = 200,000 lb; assumed wing area = 2,750 sq ft.

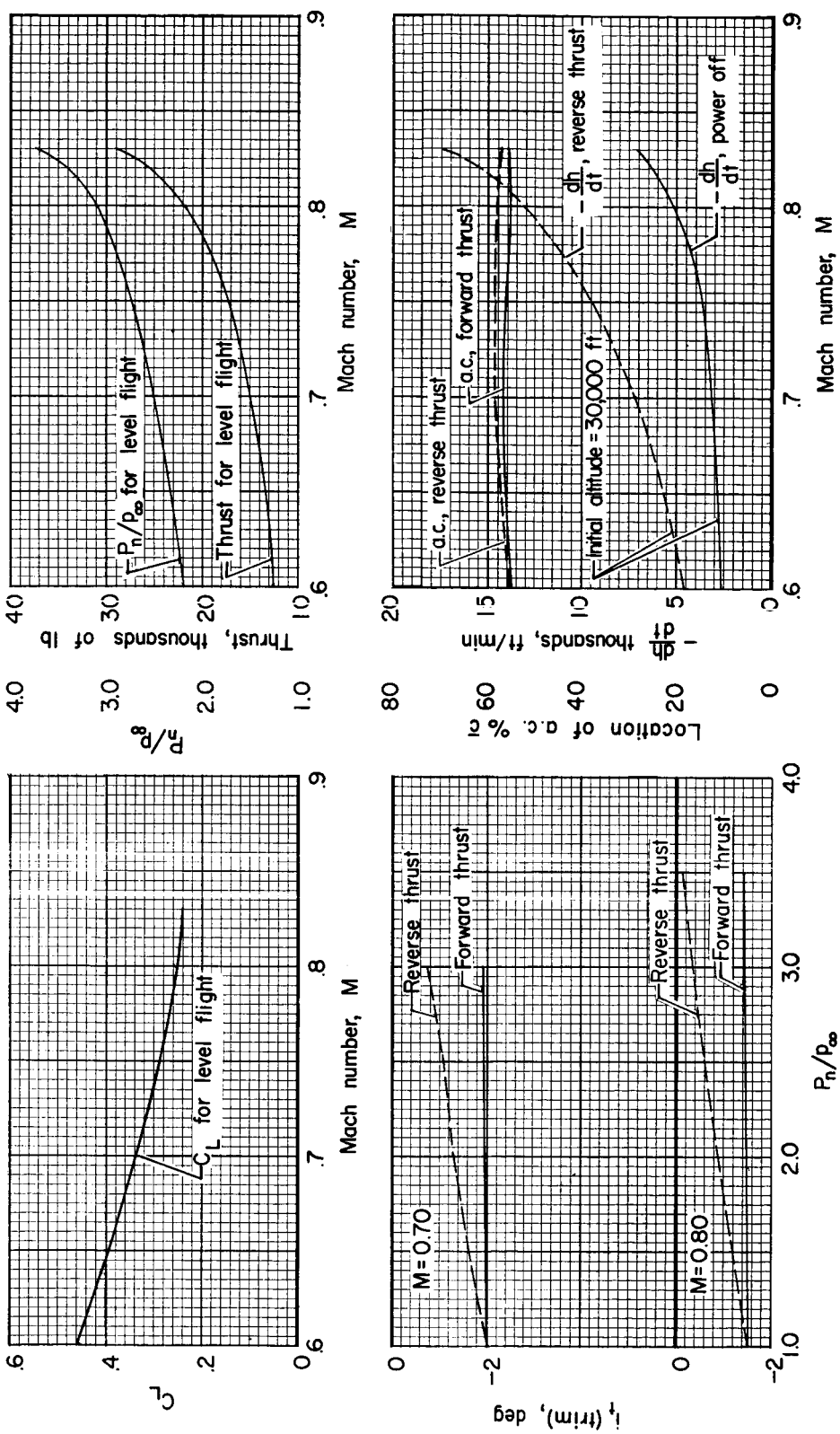

Figure 36.- Some effects of thrust reversal on the longitudinal aerodynamic characteristics of a hypothetical four-engine jet transport airplane in level flight at 30,000 feet; assumed weight = 200,000 lb; assumed wing area = 2,750 sq ft.